UiT
THE ARCTIC
UNIVERSITY
OF NORWAY

Department of geosciences

# Volume measurements and change of Longyearbreen and Tellbreen, Svalbard

—

**Marta Lidström**

*Master thesis in Geology (GEO-3900) – August 2017*

# Acknowledgements

I would like to show my supervisor Associate Professor Mette Kusk Gillespie gratitude for letting me work with her during my last year of geology studies. I am very grateful for the opportunity to write my thesis within the field of glaciology and to say the least, lucky to be able to conduct my field work on beautiful Svalbard together with Mette. Thank you for supplying me with articles, encouraging me the whole year and for corrections of my thesis. I would furthermore like to thank Mette together with Karoline Bælum for giving me their data from 2004 to work with, along with some indispensable advice. Big thanks also to UNIS for allowing me to bother you during the field work and Professor Stein Bondevik for volunteering as my main Supervisor from UiT. Thank you, Professor Jacob C. Yde for getting me on this track from the beginning with motivating lectures and the opportunity to write an exciting bachelor thesis.

As this the last (for now) episode of my long time as a student I would also like to acknowledge my family (especially mom, dad, my sisters and brother - all of them), my awesome classmates and of course Knut for all the support and encouragement during it all. Sorry for all the inconvenience it might have brought you. I will start to recompense you soon!

*Front page photograph: The stunning arctic scenery of Svalbard with Adventsfjorden in the background. View from the top of the Tenoren Mountain in between Longyearbreen and Tellbreen (Photograph: Marta Lidström, 2016).*

# Abstract

Climate change is a comprehensive field of research. The cryosphere is only a small portion of the entire spectrum but is still a very important constituent to try and understand. Thermal expansion of the oceans is the second largest cause for sea level rise around the world after the global melting of glaciers and ice sheets combined. Even the smallest valley glaciers, with small individual volumes, can altogether on a global scale have a great impact on the ocean level at the same time as they have a much faster response to climate change than the larger ice masses do (Meier et al., 2007; Bahr et al., 2009; Bahr and Radic, 2012).

This thesis evaluates the actual changes in ice volumes measured by ground penetrating radar (GPR) and the theoretical volume-area scaling method. The GPR method collects thorough ice thickness data by 2D cross profiles of a glacier which can be interpolated to ice volume models. The method provides detailed information about depth distribution, changes between different years and englacial structures, but is limited due to time consuming field work and has therefore only been carries out on a few hundred glaciers around the world. The volume-area scaling method is an alternative approach which describes the non-linear relationship between the volume and the surface area of a glacier by using exponents and proportionality coefficients derived from theoretical and empirical studies. Due to the lack of ice thickness measurements, this method is often used for volume estimations on a large scale, regionally or globally. The field work for this thesis was carried out with GPR on Longyearbreen and Tellbreen, close to Longyearbyen on Svalbard, during five consecutive days in April 2016. A total of 86 2D depth profiles collected with 100 MHz and 50 MHz rough terrain antennas (RTAs). 46 of the profiles (all 100 MHz) were interpolated to achieve a total ice volume estimate. The ice volume in 2016 was 0.085 $km^3$ for Longyearbreen and 0.110 $km^3$ for Tellbreen. The results were firstly compared with reprocessed data from 2004 which showed a decreased ice volume for both glaciers by 15.8 % for Longyearbreen and 16.9 % for Tellbreen. Secondly, both GPR surveys was compared to the ice volume estimates calculated by the volume-area scaling results. The comparison shows that the volume-area scaling method is likely to overestimate the volume for small valley glaciers similarly to Longyearbreen and Tellbreen.

# Table of Contents

# 1 Introduction

## *1.1 Background information and objective*

As advances are being made in climate research, more details about the actual changes occurring today and in the previous decades are needed to yield as realistic predictions as possible for the future. Glaciers are good climate indicators as they are geological features that react fast to changes in temperature and precipitation. A glacier can for example reduce largely in size or totally disappear in only a few tens of years, as they did in Glacier National Park (GNP) in the US (Usgs.gov, 2017). When the GNP opened in 1910 there were around 150 glaciers to be seen, while only 25 remained in 2010.

The glacial response to climate change poses uncertainties towards the environmental development in our adjacent future. There are about 211.000 glaciers all around the world when the great ice sheets (Antarctica and Greenland) are not counted in (Navarro et al., 2016). Even the smallest glaciers are so numerous that they will have an important role in the world's total ice volume and are expected to contribute the most in the near future sea level rise (Meier et al., 2007; Bahr et al., 2009; Bahr and Radic, 2012). Glaciers provide for a successively eustatic sea level rise as they are gradually losing their mass to runoff water (Navarro et al., 2016). About half of the total sea-level rise is caused by the thermal expansion of the sea due to higher global temperatures, while the other half is supplied from melting ice around the globe (Bahr et al., 2009; Climate.nasa.gov, 2017). As of today the worldwide-distributed glaciers contribute about 28% more to the sea level rise than the large ice sheets. This is a direct reflection of that the smaller glaciers, which are situated in warmer regions, has a faster response time to climate (IPCC, 2007; Navarro et al., 2016). These glacial melt water runoffs are also contemporary important as energy and water resources all around the world as they influence the regime of large river systems all around the world (IPCC, 2007). Volume estimations are an important parameter required for future climate related estimations. Accurate volume estimations of glaciers are therefore desiderated to be able to implement a precautionary approach towards a sustainable future (Bahr et al., 2009; Bahr and Radic, 2012).

Ground-penetrating radar (GPR) surveys are time consuming and therefore relatively costly type of data acquisition and have only been used at a few hundred glaciers around the world (Navarro et al., 2016). Because of the lack of ice thickness measurements on glaciers, other methods such as the empirical volume-area scaling relationship (see section 3.6) are applied when estimating the glacier volume of the world's glaciers (Navarro et al., 2016). Improved understandings of glacier dynamics have also allowed researchers to develop numerical models for volume estimation (Andreassen et al, 2015). A GPR measurement does however enable precise volume calculations, which later can be used to calibrate/adjust the inputs and validate the results of other more general methods (Navarro et al., 2016).

Almost 60% of Svalbard's land area is covered with glaciers. Most of them are cold ones since the entire archipelago lies in a cold high arctic climate with a mean annual temperature of -5°C (Yde et al., 2008). The larger glaciers lie in the east and north since the yearly precipitation is higher in these parts, whereas some parts in the south and west are defined as arctic desserts (~300 mm $yr^{-1}$).

This thesis analyses the change in volume of two small glaciers in the central parts of Svalbard during the last decade. The data collected with GPR on Longyearbreen and Tellbreen during the 2016 field work is compared to reprocessed data from the same glaciers in 2004 in order to measure their volume development. The interpolated measurement values from these studies are then compared to the presumed change in volume from the simple nonlinear power law equation: $V = cA^{Y}$. This volume-area scaling relationship based on empirical studies and is often used for volume estimations of glaciers on a large regional or global scale. A comparison between the two methods can determine the quality of volume estimations for small valley glaciers.

# 2 Study area

## *2.1 Svalbard*

Svalbard is a large archipelago in the Barents Sea (Figure 1). The land areas stretches as an oblique triangle over 63.000 km$^2$ between 81°N 35°E in the north and 74°N 10°E in the south. Spitsbergen is the largest island of Svalbard (~60% of the land area) with a total of 2600 inhabitants of which around 2000 people live in Longyearbyen. Longyearbyen is the administrative centre of Svalbard with the world renowned University Centre of Svalbard, UNIS, which specializes in environmental and technological research (Unis.no, 2017). There are only three other small settlements on Svalbard (except for smaller research stations), which also lies on the west side of Spitsbergen and exists due to mining and research activity.

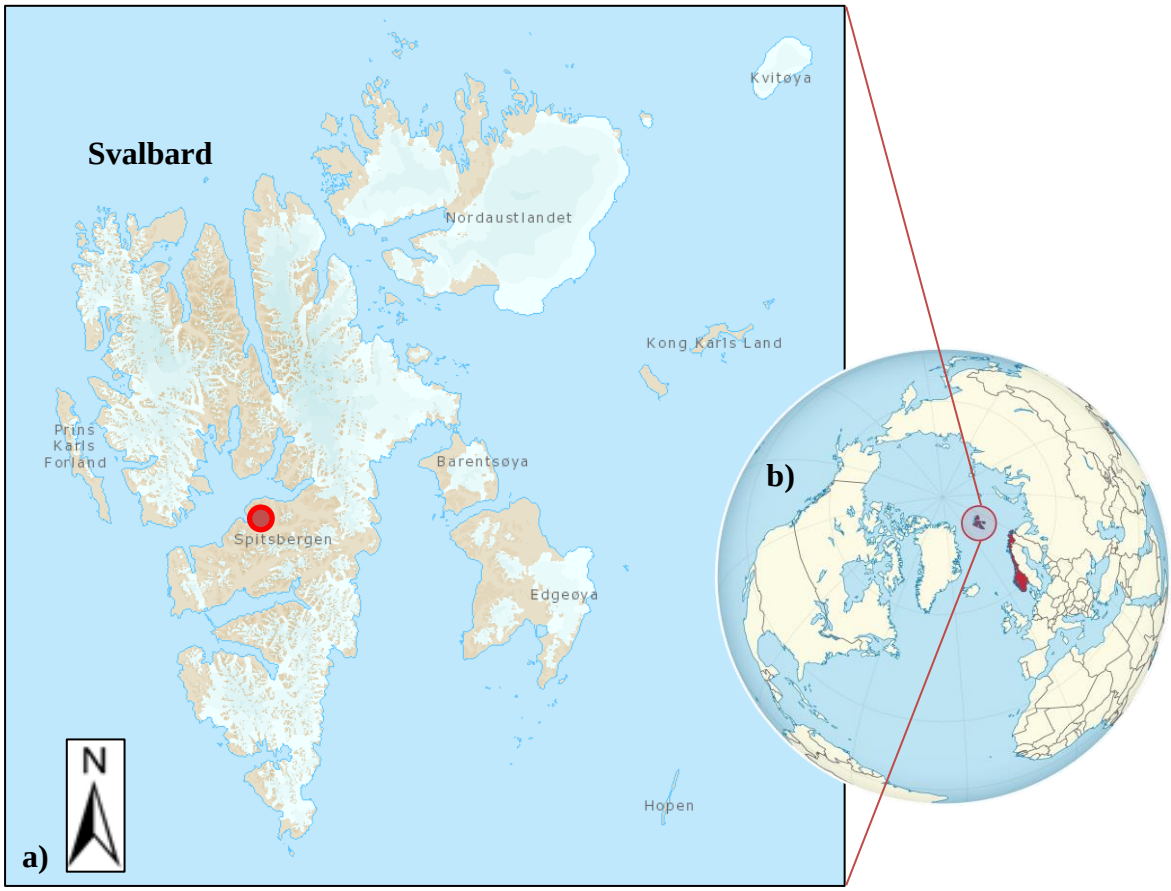


**Figure 1 – a) Map over the Svalbard Arcipelago with the Adventdalen area marked with a red dot. b) Svalbard marked with a red circle in between the Greenland Sea to the west and Barents Sea to the east. Norway is marked in red.**

## *2.2 Geological and geomorphological settings*

Svalbard is thought to have been formed and raised above sea level as the Greenlandic (Laurentia) and European (Baltica) plate collided during the creation of the Caledonian mountain range. The archipelago is built up as a puzzle of rock type sequences with an unusual amount of different bedrocks and geology formations (Figure 2). The rock types range from heavily folded and metamorphosed rocks (the Caledonian orogeny) from the mountain building Silurian age to thick erosional and sedimentation deposits characterized as red sandstones deposited during the Devonian age. Several additional folding and sedimentation processes have occurred during later geological eras.

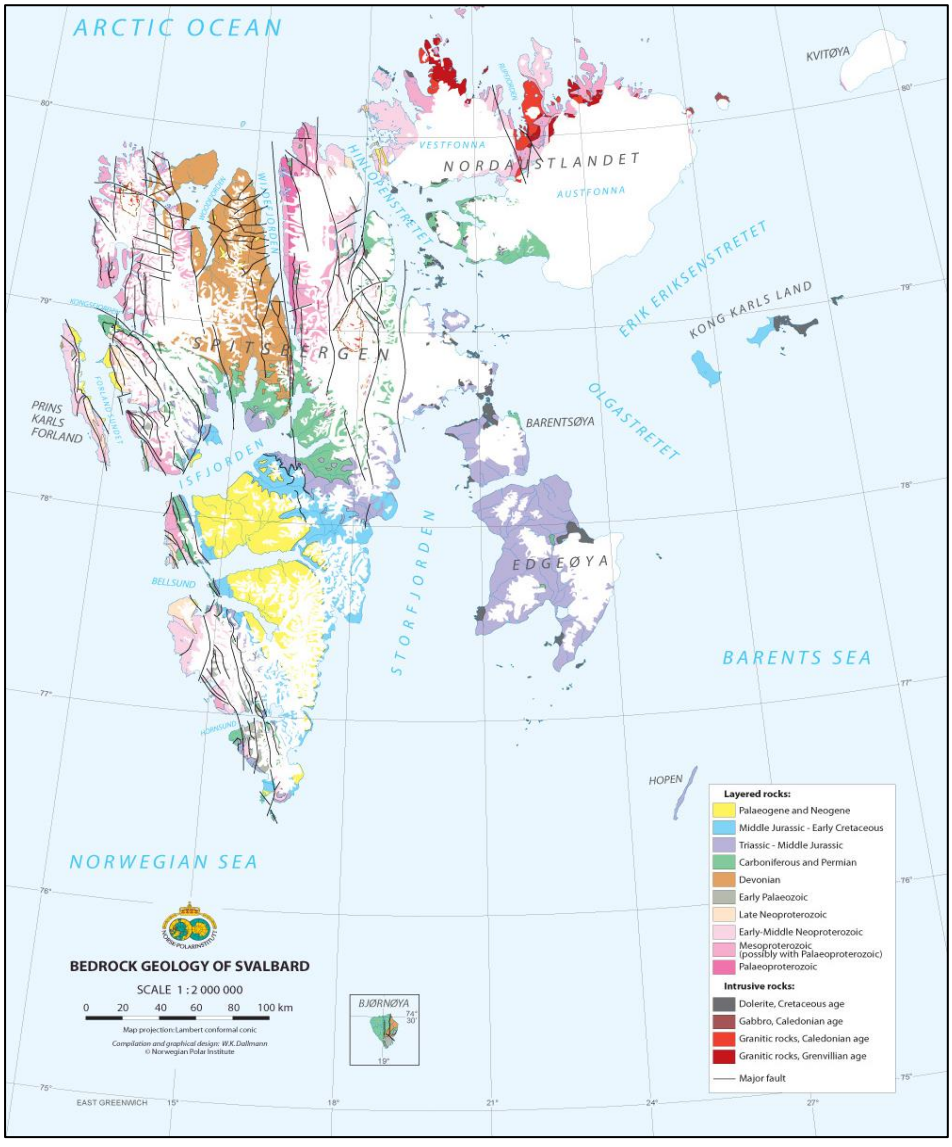


**Figure 2 – Bedrock geology of Svalbard (Norwegian Polar Institute, 2017a).**

The area around Adventsdalen consists of plateau mountainous landscape with sandstone, siltstone and shale rocks from the middle Jurassic to early Cretaceous and Palaeogene (Norwegian Polar Institute, 2017a). These mountains have close to horizontal layering and consist of highly unconsolidated rocks which are very easily erodible (Bryhni et al., 2007) and are recognizable form their nearly flat tops and steep sides with erosional spines. The glaciers around Adventsdalen have a strong erosional potential, due to the unconsolidated rocks, which will shape the whole area.

## *2.3 Climate*

The archipelago lies between the Fram Strait in the west, the Barents Sea in the east and the Arctic Ocean in north. Both large and small fjords and straits dominate the entire archipelago. The high arctic climate areas are characterized by small diurnal changes in air temperatures, whereas there are large annual variations (Figure 3) (Nuth et al., 2008; Eklima.met.no, 2017). The climate in Svalbard is largely influenced by the West Spitsbergen current that runs through Fram Strait. This is the final branch of the warm Atlantic current on the western coast of the peninsula. The oceanographic conditions and marine settings causes a locally milder climate compared to the rest of the Arctic areas on the same latitudes and keeps the west and north of Spitsbergen free of sea ice for most of the year (Norwegian Polar Institute, 2017b).

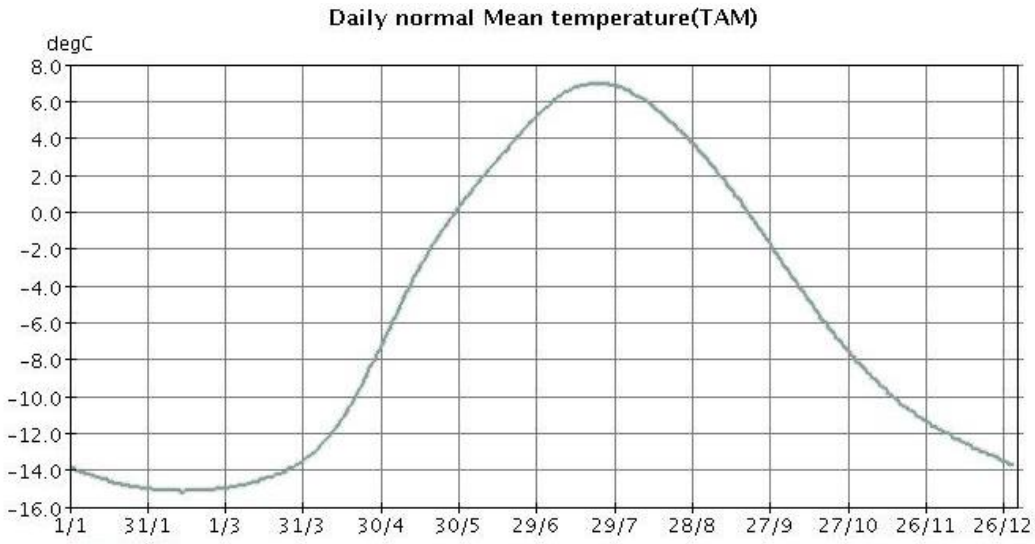


**Figure 3 – Example of daily normal mean temperature during one year at Svalbard Lufthavn, 2016 (eklima.met.no).**

There's a pronounced difference in climate from the east and west due to warm waters on the west side and cold waters leaving the Arctic Ocean to the Barents sea on Svalbard's eastern side. The northeast is more affected by hash Arctic conditions due to cold waters and the cold and dry polar easterly wind patterns (Figure 4), which also feeds the northeast with perennial sea ice (Isaksson et al., 2005). The sea ice will in turn shield the northeast from ocean humidity during the winter, which results in generally more arid northern parts of Svalbard. However, the sea ice extent has been proven to decrease in the arctic since the late 90's. It varies widely from year to year and is now often non-existent on the west coast while the east coast still has a larger extent of sea ice around the coastline in wintertime (Meterological Institute, 2017).

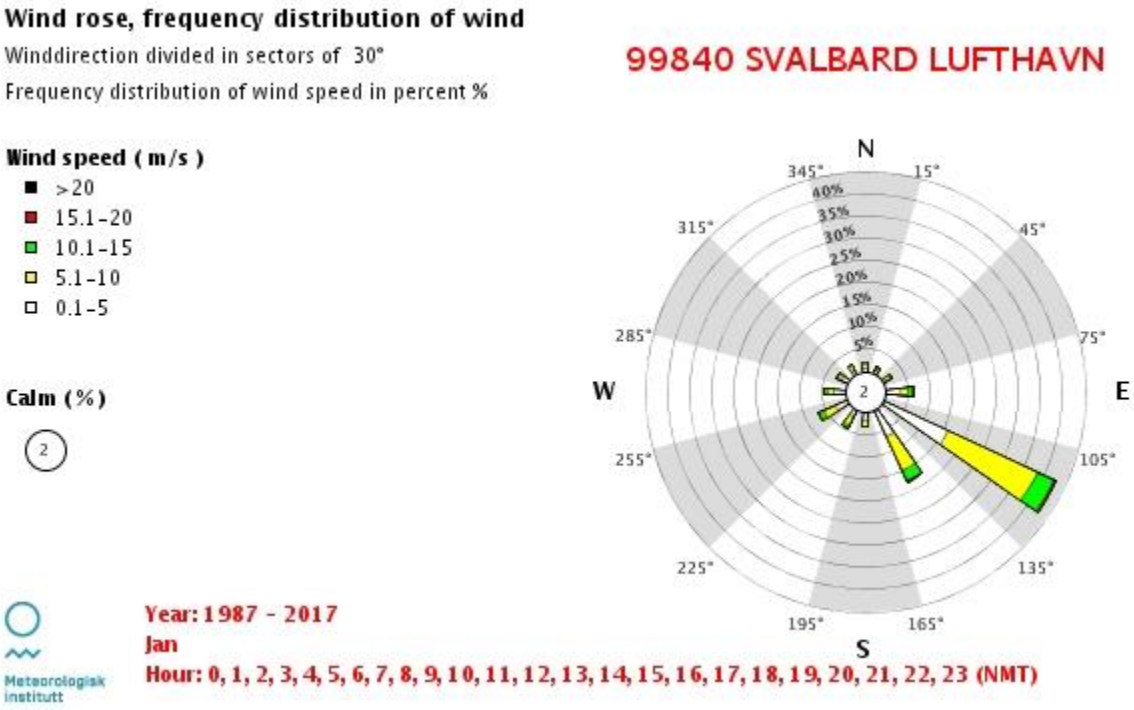


**Figure 4 – The wind rose from Svalbard Lufthavn for the last 20 years (1987-2017) shows a strong pattern with easterly winds (eklima.met.no).**

Meteorological observations around the central parts of Svalbard have been recorded since the early 20th century (1911) and show a steadily rising temperature with exception of a colder period around the 1960's (Meteorological Institute, 2017). Summer and winter temperatures have increased during the last couple of decades, both increasingly since the mid 1990's (Figure 5and Figure 6). The climate on Svalbard is called "polar desert" as the precipitation is generally low. The

contemporary annual precipitation in Spitsbergen range from 180-440 mm $yr^{-1}$ (with some higher exceptions). This is an increase by ~15-25 % since the earliest observations (Figure 7) (Førland and Hansen-Bauer, 2003). There is also a predominant increase in snow accumulation towards the eastern side as well as towards the south, which normally have about 400 mm $yr^{-1}$. The amount of precipitation is often somewhat higher over the glaciers due to orographic effects but seldom exceeds 2-3 m of snow (Hagen et al., 1993) and is often highly affected by wind-loading or drifting of snow.

Even though Svalbard has a predominantly cold winter caused by polar fronts from the north, low pressures from around Iceland and Greenland will periodically extend up towards Svalbard during winter. These low pressures will give rise to cyclone events, fast rising temperatures and even mid-winter rainfall. Svalbard has experienced an increase in annual mean temperatures during the last decade, which in turn is expected to induce a change (increase) in the yearly precipitation (Bahr et al., 2009).

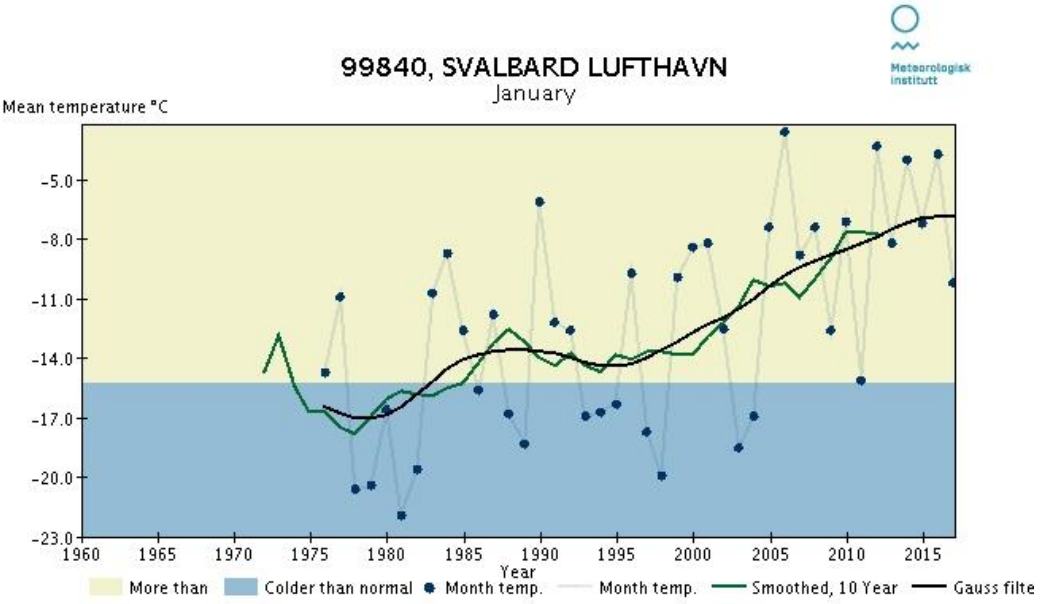


**Figure 5 – Increasing winter (January) mean temperature between 1980 and 2017 (Meterological Institute, 2017).**

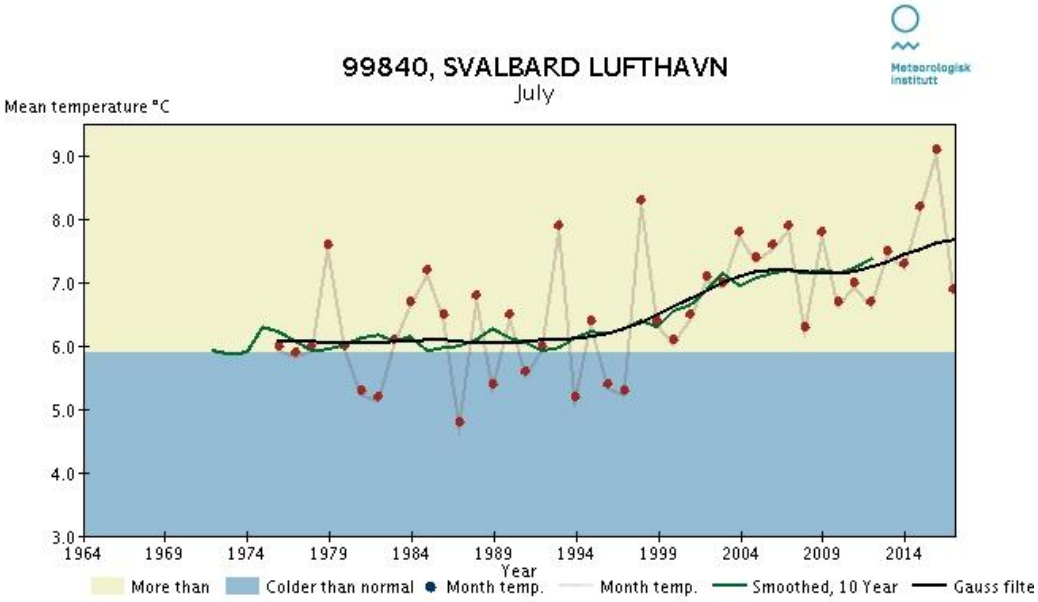


**Figure 6 – Increasing summer (July) temperatures from 1990 to 2017 (Meterological Institute, 2017).**

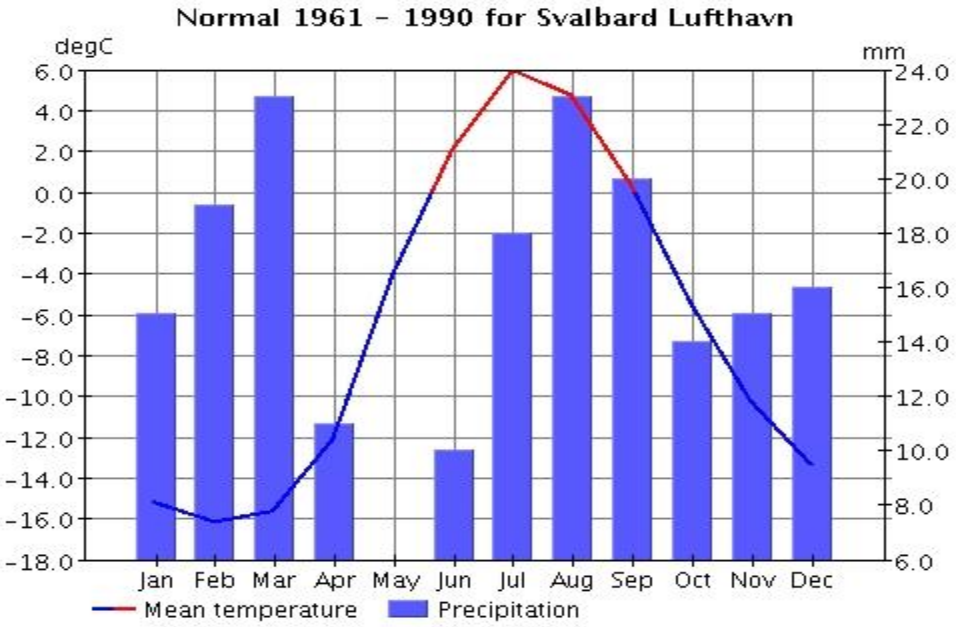


**Figure 7 – Normal mean temperature and precipitation at Svalbard Lufthavm between 1961-1990 (eklima.met.no)**

About 60 % of Svalbard is covered by ice (34.600 $km^2$), compared to only 10 % vegetation and 30 % exposed bedrock (Etzelmüller et al., 2000). The sparse flora is widely protected due to their endangerment and vulnerability and survives to a large degree because of the 3-4,5 months long period of midnight sun, which contrarily lies below the horizon and leaves the area in obscurity the rest of the year. The inland

areas of Svalbard have continuous permafrost with a varying thickness of 200-450 m, while the permafrost in the coastal areas now can be entirely absent (Unis.no, 2017). The seasonally active layer above the permafrost oscillates between 0,1-1 m. Most of the glaciers on Svalbard have cold based outer margins (below the pressure melting point) (Etzelmüller et al., 2000). Depending on their thickness some of the glaciers have limited areas of temperate ice, making them polythermal (Etzelmüller et al., 2000).

## *2.4 Glaciers*

The most typical type of glaciers on Svalbard are large ice caps that spreads out and divides around mountain ridges of nunataks into valley glaciers. These complexes are often referred to as Spitsbergen type glaciers (Hagen, 1993). Another common phenomenon on Svalbard is the numerous surge-type glaciers, which has long time-intervals of slow to no movement before suddenly shifting in to a higher yearly velocity for a shorter period of time (Sevestre, 2015; Yde et al., 2014).

There are large differences in size between the smaller valley and cirque glaciers in the mountainous areas and the numerous plateau glaciers and large ice caps in the flatter areas. The largest ice masses on Svalbard are the Austfonna (~8000 $km^2$) and Vestfonna (~2000 $km^2$) ice caps in the cold north-eastern part. Valley glaciers are abundant in the more mountainous areas in the central and northern Spitsbergen, and are often are smaller than 5 $km^2$ in comparison. While the large ice caps thrive along the cold coastal areas, the valley glaciers reflect where the topographic effects and wind conditions are most favourable for glacier development. The sea-terminating glaciers covering Svalbard has a high annual mean flow speed of up to ~1.5 m $d^{-1}$ compared to the lower speed land- terminating glaciers which typically move less than 10 m $a^{-1}$ (Lefaconnier et al., 1994). The glaciers on Svalbard are predominantly characterized as either polythermal or cold, meaning that they exist at or under the pressure-melting point with cold or/and temperate ice. It's generally the small glaciers that cannot reach the pressure-melting point limit that are entirely cold. The greater the extent and depth of the glacier, the higher the temperatures get towards the base due to thermal conductivity of strain or frictional heating, increased pressure, advection of ice and water, conservation of geothermal heat flux from the ground and

increased insulation from local weather conditions (Björnsson et al., 1996). It's only about 10-20 m of the top ice column in a glacier that is subjected to seasonal weather variations.

The GPR survey presented in this thesis was conducted at Longyearbreen and Tellbreen at 78°N 15°E (Etzelmüller et al., 2000). These glaciers are two of the valley glaciers closest to Longyearbyen (Figure 8), both of which are well studied glaciers due to its closeness to UNIS. They do both terminate on land and are cold based glaciers, meaning that they are frozen to the ground below and does not reach the pressure melting points. Both glaciers are, like most other glaciers on Svalbard, thought to have had their maximum extent during The Little Ice Age (LIA) and none of them are defined as surging glaciers (Etzenmüller, 2000; Bælum, 2010; Seveste, 2015; Yde et al., 2008).

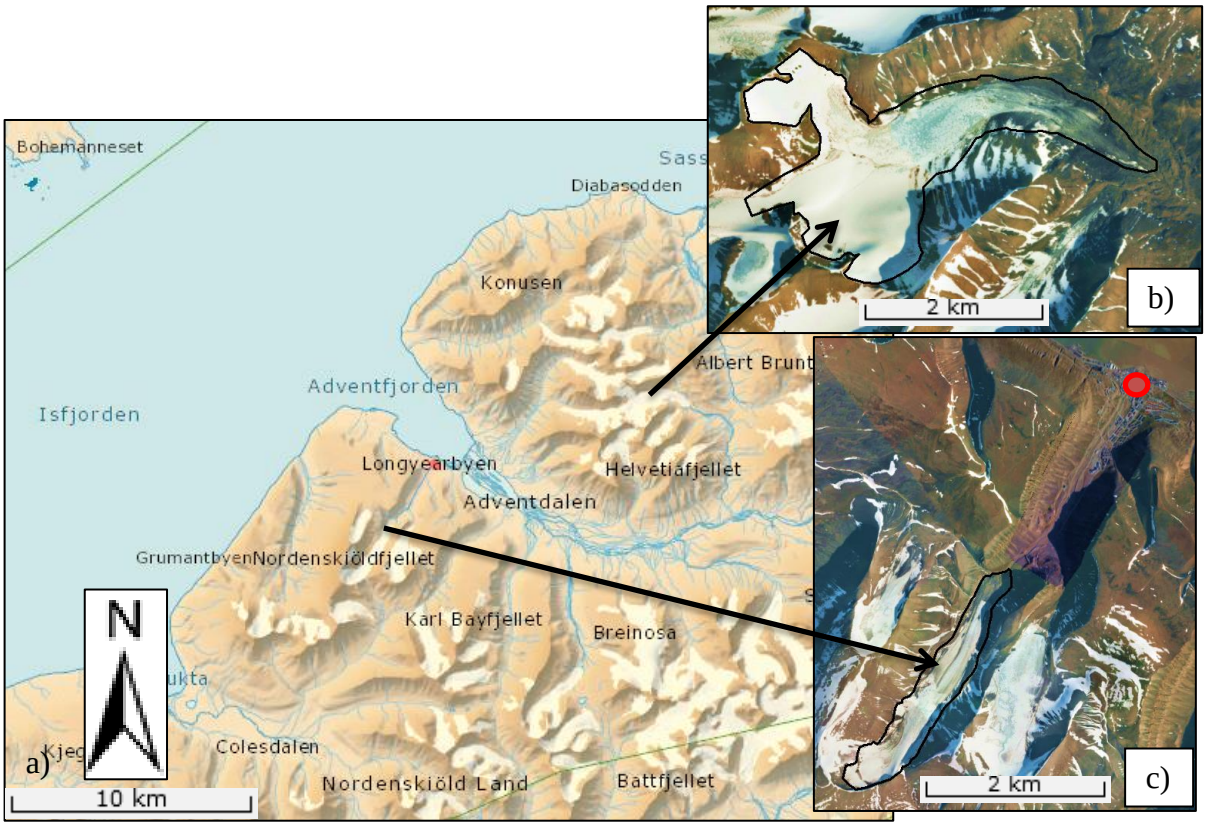


**Figure 8 – a) Map over the area around Adventfjorden. b) Tellbreen outlined northeast of Adventdalen. c) Longyearbreen outlined southwest of Longyearbyen (marked with a red dot). Larsbreen is seen to the right and Platåbreen glacier lies on the west of Longyearbreen.**

## *2.5 Longyearbreen*

Longyearbreen lies about 4 km southwest of Longyearbyen (Figure 8c). The glacier stretches 4.8 km through a narrow north-east oriented valley and covers an area of

about 2.7 km$^2$ between 210-850 m a.s.l. (Figure 10 and Figure 11) which is within the continuous permafrost zone (Yde, 2008, Etzelmüller et al., 2000). The outlet, which drains a 10.68 km$^2$ large catchment area, runs down past an ice-cored debris covered terminal moraine before it continues further down through Longyearbyen to Adventfjorden (Riger-Kusk, 2006). About 43 % of the catchment area was covered by glaciers in the late 90's (Riger-Kusk, 2006). Longyearbreen, Larsbreen and Platåbreen to the west of Longyearbreen (Figure 8c) end their yearly snow melting period around the end of July.

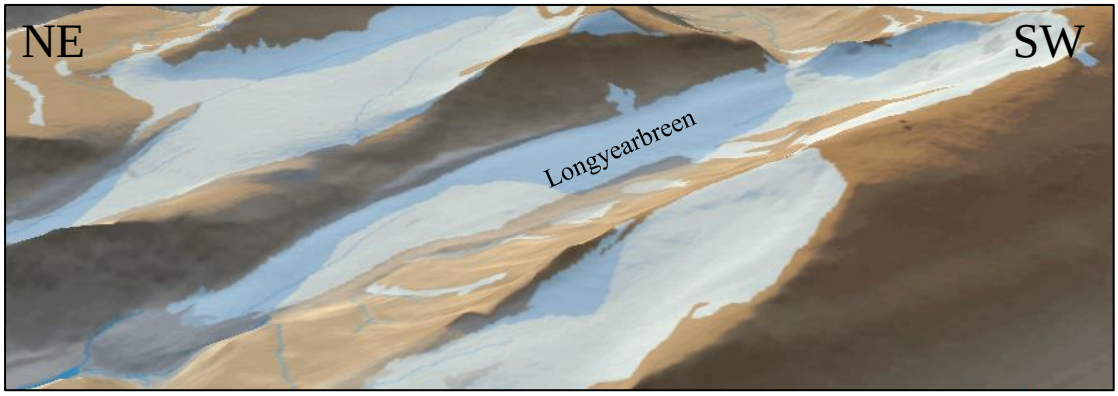


**Figure 9 – 3D image of Longyearbreen seen from the northeast.**

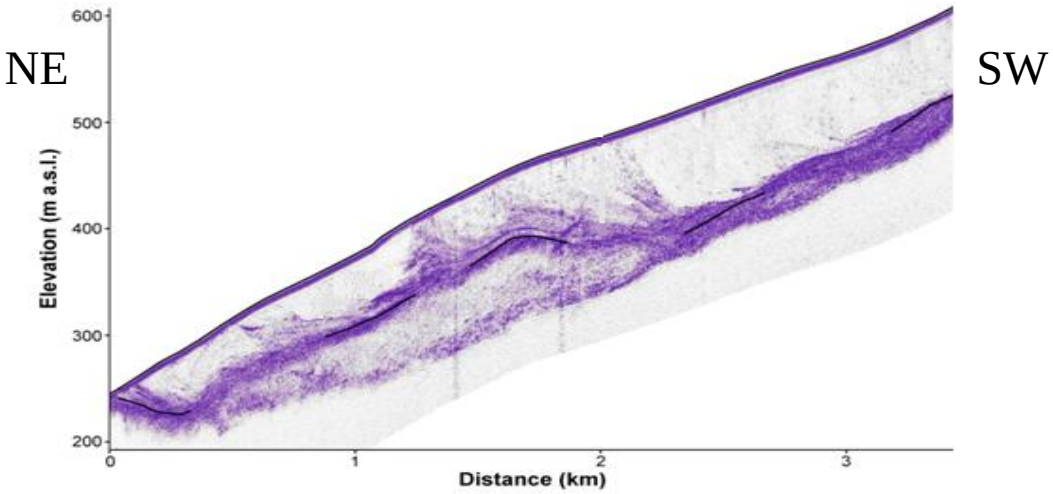


**Figure 10 – Centerline glacier profile of Longyearbreen collected with a 100 MHz antenna in 2009, corrected for elevation. Top pick from centerline of the glacier and basal pick from glacier bed reflector (Modified from Sevestre 2015).**

Longyearbreen has been the subject for several earlier studies. Most relevant for this study are the GPR surveys from 1993 and 2004. The 1993 study found a total volume of 0.13 km$^3$ (Etzelmüller et al., 2000) while the next GPR study made by Riger-Kusk

in 2004 found it to be 0.08 $km^3$ (Riger-Kusk, 2006). There have been different interpretations of radio-echo reflections and GPR surveys in the middle and upper part of the glacier. What was first assumed to be temperate ice in the upper parts (Etzelmüller et al., 2000) has later been interpreted as debris-rich basal ice (Riger-Kusk, 2006). The glacier is therefore believed to be entirely cold based. This is based on earlier GPR surveys where no evidence of temperate ice was found. A modest maximum depth of ~120 m in 2004 and a V-shaped subglacial relief indicating little basal erosion (due to subzero temperature at the glacial bed) also supports that Longyearbreen is an entirely cold glacier (Riger-Kusk, 2006; Sevestre, 2015).

The glacier has been proved to be melting as mass balance measurements between 1977 and 1982 on Longyearbreen showed an annual mass loss of -0.55 m water equivalent per year (Hagen and Liestøl, 1990; Hagen et al., 2003a). The equilibrium-line altitude (ELA) where the accumulation and ablation is balanced was at ~615 m in 2001 according to Bringedal (2004), but strongly negative mass balances the last couple of years has left Longyearbreen with almost no remaining accumulation zone at all (Sevestre, 2015). The movement velocity in this area of the glacier was about ~2-4 m $yr^{-1}$ in 2000 (Etzelmüller et al., 2000, Yde et al., 2008). Longyearbreen is a typical low-activity glacier and the speed decreases even more towards the glacial terminus to about 1 m $yr^{-1}$, which is common for valley glaciers (Etzelmüller et al., 2000; Benn and Evans, 2010; Sevestre, 2015).

The sediment-rich convex shaped ice layers on the surface of Longyearbreen are almost perpendicular to the flow direction. These layers are substantially more parallel to the flow line along the lateral sides of the glacier where the ice velocity is much lower due to the higher frictional forces. The debris-covered ice (Figure 11) consists of a 0.5-1.5 m thick layer of angular gravel to stones sizes in a fine matrix above the ice-core (Etzelmüller et al., 2000). The thick moraine debris covering and protecting the ice from sun and heat in the northernmost part is assumed to have caused the slow decrease in longitudinal extent of Longyearbreen compared to other glaciers in the area (Benn and Evans, 20120; Sevestre, 2015) during the last decades. Comparing photos of the glacier from 1934and 2008 (74 years) shows little to no ret reat of the glacial front (Figure 11). There are also lateral moraines on both

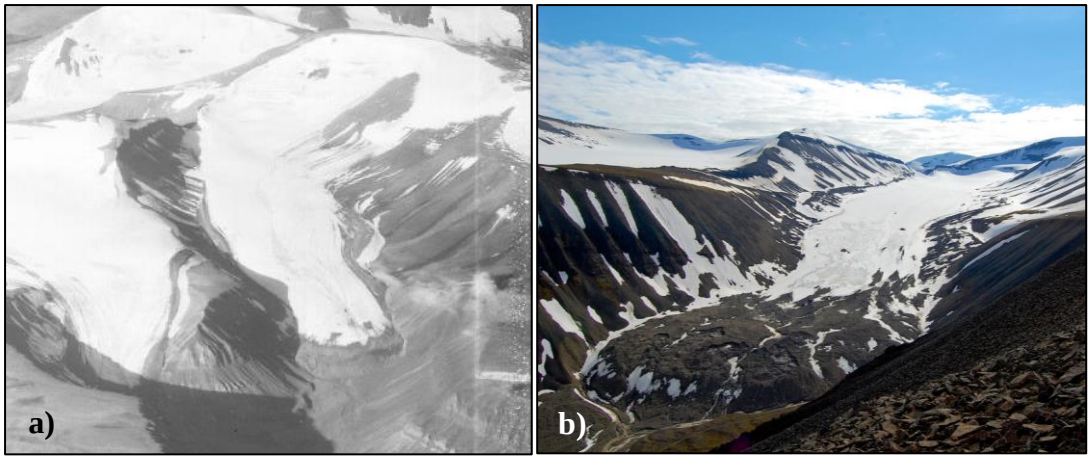


**Figure 11 – a) Aerial picture of Longyearbreen from the north in 1934 (Norwegian Polar Institute, 2017a). b) Longyearbreen seen from the north with the large ice cored moraine in the front and its thinning glacial body above the moraine and along the sides. Larsbreen can be seen on the left in the picture. (Photograph: Markus Eckerstorfer, July 2008)**

sides up to the ELA.The relatively flat surface of Longyearbreen has few crevasses in the cold surface and cold temperature of the ice which is why the main drainage method on the central glacial body is through supraglacial conduits. The number of crevasses increases towards the lateral parts of the glacier and will therefore reroute the melt water through englacial and subglacial conduits (Etzelmüller et al., 2000; Bælum, 2006). These conduits develop into large tunnels due to the slow yearly movement of the cold glacier and can safely be visited during wintertime to get a firsthand opportunity to see the inner structures of the glacier and its hydrological system (Figure 12).

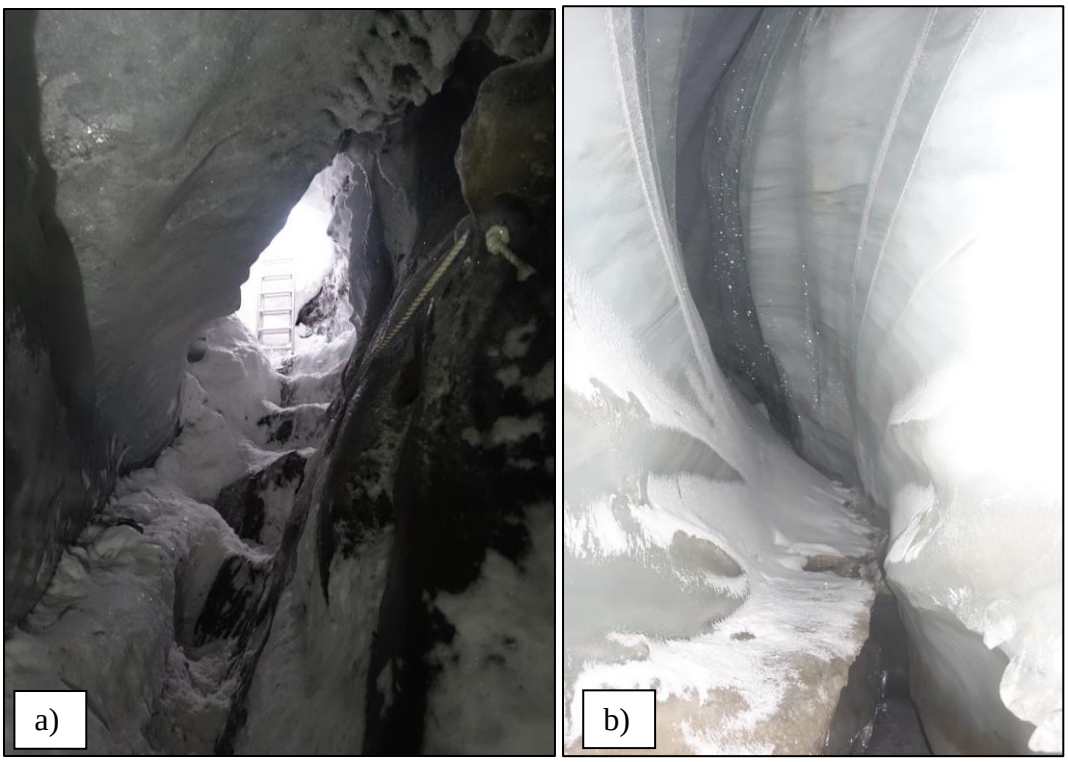


**Figure 12 – a) A large supraglacial melt water tunnel on Longyearbreen with a ladder as a scale in the opening. b) The flow lines from the melt water can be seen on the top while an old layer of debris-rich ice can be seen as a "shelf " covered with snow of less easy erodible ice in the basal of the picture.**

## *2.6 Tellbreen*

Tellbreen is almost double the size of Longyearbreen in area with ~3.9 $km^2$ (Sevestre, 2015) and lies about 20 km northeast of Longyearbyen (Figure 8b). Like Longyearbreen, it stretches over 4 km (centreline) towards the north-east but with a more complex shape in the upper regions, where ice drains into Tellbreen from tributary ice masses to the north and south of the main valley. Tellbreen is a land terminating valley glacier and lies between 340-800 m a.s.l. (Figure 13 and Figure 14) within the continuous permafrost zone. It has a distinct catchment area but does, unlike Longyearbreen, connect to valley glaciers running to opposite directions over mountain passes near the top parts. It's a cold glacier with suspicions of minor temperate zones of temperate ice, such as a thin temperate basal layer under the thickest parts of the glacier (Bælum and Benn, 2011). The glacier is otherwise frozen to its bed with signs of former wet-based conditions, such as subglacial traction till and foliated debris-rich basal ice from shearing and stress-induced metamorphism of the basal ice-till interface (Sevestre, 2015). Tellbreen has an average surface velocity

of ~1 m $yr^{-1}$ and a negative mass balance of -2.3 × $10^6$ $m^3$ water equivalent averaged between 2010-2014 (Sevestre, 2015, as cited from Report AGF212 (2014)).

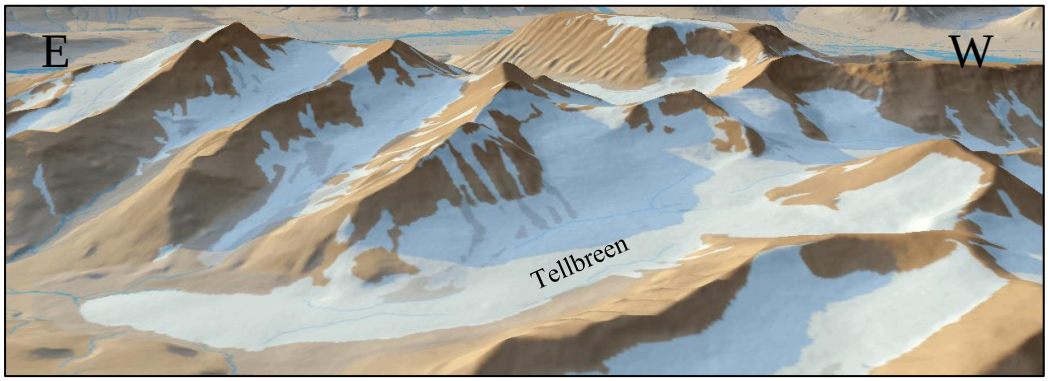


**Figure 13 – 3D image of Tellbreen seen from the northeast.**

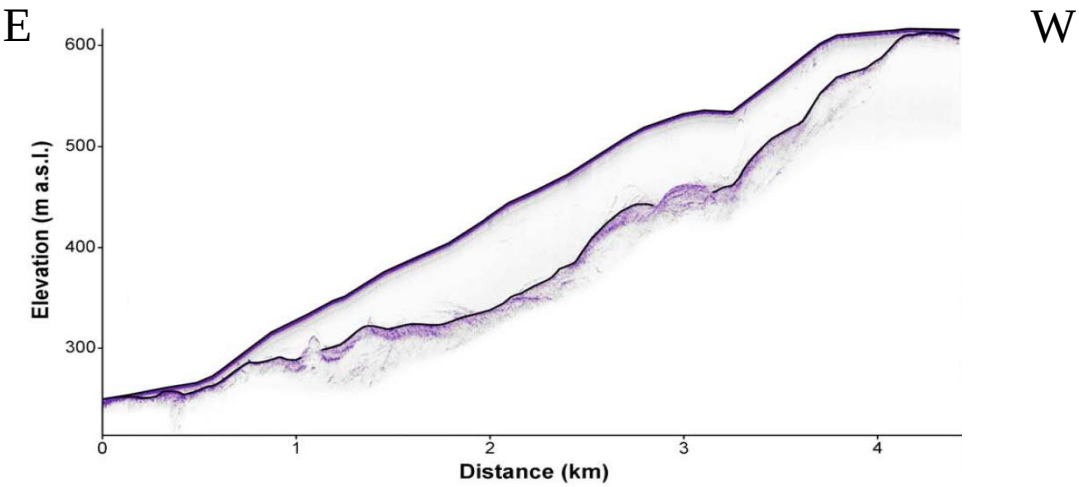


**Figure 14 – Centerline glacier profile of Tellbreen collected with a 100 MHz antenna in 2009, corrected for elevation. Top pick from centerline of the glacier and basal pick from glacier bed reflector (Modified from Sevestre 2015).**

The retreat of Tellbreen has been subsequent and has lost about 60-70 % of its volume since LIA, as is the case for most small glaciers on Svalbard (Hagen et al., 2003a; Bælum and Benn, 2011). The glacier ends up in a terminal moraine in the far eastern part while lateral and push moraines are present around the glacier margins. The moraines in the front of the glacier and on the valley sides probably originate from the last advance of LIA. The ELA has retreated up glacier the last couple of decades and was at about 480 m a.s.l. in 2006 (Bælum, 2006). The negative mass balance has since then caused the accumulation zone to disappear completely (Sevestre, 2015). The ice area and volume during the LIA maximum has been estimated to be 6.4 $km^2$ and 0.55 $km^3$ respectively, based on height and distribution of LIA moraines (Bælum

and Benn, 2011; Hagen, 1993). Data from 2009 indicates a regression of Tellbreen as the values has decreased to 2.8 $km^2$ (area) and 0.17 $km^3$ (volume) (Bælum and Benn, 2011; Hagen 1993). The mean ice thickness at LIA maximum, estimated to be 86 m, had decreased to 59 m in 2009 (Bælum and Benn, 2011; Hagen, 1993).

# 3 Theory

Changes in ice thickness occur due to accumulation and ablation variations or dynamic processes in a glacier (Benn and Evans, 2010, 145). Basal melting and freeze-on also influence the mass balance but are often overlooked due to limited contributions on large scale measurements. Ice thickness will remain constant if the negative mass loss in the ablation area is equal to the positive mass balance in the accumulation area. A negative imbalance will therefore result in volume reduction of the glacier (Benn and Evans, 2010). Both Longyearbreen and Tellbreen have almost no existing accumulation zone left due to years of negative mass balances (Sevestre, 2015). It is therefore interesting to study the actual change in volume.

One way of measuring the ice thickness of a glacier is through GPR, an active remote-sensing technique. The method shares many similarities with reflections seismic with the difference that GRP measurements use electromagnetic (EM) waves instead of sound waves. The method is a non-destructive way to investigate subsurface features. It's a versatile method and the GPR equipment therefore offers a broad range of applications for different fields of investigation. GPR has been a widely used method since the 1970´s for mapping and detecting internal subsurface structures in sediments, groundwater and saltwater investigations, utility detection, construction profiling, mineral exploration, arctic studies and climate research including glacier thickness studies as in this study (Malå, 2017a). It is also used as a complementary tool together with for example satellite and seismic data.

## *3.1 Principle of GPR method*

The EM waves are sent out from a transmitting antenna in all directions. The return signal from the downward directed waves are subsequently recorded by a receiving antenna placed in a fixed distance behind the transmitter (Figure 15). The four different types of waves recorded by the receiver and produced by the same transmitted signal are the direct air wave (1), the direct ground wave (2), the refracted wave (3) and the reflected wave (4) (Figure 16). The antennas are so close together compared to the measuring depth in GPR so that the refracted wave can be ignored.

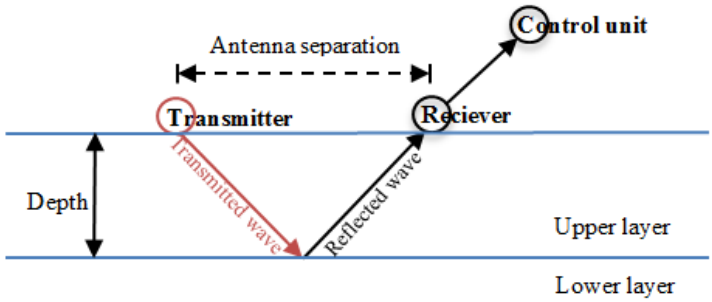


**Figure 15 – GPR setup simplified. The depth will in reality be much deeper than (tens to hundreds of meters) the antenna separation (few meters).**

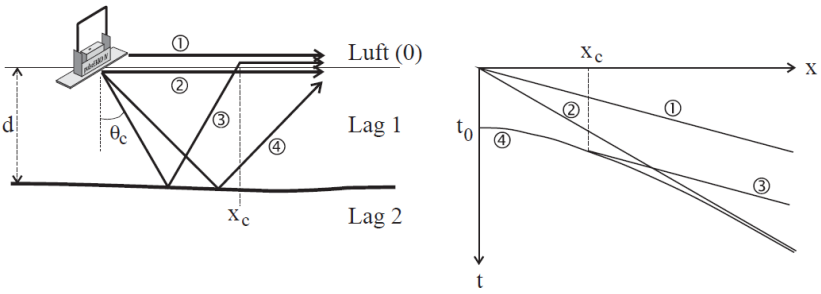


**Figure 16 – Schematic display of the different EM wave pathways (left) and how these would be displayed in a graph (right) (Annan and Cosway, 1992).**

The signal that the GPR sends out interacts with various structures and objects in the ground that will reflect waves backwards. As the return signal is received a control unit store the information of wave intensity (amplitude) and shape (phase). In GPR investigations it's only the reflected wave that's used to determine the depth of subsurface features. Since the antenna separation is incomparably small to the depth, one can assume that the wave path of the reflected waves are equal both ways and therefore is dividable by two too find the one way time down to the reflecting layer. When measuring the depth, the velocity of the material (see section 3.2) is used to determine how fast the waves have travelled a round-trip from the transmitter and back to the receiver, the two-way-travel time (TWT). The depth equation (Eq. 1) assumes that the separation between the transmitting and receiving antenna is indefinitely small ($\approx 0m$) and that the point of measurement lies in the middle between the two (Mauring et al., 1995). Also, compared to the depth of the reflection layer the separation is likely insignificantly small.

$$depth = \frac{TWT \times velocity_{ice}}{2} \qquad \text{Eq. 1}$$

## *3.2 Electromagnetic waves*

When using the GPR method a repetitive signal of high frequency electromagnetic impulses in the radio spectrum are sent out from a transmitter (Figure 15). These waves are directed downwards into the ground and will descend with different characteristics depending on the underlying mediums. The EM waves travel at approximately the speed of light ($0.2998\frac{m}{ns}$) in free air but will adjust its speed for the current medium. For the waves to not just continue downwards, as they would do in an entirely homogenous medium, the ground has to be heterogeneous and contain alternating layers of materials with different properties. The electric properties for geologic materials vary and typical values are listed in Table 1. The propagation velocity, attenuation and reflection of the signal depend on the magnetic permeability ($\mu$), dielectric constant ($\varepsilon_r$), and electric conductivity ($\sigma$) of the geological material (Plewes and Hubbard, 2001). The magnetic permeability can be disregarded in this thesis since geological materials generally have a low magnetic susceptibility.

The dielectric constant describes how well the medium stores an electric charge compared to the permittivity of vacuum. It's the contrast in the relative permittivity between different layers that cause reflections used in GPR. It is the most important property for the propagation velocity in most materials, which in turn often is dependent on amount of water content (increased by water content) (Mauring et al., 1995; Mussett and Khan, 2000; Plewes and Hubbard, 2001). This can be seen in Table 1 as water has a 10-20 times higher dielectric constant than most other geological materials.

The dielectric constant (relative permittivity) is not temperature controlled in frequencies above 50 MHz, but temperature does have an indirect effect since higher temperatures may cause higher water content in glacial environments (Mauring et al., 1995). The dielectric constant can also be affected by internal crystal orientation within the ice, the percentage of impurities and density.

**Table 1 – Electrical properties of geological materials. Modified from Plewels and Hubbard (2001) and MALÅ Geoscience (2011).**

| Medium | Velocity v (m ns$^{-1}$) | Dielectric constant ($\varepsilon_r$) | Conductivity σ (mS m$^{-1}$) | Attenuation α (dB m$^{-1}$) | Wavelength (m) | Vertical resolution (cm) |
|---|---|---|---|---|---|---|
| **Air** | 0.3 | 1 | 0 | 0 | 3.0 | 100-150 |
| **Ice** | 0.15-0.173 | 3-4 | 0.01 | 0.01 | 1.7 | 57-85 |
| **Polar ice** | 0.168 (used in this thesis) | 3-3.15 | - | - | - | - |
| **Polar snow** | 0.194-2.52 (0.21 often used) | 1.4-3 | - | - | - | - |
| **Permafrost** | 1.06-1.5 | 4-8 | - | - | - | - |
| **Fresh water** | 0.033 | 80 | 0.5 | 0.1 | 0.33 | 11-17 |
| **Sea water** | 0.01 | 80 | $3*10^3$ | $10^3$ | - | - |
| **Distilled water** | 0.033 | 80 | 0.01 | 0.002 | - | - |
| **Sediment rich ice** | 0.12 | - | - | - | 1.2 | 40-60 |
| **Granite** | 0.13 | 4-6 | 0.01-1 | 0.01-1 | - | - |
| **Clays** | 0.6 | 4-40 | 2-1000 | 1-300 | - | - |

The conductivity (σ) is a measure of how well an electric current is conducted through a certain medium in mS m$^{-1}$ (increases with ionic content). The signal attenuation increases with increased conductivity (for example in clayey or salty environments) and GPR surveillance is therefore more suitable in low conductivity (resistive) environments (σ > 10 ms m$^{-1}$) (Plewes and Hubbard, 2001). Ice is produced by precipitation (snow from fresh water) which normally has a very low ionic content (the less ions, the less conductivity). When water freezes, as much ions as possible are excluded giving more pure and less conductive ice. The low existing conductivity of ice, 0.01 mS m$^{-1}$, is therefore mainly produced by impurities in the ice which in turn is determined by different factors such as salt content, volcanic deposits, pressure and temperature.

Cold polar ice has higher conductivity than temperate ice due to a higher salt content derived from sea-salt (yde et al., 2008). Despite this, a cold glacier would still give deeper EM penetration depths due to lower water content (dryer). High dielectric properties in a material can yield good results since this enhances the propagation of the EM waves. The velocity of radar waves in different materials can be calculated using (Eq. 2):

$V = \frac{Speed\ of\ light}{\sqrt{\varepsilon_r}}$, where the speed of light is $= 2.998 \times 10^8 ms^{-1}$ Eq. 2

The velocity of ice can vary somewhat with the geophysical properties such as water content and impurities but is normally calculated as between 0.167 and 0.17 m $ns^{-1}$. In this thesis the velocity used was set to 0.168 m $ns^{-1}$ for all profiles since this gave the best results in processing (see section 4.2.6). This velocity compares well with previously assigned velocities of cold glaciers (Ødegård et al., 1997; Plewels and Hubbard, 2001; Navarro et al., 2005).

The speed of EM waves in vacuum would be 0.3 m $s^{-1}$ whilst it will reduce in speed on other materials depending on their relative permittivity. The velocity in ice is calculated to be 0.15-0.173 m $ns^{-1}$ (Annan, 1992; Hubbard and Glasser, 2005; Bradford et al., 2009). The variety in velocities is derived from different types of ice with different contents of impurities, water and air inclusions in different seasons. The velocities will vary according to seasons since the ablation season will increase the water content through melting and rain while glaciers often are insulated by a snow cover in the accumulation season allowing the glacier to stay relatively warm and dry during the winter (still colder than in summer).

## *3.3 Selection of GPR frequencies*

As a wave travels downward it will be influenced by continuous absorption and geometrical spreading. Every time a wave meets a reflective boundary, for example a layer with different density, a buried rock, a water channel or a crack filled with air etc, the EM impulse will also attenuate by scattering (reflection, refraction and diffraction) back towards the surface (Figure17). Signal attenuation (α) is the collective term for all of the dampening effects and is measured in loss of decibel strength per meter ($dBm^{-1}$). Since the attenuation in ice is low the signal penetration depth is high.

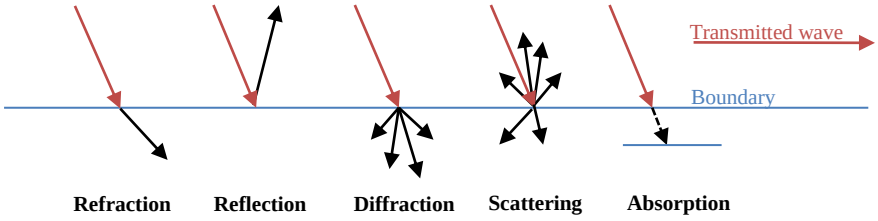


**Figure 17 – Simplified sketch of a wave-boundary interactions.**

The normal scenario is that EM waves moves more easily through materials with less electrical conductivity, making the signal gradually more and more attenuated with depth. The wave will reflect and refract etc. uncoordinatedly between particles and spread the energy in different directions so that they are lost to the receiver antenna.

The spreading increases with increased frequencies and the amplitude of a wave decreases by the same factor for each wavelength travelled through a material (Mussett and Khan, 2000). The higher the frequency is the lower the length of the wave becomes, as (Eq. 3):

$$Frequency\ \boldsymbol{f}\ (Hz) * Wavelength\ \boldsymbol{\lambda}\ (m) = Velocity\ \boldsymbol{v}\ (m\ s^{-1}). \qquad \text{Eq. 3}$$

A high frequency EM signal will therefore oscillate more often than a low frequency wave in a material with the same velocity. More frequent short wavelengths (higher frequencies) will attenuate faster than long slow waves (low frequencies) and is also why antennas should be chosen carefully before conducting a GPR investigation (Figure 18) (Mauring et al., 1995; Mussett and Khan, 2000).

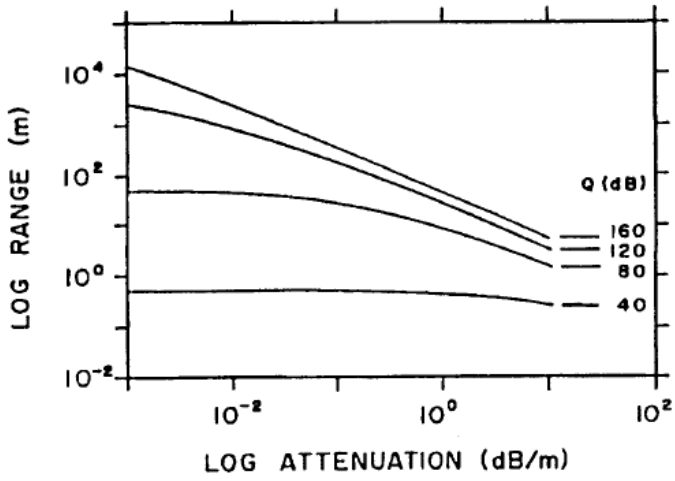


**Figure 18 – Context between range and attenuation for different antenna frequencies (Q) (Davis and Annan, 1989).**

The minimum antenna frequency can be calculated by (Eq. 4) (Mauring et al., 1995):

$$f = \frac{150}{x\sqrt{\varepsilon_r}} \qquad \text{Eq. 4}$$

where x is the distance between two vertically separated layers desired to be identifiable. The loss of energy in ice is though quite low compared to the energy loss in bedrock or soil, meaning that a high frequency would still be able to distinguish deeper reflectors as long as the glacier is not too deep and consists of too many strong reflectors.

Skin depth is the depth where the amplitude has been reduced to 1 $e^{-1}$ ($e$ being the exponential 2.718) which is $\approx \frac{1}{3}$ (or 37%) of the original amplitude. At this point the attenuation will be too strong for good results and it therefore defines the maximum penetration depth of a certain antenna frequency (Mauring et al., 1995). The skin depth is mainly dependent on the antenna frequency since the conductivity in ice is very low, proving that higher frequencies will have lower maximum depth than low frequencies. The EM wave frequencies used in GPR surveys, 10–1000 MHz, are amongst the shortest and highest frequencies of all EM geophysical techniques (Figure 19) (Mussett and Khan, 2000).

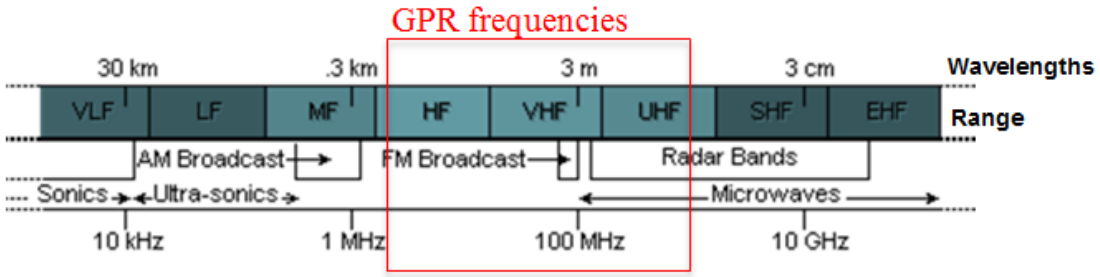


**Figure 19 – EM wave spectrum.**

## *3.4 Reflection and resolution*

Subsurface features with sizes from a couple of cm up to tens of meters can be detected by GPR depending on the centre frequency of the antennas, and it is therefore necessary to use different frequencies for different purposes. Lower frequencies are used to reach deeper targets, but the depth qualities come at the expense of resolution. This is because vertical resolution is improved by a shorter pulse (wavelength), and therefore higher frequencies are used when shallower but detailed depictions are required. A rough estimate for the maximum penetration depth in a material, antenna frequency aside, is given by (Eq. 5):

$$d_{max} < \frac{35}{\sigma} \qquad \text{Eq. 5}$$

where σ is the conductivity of the material in mS $m^{-1}$. This gives < 3500 m of $d_{max}$ for ice with σ = 0.01, when antenna frequency is not accounted for. The moisture level of the mediums is of high importance to the maximum penetration depth as the dielectric constant increases with water content. When conducting surveys over ground, cold frozen ground consequently gives the best penetration depths and distinct reflections (Mauring et al., 1995).

The reflection strength of the EM waves depends on the shape and roughness, electrical properties and the depth of the reflector (Mauring et al., 1995). Dielectric changes between materials will reflect the signal and the stronger the dielectric constant is the larger the reflection will be. To know if a boundary between two materials will yield visible reflections the reflection coefficient (R) is used. The

reflection coefficient measures the amounts of energy that will be reflected at impedance contrasts between two know materials and can be estimated with (Eq. 6):

$$R = \left|\frac{\sqrt{\varepsilon_{rv}}-\sqrt{\varepsilon_{ro}}}{\sqrt{\varepsilon_{rv}}+\sqrt{\varepsilon_{ro}}}\right|^2 > 0.01 \qquad \text{Eq. 6}$$

where $\varepsilon_{rv}$ and $\varepsilon_{ro}$ are the dielectric constants in the main material and the boundary material respectively. $v_1$ and $v_2$ are the velocities of the upper and lower layer respectively. The equation shows the ratio between the emitted and reflected waves. Table 2 contains example values between ice and typical surrounding materials.

**Table 2 – Reflection coefficient of ice and common surrounding materials.**

| From | $\varepsilon_r$ | To | $\varepsilon_r$ | **R** |
|---|---|---|---|---|
| **Ice** | 3.2 | Air | 1.0 | 0.28 |
| **Ice** | 3.2 | Water | 80 | -0.67 |
| **Ice** | 3.2 | Granite | 5.0 | -0.11 |
| **Ice** | 3.2 | Shale | 10 | -0.28 |
| **Ice** | 3.2 | Saturated sand | 25 | -0.47 |

The amount of reflected energy increases with increasing difference of dielectric constants between the two materials. Therefore the higher number (both positive and negative) gives the stronger reflection but also the less energy left for deeper reflectors, making deeper features harder to see below a strong reflector. The average small glacier with a relative permittivity of 3.2 has an equivalent water content of ~1.5%. A wave will move downwards with a specific geometrical orientation of the oscillations, called wave polarity. A negative reflection coefficient value means that the EM wave will shift its polarity as is encounters the impedance contrast and be reflected with reversed polarity (Figure 20).

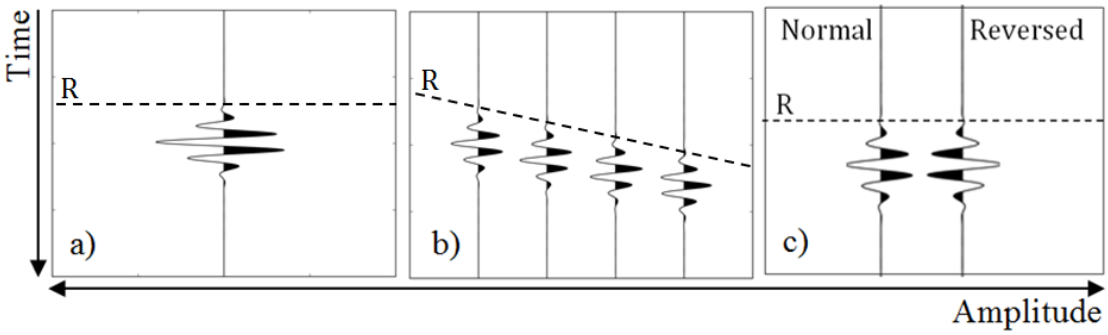


**Figure 20 – a) An example of one simple wavelet from a EM wave. b) A series of wavelets produced by EM waves at a dipping reflector. c) Normal and reversed EM wavelet produced by a reflecting layer.**

The vertical resolution is, as mentioned above, dependent on the wave velocity of the medium together with the frequency used. It's the minimum distance between reflectors that is needed to tell them apart and is usually between $\frac{\lambda}{2}$ (usually) and $\frac{\lambda}{4}$ (theoretical). The wavelength can be determined by (Eq. 7):

$$\lambda = \frac{V}{f}, \lambda = \frac{c}{f\sqrt{\varepsilon_r}} \qquad \text{Eq. 7}$$

## *3.5GPR Settings*

GPR measurements are usually gathered by the "profiling" technique meaning that the transmitter and receiver are moved along a line with a fixed distance (s) to each other while measuring (Figure 21). The setup is moved forward according to the Nyquist interval (*a*) which defines the minimum recommended moving distance between each measurement ($\sim\frac{\lambda}{4}$) to eliminate spatial aliasing (Mauring et al., 1995).

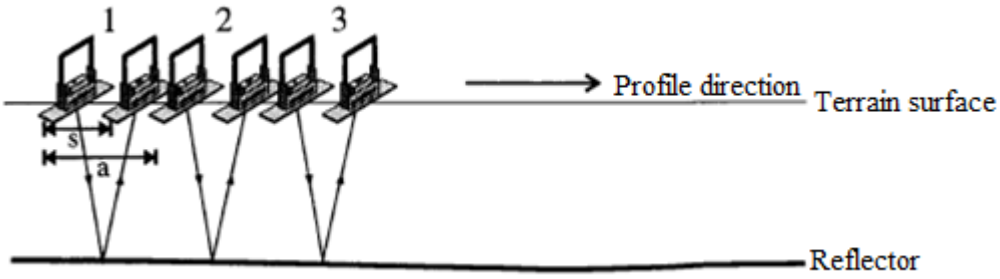


**Figure 21 – Setup of "the profiling" technique. S is the separation distance between the tranciever and receiving antenna while A is the distance between each measuring point (Modified from Mauring et al., 1995).**

The Nyquist interval can be calculated as (Eq. 8):

$$a = \frac{c}{4f\sqrt{\varepsilon_r}} = \frac{7.5\times10^7}{f\sqrt{\varepsilon_r}} \quad \text{Eq. 8}$$

The Nyquist interval in ice is 0.42-0.43 m for 100 MHz and 0.84-0.86 m for the 50 MHz antennas (Input $\varepsilon_r$ between 3-3.15). The time interval between each measurement is then acquired by dividing the distance between each measurement point with the expected velocity forward (Eq. 9).

$$time\ interval = \frac{a}{v} \quad \text{Eq. 9}$$

The time window ($T_w$) defines how long time the antenna is able to receive the transmitted signal from one point, before moving on to the next and consider the former as noise to avoid disturbances. Because of the large time interval compared to the time window, any reflections from the previous measurements will be so weak that is won't be able to influence the next measurement. The equation for time window is (Eq. 10):

$$T_w = 1.3\frac{2D\sqrt{\varepsilon_r}}{c} \quad \text{Eq. 10}$$

where D is the depth of the deepest reflector of interest, which in our case was the glacier bottom with an anticipated depth of ~100 m+. To be certain of reaching the basal reflector at all time the time window can be exaggerated some and set to a higher time count.

Sampling frequency is the number of sampling points along each trace (measurements) within a unit of time. As long as this frequency is at least twice as high as the centre frequency of the antenna, no information will be lost. The higher the sampling frequency gets, the higher the vertical resolution will become. The half of the sampling frequency is called the Nyquist frequency ($f_N$) and can be calculated by (Eq. 11) (Mauring et al., 1995):

$$f_N = \frac{1}{2}\Delta t \qquad \text{Eq. 11}$$

where $\Delta t$ is the sampling interval. The equation gives the maximum moving distance between each measurement and ensures.

The signals are recorded in to traces where one trace is a collection of stacks from one point. Stacks are the summation of samples stored for each trace to eliminate background noise. The samples are gathered to find the mean trace.

## *3.6 Volume – area scaling relationship*

The volume-area scaling relationship describes the non-linear relationship between the volume and the surface area of a glacier (Eq. 8) (Bahr et al., 1997):

$$V = cA^{\gamma} \qquad \text{Eq. 8}$$

*A* is the area, *c* is a coefficient of proportionality and $\gamma$ gives the scaling relationship between the area and volume as a dimensionless exponent. The method allows for a simple estimation of a glacier volume since *A* is easily derived by remote sensing (satellite or aerial photographs) compared to the volume of glaciers which has only been measured on a limited amount of glaciers around the world.

$\gamma$ is influenced by the mass balance of the glacier due to its volume changes (greater value with negative mass balance), the inclination of the glacier (greater value with less inclination), the size of the glacier (lower value for large glaciers), friction from the surrounding rocks and flow ability of the glacier (Bahr et al., 1997). The theoretical value of $\gamma$ (1.375) is calculated from average values from glaciers in balance with the local climate and for a glacier in steady state, *c* would have a value of 1 (Bahr et al., 1997). The values derived from Bahr et al. (1997) are also supported by empirical data from Chen and Ohmura (1990) who collected the volume of over 60 glaciers by radar and averaged the results into values between 0.12-0.22 $m^{3-2\gamma}$ for *c* and between 1.15-1.52 for $\gamma$ (Yde et al., 2014).

The volume-area scaling method is because of $\gamma$ and $c$, dependent on the characteristics of each individual glacier and its balance with the local climate. Example approximate values used for $\gamma$ and $c$ of non-steady state valley glaciers are 1.36 and 0.033 $km^{3-2y}$ respectively (Bahr, 2011). As the $\gamma$ component is dependent on each glaciers individual characteristics, the individual glaciers will have a large variety of $\gamma$ values different from those found by theoretical or empirical methods (Bahr et al., 1997). Small variations in the scaling parameters can produce large differences in volume estimations and since most glaciers are in non-balance with the contemporary local climate, the uncertainty of the method can vary a lot (Yde, 2014). Though, the uncertainty will be lower for glaciers close to the average within a group of glaciers with similar characteristics.

# 4 Method

## *4.1 Data collection*

The data collection at Longyearbreen and Tellbreen was conducted during 5 succeeding days in April 2016. The choice of time period originate from practical reasons as the continuous snow cover over the glaciers simplifies the actual data collection as it covers the rough glacier surface and allows for towing of the GPR with snowmobile. The weather in April is also often milder and the data collection can continue long hours every day thanks to the midnight sun which arrives at this time. The data will also give some better penetration depth when collected in cold ice and dry snow cover since electromagnetic waves attenuate more rapidly upon contact with water pockets in the ice during the ablation season (Plewels and Hubbard, 2001).

The Malå Professional explorer (ProEx) was used mounted in a backpack with 100 MHz and 50 MHz rough terrain antennas (RTA) together with a Malå XV Monitor. This normally allows the researcher to control the results continuously during the data collection by its easy manageable monitor carried within the field of view of the handler (Malå, 2017). Although, during the data collection the monitor was fastened on a plastic sledge behind the snowmobile together with the control unit to increase the distance to the equipment and therefore minimize the noise effect from the snowmobile. Figure 22 shows a picture of the setup during the data collection. The control unit was mounted in the front of the sledge. The global positioning system (GPS) was connected to the monitor and fastened in the back of the sledge under the orange tarp which protected the screen from being covered with snow. The RTA was fastened behind the sledge, straightened up before every new profile and then dragged along in the snowmobile track.

The RTAs used are long flexible snake-like (one-piece) antennas where the transmitting and receiving antennas lay in-line respectively first and last in fixed distances (Figure 22). They’re easily maneuvered in rough terrain and lightweight (6-7 kg). The distance between the transmitter and the receiver depends on the frequency of the antenna. The separation is 4.2 m for the 50 MHz antenna and only 2.2 m for the 100 MHz antenna.

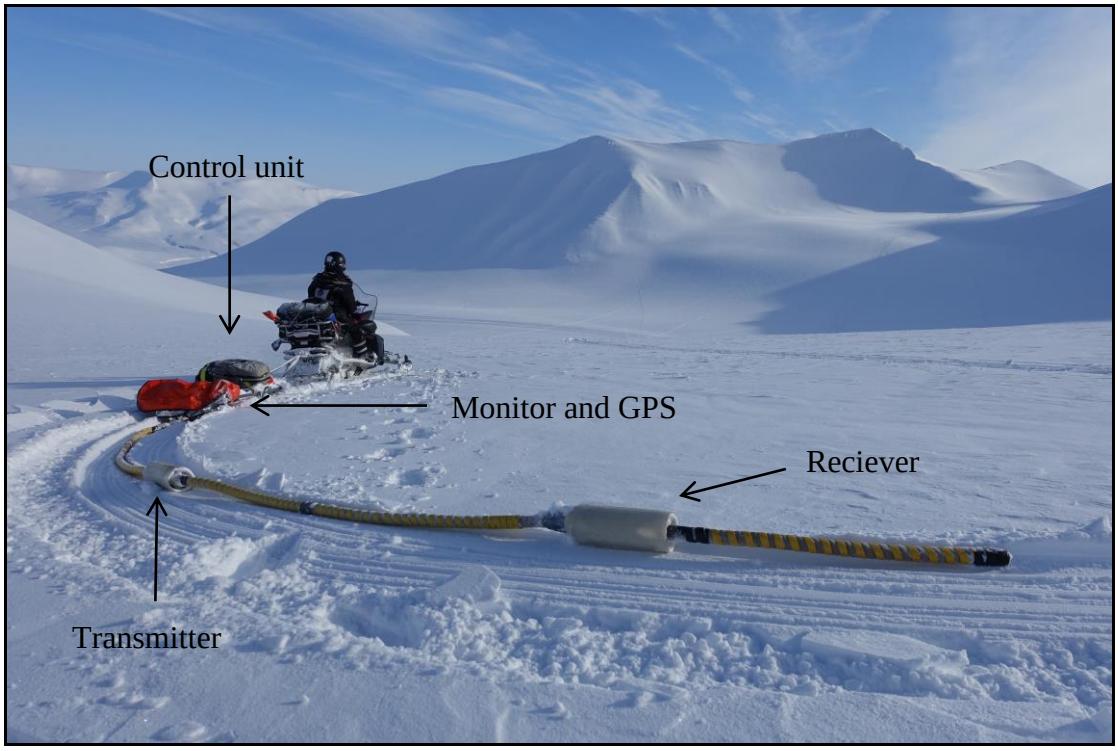


**Figure 22 - Data acquisition on Tellbreen with the shorter 100 MHz RTA. The setup was straightened up after each profile and then dragged along in the close to straight snowmobile track.**

Data collection with GPR should follow a constant speed forward and as lower frequencies need longer separation due to deeper penetration (longer two-way-travel times of the EM waves) the distance has to be larger between the transmitter and receiver. All the specifications about the antennas are listed in Table 3.

The point of measurement is located in the middle between the transmitter and the receiver whereas the connected GPS unit is fixed close to the control unit causing a slight offset in the positioning of the individual measurements. This offset is 5-7 m, however considered acceptable as the accuracy for the GPS itself is ±4 m (MALÅ, 2017b). All the start and end points to every profile were also measured with a handhold GPS for backup. This GPS was also used to follow the lines from the 2004 survey as close as possible. Naturally, it was hard to repeat the lines in some places as the glacier has changed its geometry the last decade. The 2016 fieldwork was also aimed to collect a more dense distribution of profiles as a more detailed survey of the glacier was desired. The separations between the profiles from 2004 and from 2016 are up to 80 m in some areas, while completely parallel in other.

**Table 3 – Specifications of the antennas used during the 2016 fieldwork (Malå, 2017b). The 500 MHz antenna was used as a snow radar (data not included in this thesis) and is showed as a comparison to the other two antennas.**

| Antenna | 50 MHz | 100 MHz | 500 MHz |
|---|---|---|---|
| **Name** | Malå RTA | Malå RTA | Malå SA |
| **Modell** | Cable | Cable | Single housing |
| **Type** | Rough terrain | Rough terrain | Shielded |
| **Size** | 9.25 m | 6.56 m | 50 x 30 x 16 cm |
| **Weight (kg) incl. batteries** | 7.0 kg | 6.0 kg | 5.9 kg |
| **Separation (D: Tx-Rx)** | 4 m | 2 m | 0 |
| **Resolution** | Ok | Good | Great |
| **Length between measurements point and GPS** | 2 m + | 1 m + | <1 m |
| **Penetration (Depth)** | Deep-medium | Medium | Shallow-medium |

The control unit administers the data collection and is designed for outdoor usage. It is easily carried by one person in a backpack and is assembled with batteries and an antenna through optical fibres. The control unit communicates with the RTAs through the optical cables that are favourable for this equipment since they do not interfere with the radar waves. All measuring settings could easily be set out in the field with the monitor with some pre-calculated values. When the antenna choice is set some settings are suggested by default, but others are not.

The sampling frequencies used were 509 MHz for the 50 MHz antenna and 1018 MHz for the 100 MHz antenna. Since the data was collected with a snow mobile, a reasonable speed had to be held to be able to drive it forward (~10 km $h^{-1}$) and appropriate time intervals was calculated according to the speed to be every 0.08 s and 0.1 s for the 100 MHz and 50 MHz antennas respectively. The sampling frequency was set to be ~10 × antenna frequency, i.e. 1000 MHz (100 MHz antenna) and 500 MHz (50 MHz antenna). The signals are recorded in to traces (a collection of stacks) from one point. Stacks are the number of averages stored for each trace to eliminate background noise and was set to 4 in our case, which is appropriate considering the speed. The velocity was set to 0.168 m $ns^{-1}$ (see section 3.2) and the time window was set to 1769.4ns and 1895.1 for the 100 MHz and 50 MHz antennas

respectively. This corresponds to between 150-170 m of ice and is well within the anticipated ice depths on both glaciers.

### *4.1.1 Snow radar*

The snow layer on a glacier will have an effect on the GPR profiles since the velocity of snow and ice is different from each other (0.21 m $ns^{-1}$ and 0.168 m $ns^{-1}$ respectively) (Ødegård et al., 1997; Plewels and Hubbard, 2001; Navarro et al., 2005). The best results would therefore be achieved by summing up the amount of snow on each glacier with the right velocity to then subtract from the measured ice thickness. The field work was therefore carried out with a 500 MHz antenna (so-called snow radar). These data profiles (46 profiles) were not used in this thesis, other than to confirm to snow depths (see section 6.1.2) of the GPR profiles, to limit the scope of the data processing and thesis. Though, the data did show good results and can be used in later work. The actual snow depth distributed over a glacier can vary by orographic effects every winter. One snow pit was dug on Longyearbreen (Figure 23) directly under a cross profile to measure the actual depth of the snow cover and compare it to the GPR data (see section 6.1.3). The measured snow depth in the snow pit was 0.9 m.

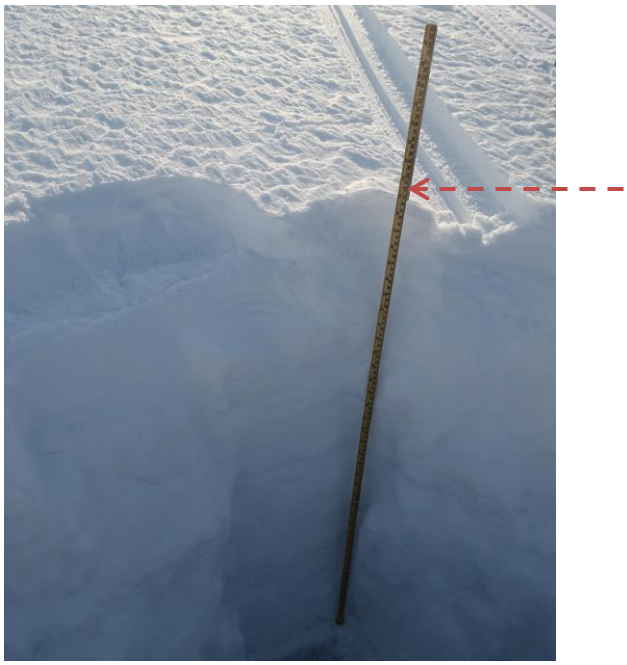

**Figure 23 – Snow pit shows a snow depth of ~0.9 m just above the terminal moraine on Longyearbreen. Red dotted line indicates the 1 m level.**

### *4.1.2 Survey profiles*

All profiles of the 2004 and 2016 surveys are shown in Figure 24 and Figure 25.The zigzag track with cross profiles was collected starting from east/northeast and ending up towards the south/southwest (with rising numbers/letters). The longitudinal profiles were collected the other way around, from west/southwest, on the return.

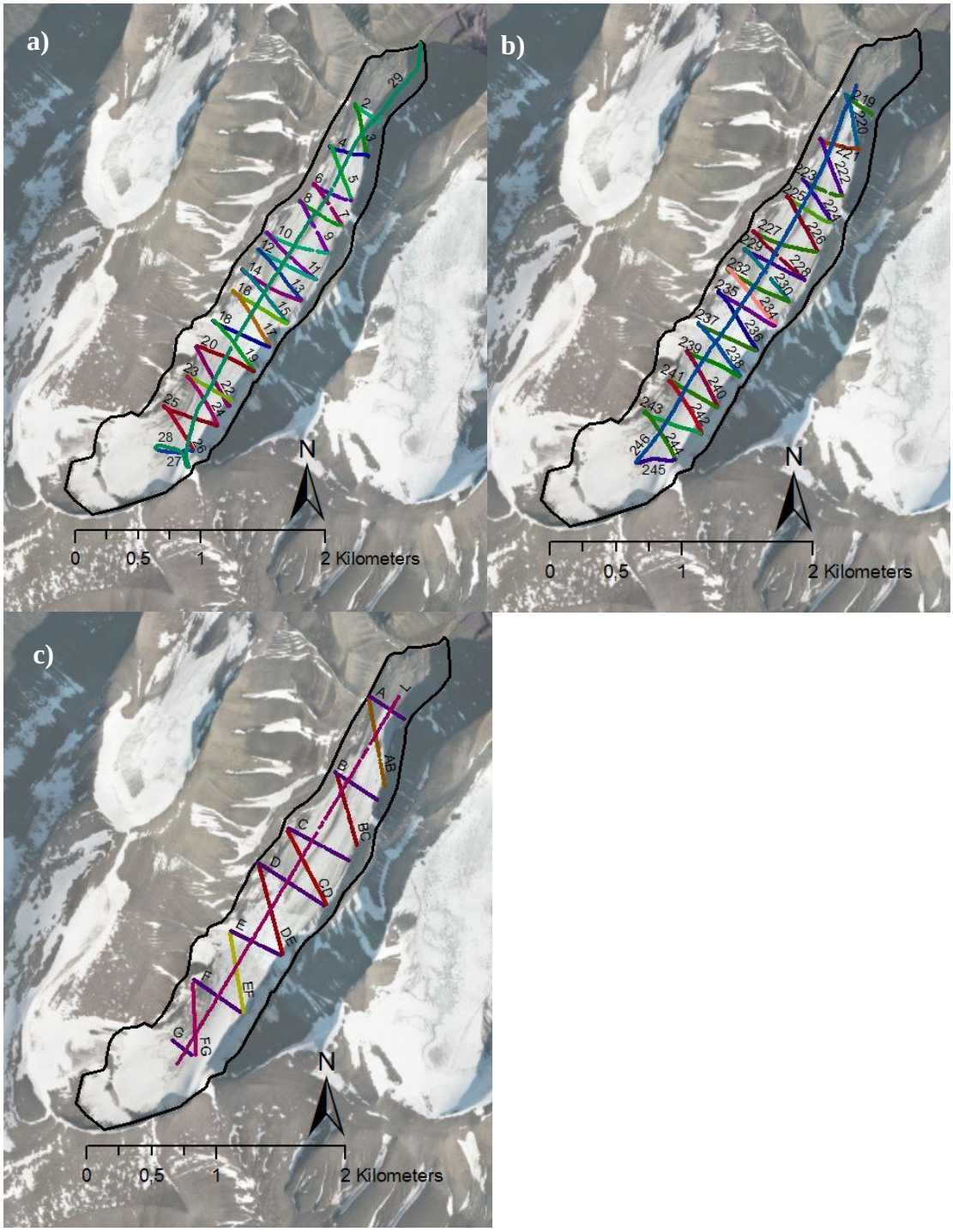


**Figure 24 – a) All 50 MHz profiles on LYB 2016, b) all 100 MHz profiles on LYB 2016 and c) all 100 MHz profiles on LYB 2004.**

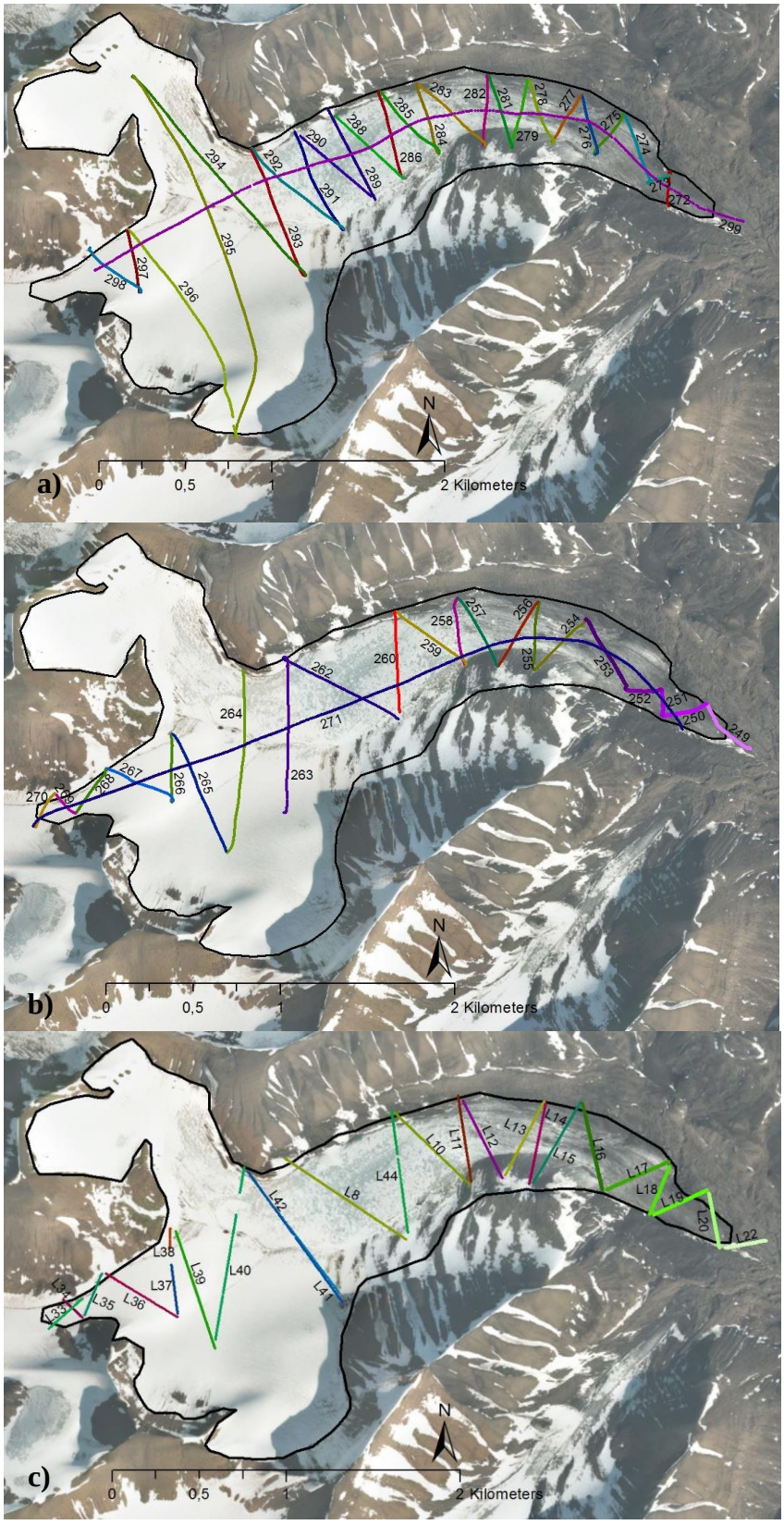


**Figure 25 – a) All 50 MHz profiles on TB 2016, b) all 100 MHz profiles on TB 2016 and c) all 100 MHz profiles on TB 2004. Uninterpretable data left as "holes" in profile picks can be seen as gaps in the profiles to the west.**

## *4.2 Data processing*

RadExplorer version 1.42 (2004-2008), which is an associated software to the Malå GeoScience equipment, was used to process the collected data from 2016 as well as the data collected in 2004. The different processing routines in the software are listed in a specific order which normally is the best to follow. Although where better results was achieved in another order this was preferred. The cross profiles in this thesis where all processed with the same 5(6) steps in the subsequent order; geometry definition (not used on all profiles), time adjustment, spacial interpolation, bandpass filtering, amplitude correction and Stolt F-K migration (Figure 26-Figure 28). The longitudinal profiles were processed with all except for migration since it does not have the same effect to longitudinal profiles along the valley where there is not steeply sloping bedrock topography underneath.

### *4.2.1. Geometry definition*

The data collected with the Malå science equipment during the 2016 fieldwork continuously logs all GPS points automatically through the connected GPS. These profiles do therefore already contain geometric information and doesn't need manual definition. In some cases though, the GPS was disrupted during the data acquisition and the start and end points had to be added manually from the first to last trace recorded. This was also the case with the 2004 data from both Longyearbreen and Tellbreen since they only had GPS coordinates registered with a handhold GPS at every start and end point. This makes it even more important to collect data with constant speed to not distort the data during processing (see section 4.5).

### *4.2.2 Time-Adjustment*

The time-zero adjustment configures the correct zero-point of the vertical time scale to the actual moment when the wave left the transmitter antenna (Figure 26) (MALÅ, 2005). There are also options to define the spacing between the two antennas, to eliminate any time delay due to the horizontal distance, and to define the medium velocity. The spacing was set to 2 and 4 m for the 100 MHz and 50 MHz antenna respectively.

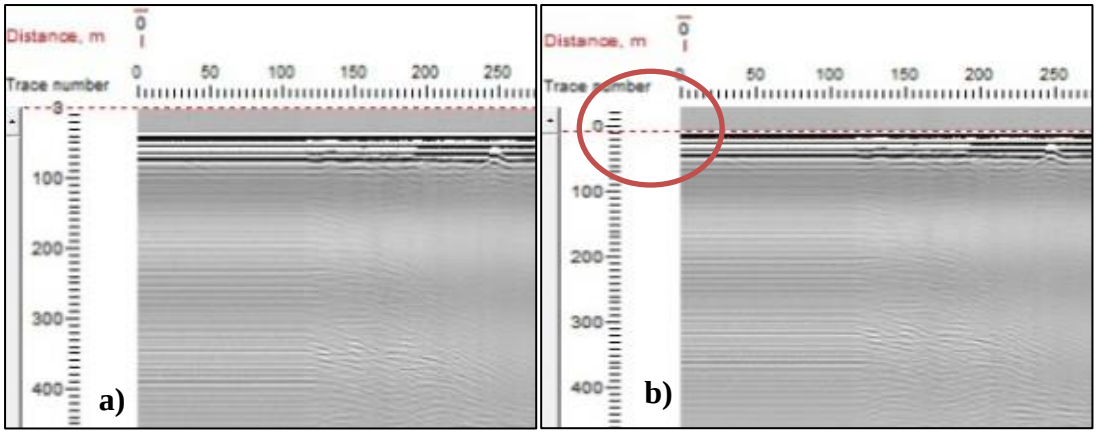


**Figure 26 – Time-adjustment of example profile. The red dotted line indicates the 0 ns level. a) Profile without time-zero adjustment and b) profile with time-zero adjustment where 0 ns is adjusted to the correct position when the first EM wave is registered.**

### *4.2.3 Spacial interpolation*

Due to small variations in travel speed of the snow scooter, traces are located at different spacings along the survey lines. The spatial interpolation filter creates a radargram where traces are equally spaced, which is a requisite for the migration routine (explained in section for migration). In other words it uses the average of a set of known points surrounding an unknown point to predict what the unknown value should be. Therefore creating a continuous data set by recalculation of the traces in the horizontal plane (Figure 27). The function extracts improper data, such as standstill data in the beginning and end of the profiles, and predicts applicable values by a specified interval using the attached GPS coordinates to separate profiles. When using this tool a calculated default value is suggested for each separate profile. In this master thesis the value was set to 0.2 at every profile to process them as similar as possible and make them more comparable.

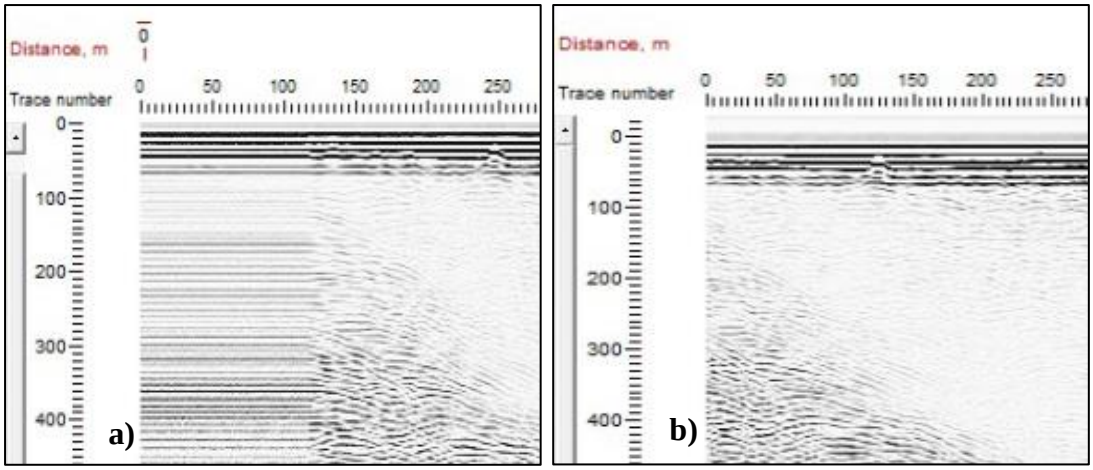


**Figure 27 – a) Horizontal stripes effect from stand still data collection at start and stop of every profile. b) Spacial interpolation removes incorrect data by eliminating monotonous data.**

### *4.2.4 Bandpass filtering*

Bandpass filtering increases the signal to noise ratio in the frequency domain between specified values by attenuating unwanted noise outside a desired frequency range (Figure 28b). All profiles were filtered with default settings and the best results were obtained when this routine was performed before amplitude correction. The values used for low/high cut and low/high pass varied for all profiles.

### *4.2.5 Amplitude correction*

Amplitude correction is a gain control routine (Figure 28c) where the EM signal is

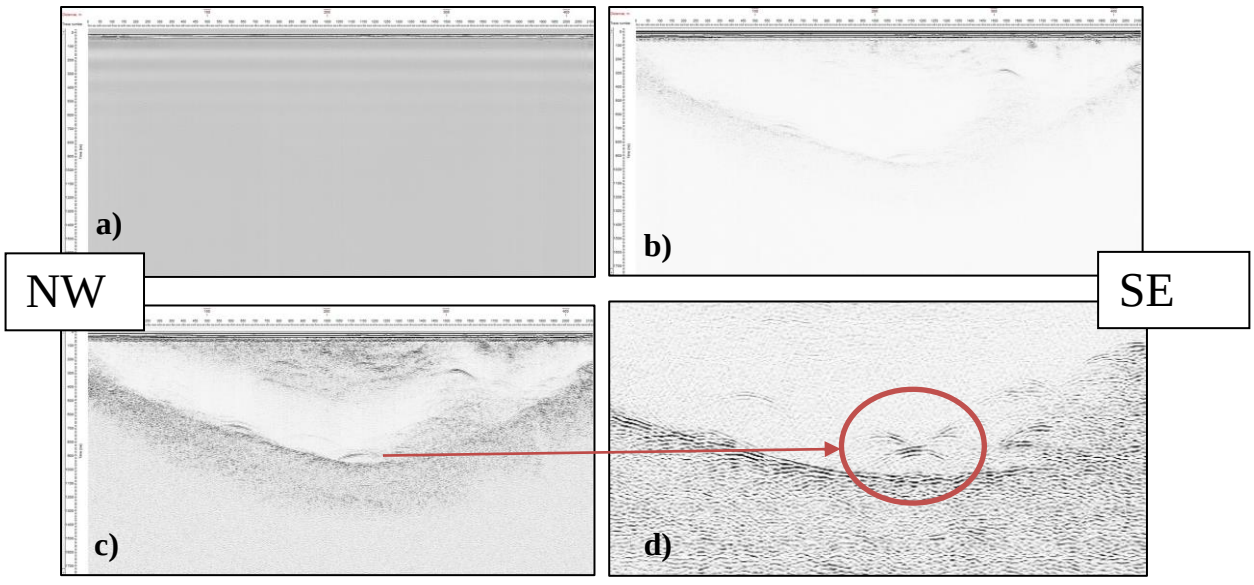


**Figure 28 – a) An unprocessed profile with few interpretable structures, b) profile with Bandpass filtering eliminating background noise outside the desired frequency range, c) profile with Amplitude correction which increases the gain with depth in the profile, making the deeper reflections more visible and d) Migration of profiles restores the point reflections to their true shape (collapsing hyperbolas etc.).**

strengthened with increased time (depth). This routine is important for GPR measurements since the EM energy used attenuates rapidly with depth through scattering, damping and spreading (Annan, 1992). Shallower reflectors are therefore stronger (higher amplitude) than deeper reflectors without gain correction. It is often necessary to use this routine and amplify the return signal, especially in glacial surveys since the basal reflector often is the most important one, even though the relative amplitude strength between the reflections will be lost.

There are multiple different methods for amplitude correction but our data has only been adjusted with automatic gain control (AGC) with default values for each individual profile since this gave the best results. The AGC works by equalizing the amplitudes along each vertical trace, within a specified time window, by multiplying with the inverse amplitude value at every point.

### *4.2.6 Migration*

The GPR always assume that the reflecting signal is derived from a reflector or change in EM properties directly below the antennas. But since EM waves travel outwards in all directions they will also record false structures or incorrect positions of for example dipping reflectors, faults, syncline formations ("bow-ties"), debris, melt-water channels etc. (see section 5.1.1). The signal reflects off such points in different directions and will be recorded as false dip angles or diffraction hyperbolas (upside down smiley) as the antennas move towards and past it. Migration is a processing routine which restores reflections to their real source within the radar image by repositioning the reflected energy to their true geometrical location (Figure 28d) (Annan, 1992). Rad Explorer uses the Stolt-FK migration algorithm which operates in the frequency-wave domain. It is fast, but does not take vertically varying wave velocity propagation into consideration. This entails a limitation to the migration as imprecise velocity values tend to over- or under migrate the data easily; creating smiley effects or not collapse the hyperbola effects completely. One way to determine the appropriate migration velocity is to compare the diffraction hyperbolas in the profiles with the "Hyperbola" tool. Since the distance travelled is known and the steepness of the hyperbola sides indicates the velocity of the material the "hyperbola" tool should be adjusted to fit the entire form in the best way possible. In

our case the best matched hyperbolas indicated a velocity of 0.168 m $ns^{-1}$ which was then used to migrate all the profiles.

## *4.3 Picks*

When all above mentioned processing steps had been implemented the basal reflection of the profiles were handpicked, making horizon correlation lines (Figure 29a). The picks were positioned after the best ability along the strongest and most continuous reflector. The basal reflector was distinguishable in the majority of the profiles and mostly good enough to follow. However, there where areas in a few profiles with weak basal reflections or lateral parts hard to distinguish. In a few cases the segment with too weak reflection was left un-interpreted as a "jump" in the horizon picks (Figure 29b). In other examples the neighbouring profiles were sometimes used as help to see at which height their basal reflector was positioned and thereby deduce the real extent of the one in progress. As the most probable reflection had been chosen the picks were exported into text files with XY coordinates, trace number, TWT and Depth which is readable in ArcMap (Figure 30).

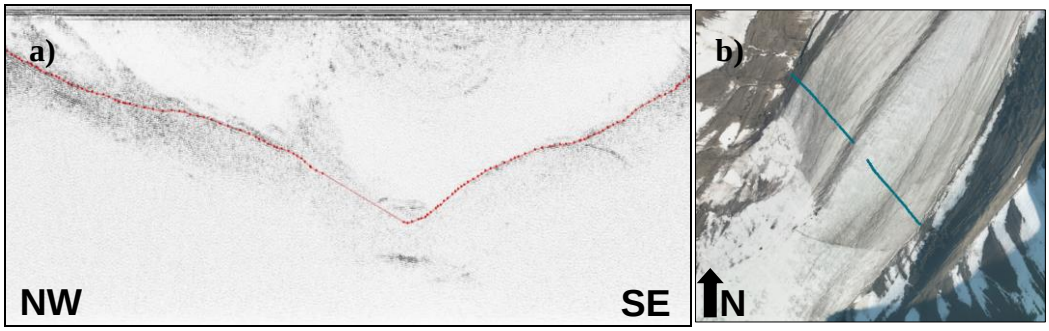


**Figure 29 – a) Picks of basal reflector shown as red dots connected with a red line. b)"Jump" in distinguishable basal reflection shown as a simple red line without dots in the horizon pick to the left and as a gap in the profile line. Profile nr 230 shown as an example (100 MHz at Longyearbreen).**

| X | Y | LAT | LON | TRNR | TWT | Z |
|---|---|---|---|---|---|---|
| 8678502.9 | 511183.53 | 78.180008 | 15.489080 | 2 | 234.49122 | 19.666523 |
| 8678501.2 | 511186.63 | 78.179993 | 15.489215 | 21 | 242.34668 | 20.327381 |
| 8678498.6 | 511189.03 | 78.179969 | 15.489319 | 39 | 259.03952 | 21.731499 |
| 8678496.6 | 511191.08 | 78.179951 | 15.489408 | 53 | 270.82272 | 22.722498 |
| 8678494.6 | 511193.34 | 78.179933 | 15.489506 | 68 | 283.58783 | 23.795967 |
| 8678493.2 | 511195.03 | 78.179920 | 15.489579 | 79 | 293.40716 | 24.621643 |
| … | … | … | … | … | … | … |
| … | … | … | … | … | … | … |
| … | .. | .. | .. | .. | .. | .. |

**Figure 30 – Example of exported profile picks. The UTM coordinates (X and Y) and depth data (Z) was used to plot the profiles in ArcMap.**

There were strong basal reflections on both the 50 MHz and 100 MHz data sets. But since the 100 MHz data set held the same depth quality as the lower frequency data set and also had the best vertical resolution, this data set was preferred during further data interpolation. Cross-over points between different cross profiles and the associated longitudinal profile were used to compare the depth of the reflectors of different profiles (see section 5.1). The points were checked for large differences in depth. Most cross-points from the 2016 data sets showed a difference between 0-5 m (Table 5) and a total average difference of < 0.2 m which is well within the acceptable level of uncertainty.

#### *4.3.1 2D model*

All profiles from one and one data set were combined in excel creating documents containing XY coordinates, trace number, two-way-travel time and depth (Z). The text files were used to make 2D depth profiles of the individual lines by converting coordinates to distances between every start and end position and plot them against depth in a XY display (see section 5.1).

## *4.4 Interpolation and modelling in ArcMap*

All the profiles were imported in to Arcmap to visualize the results of the GPR profiles. Since most of the profiles collected ends within the outer limits of the glacial body, only few zero depth values were registered. This would give false depth data at interpolation, which is why the glacier outline was plotted by hand around both Longyearbreen and Tellbreen from the latest WMTS service orthophoto by the Norwegian Polar Institute from 2009 (Norwegian Polar Institute, 2017a). The outline was then converted into points and added with XY coordinates and depth equal to zero before joined with the rest of the profiles into one set of data (100 MHz or 50 MHz) of one glacier to create an outer boundary for the data. The longitudinal profiles from both 2004 and 2016 were left out of the interpolations. There were a few cross sections between longitudinal profiles and cross profiles of the 2016 data set that where not comparable in depth, causing problems with the interpolation and was therefore excluded. The 2004 profile was left out due to low quality of the profiles caused by the malfunctioning odometer wheel (see section 4.6).

The interpolation was done using a spatial geostatistical analyst tool. The radial basis function used is well suited for data sets such as these ones with a large number of points with small changes in depth within short distances. The resolution of the interpolations is 5 x 5 m.

### *4.4.1 Interpolation models*

The different sets of data imported in to ArcMap were each interpolated with the radial basis function to create surfaces between the existing points making a geo-statistical layer (see section 5.2). This is an essential routine for visualization of the data since the GPR measurements does not cover the entire glacier. The radial basis function is an interpolation technique where the created surface must pass by every measured sample value which creates an exact and smooth surface (ESRI, 2016). The interpolation was made through an oval search window divided in to 4 sectors with 45˚ offset compared to the longitudinal axis of the glaciers (Figure 31). By doing this the interpolation prefers the neighbouring data points in the longitudinal direction and

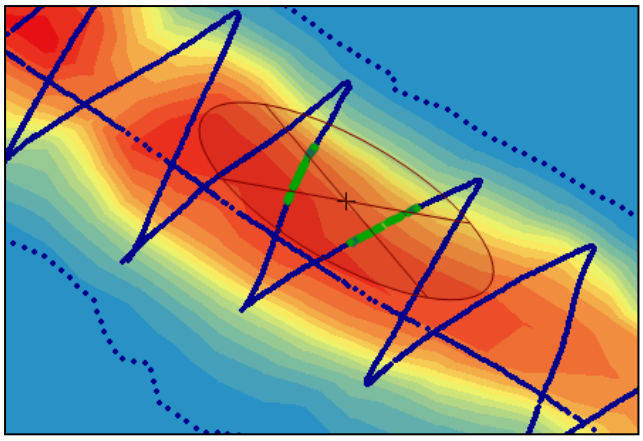

**Figure 31 – Example of search sector with 45˚ offset angle to the longitudinal direction.**

creates a more realistic model since this the depths values are more similar along the glacier rather than across the glacier due to the V-shaped bottom relief. The area of the glacier was divided in to 5 x 5 m cells where every cell was assigned an averaged value of interpolation. The data was then exported to a raster file, added contour lines and compared with each other.

Subglacial topography models were made of both Longyearbreen and Tellbreen by subtracting the interpolated ice thickness model from the digital elevation model (DEM) (Norwegian Polar Institute, 2017a).

## *4.5 Source of error*

There are a variety of uncertainties concerning GPR data, some more and some less important. The fieldwork for this thesis was carried out with 50, 100 and 500 MHz antennas. The 500 MHz (shielded) antenna data, not included in this thesis (see section 4.1.1), provided very detailed and shallow (few meters) profiles. If included, the snow radar data could have given more precise volume estimates of the 2016 data set as thorough snow levels could be mapped over the two glaciers and subtracted from the estimated volume data. However, since the data from 2004 did not include snow data, comparison between the two data sets will still be more comparable without snow data in both.

A usual source of error is the uncertainties connected to the GPS on high latitude locations such as Svalbard. Most geostationary satellites are just visible at low angles or not visible at all, giving the positioning system a higher inclination angle. The uncertainty is between 5-9 m in the horizontal plane and as much as 9-15 m in the altitude level (Bælum, 2010). Poor altitude accuracy will in turn affect the quality of the GPR survey. GPS points during the 2004 data collection were in addition collected with a handhold GPS not connected to the GPR, only giving GPS coordinates at start and end point of every profile. The GPS was primarily used as a backup as the real length of the profiles were supposed to be measured with a connected odometer wheel. Although as it proved unstable, the GPS lines were assigned with the GPS points only. This means that the data collection should be conducted in a completely constant velocity to avoid distortion of the data during processing. Such stable velocity is hard to implement properly, resulting in a changing distance between measurement points.

The velocity of ice is assumed constant (in this case 0.168 m $ns^{-1}$) during GPR surveys even though it varies with inhomogeneous (warm/cold) ice, snow coverage (see section 4.1.1) and water content. This source of error is kept to a minimum due to

the limited to non-existent temperate ice on Longyearbreen and Tellbreen, as well as low water content during field work in winter time. The snow layer on top of the ice has higher velocity tan the ice itself. By assuming a snow velocity, a maximum error ice depth can be calculated (see section 6.1.3).

One of the major uncertainties lies in the human factor as to how all the data is collected, processed and interpreted. The profiles from both data sets (2004 and 2016) do not overlap completely, which of course would give the best comparisons, and the 2004 profiles were interpreted by others at first. All the profiles from 2004 have therefore been processed once again in the same way as the 2016 data to remove the source of error due to different personal interpretations. The manually picked basal reflector will thanks to mostly strong and continuative reflections have low uncertainty. An estimate of maximum 4 m (~50 ns) depth error is within the acceptable levels as earlier GPR studies expect an overall uncertainty of 5-10 m (Björnsson et al., 1996; Tonning, 1996). The many different variables to the processing steps have also been kept to a minimum by using the same settings or default settings for all profiles. The difference in quality between the 2004 and 2016 data sets (100 MHz) was determined by comparison of as similar cross-profiles as possible (see section 6.1.1).

The last decade has changed the glacial geometry both by retraction of the ice masses and changes in the surface structure. Longyearbreen has not retreated much due to the debris covered terminal moraine whilst the first couple of profiles collected along the old tracks on Tellbreen did not have any ice at all. The glacier outline on Tellbreen for 2016 was therefore drawn along the 0 m ice depth data from the GPR sets since it has retreated since the last orthophoto found (2009). The difference in ice depth between the two years will also be affected of that the profiles of 2016 covered a larger area due to wider cross-profiles. This is most significant on Tellbreen where the 2016 GPR data covers larger parts of the two side cirques on the western part of the glacier compared to the 2004 survey. This will increase the apparent ice volume from 2016 and therefore underestimate the actual decrease in volume between the two data sets.

# 5 Results

The profiles collected in 2016 with the 50 MHz and 100 MHz antennas were of high quality and showed a strong distinguishable basal reflector. Excluding test profiles, there were in total 86 profiles collected: 50 on Longyearbreen and 36 on Tellbreen (Figure 24 and Figure 25). The 2004 surveys included 14 profiles on Longyearbreen and 24 profiles on Tellbreen. Altogether, 124 profiles have been processed. The amount of collected and processed profiles during this survey limits their presence in this section and all of them will for practical reasons not be presented in this thesis. Only some will be used as examples in the following chapters.

## *5.1 Interpretations of 2D profiles*

The ice velocity of all profiles on both glaciers was set to 0.168m $ns^{-1}$ (see section 4.2.6) which is appropriate for cold ice (Ødegård et al., 1997; Navarro et al., 2005). Since the 2004 profiles were previously interpreted with different velocities and settings, all profiles were interpreted over again in the same way as the 2016 data sets, resulting in profiles with clear basal reflections. All basal reflectors from cross profiles perpendicular (or close to perpendicular) to the length direction are combined in charts per data set and overturned so that all are shown in the same orientation in Figure 32 – Figure 35. The four figures illustrates how the valley shape of the two glaciers change along the glacier extent and how the cross sectional profile has changed during 12 years. The main shape of the profiles resemble between the two data sets on both glaciers but as all profiles start at 0 m, the width distribution can be seen to differ between the two data sets of both glaciers. This is somewhat deceptive since many of the 2016 profiles, especially on Tellbreen, were collected further out past the end of the 2004 profiles. The width of the glaciers has not grown since 2004. Both glaciers show tendencies of one steeper side and one side with lower inclination (see section 5.3). This is, unlike the ideal U-shaped form of a valley glacier relief, normal to small valley glaciers with low basal erosion (Benn and Evans, 2010; Etzenmüller, 2000). The dotted line indicates the maximum measured depth from the GPR survey at each data set, the red dot indicates the location of the deepest reflector and the legend to the right shows the name of the profiles. The deepest basal reflectors on the 2004 data sets (Figure 32 and Figure 35) align with the deepest

profiles from 2016 on both glaciers. The maximum depth has decreased with ~20 m at Longyearbreen and ~10 m at Tellbreen since 2004.

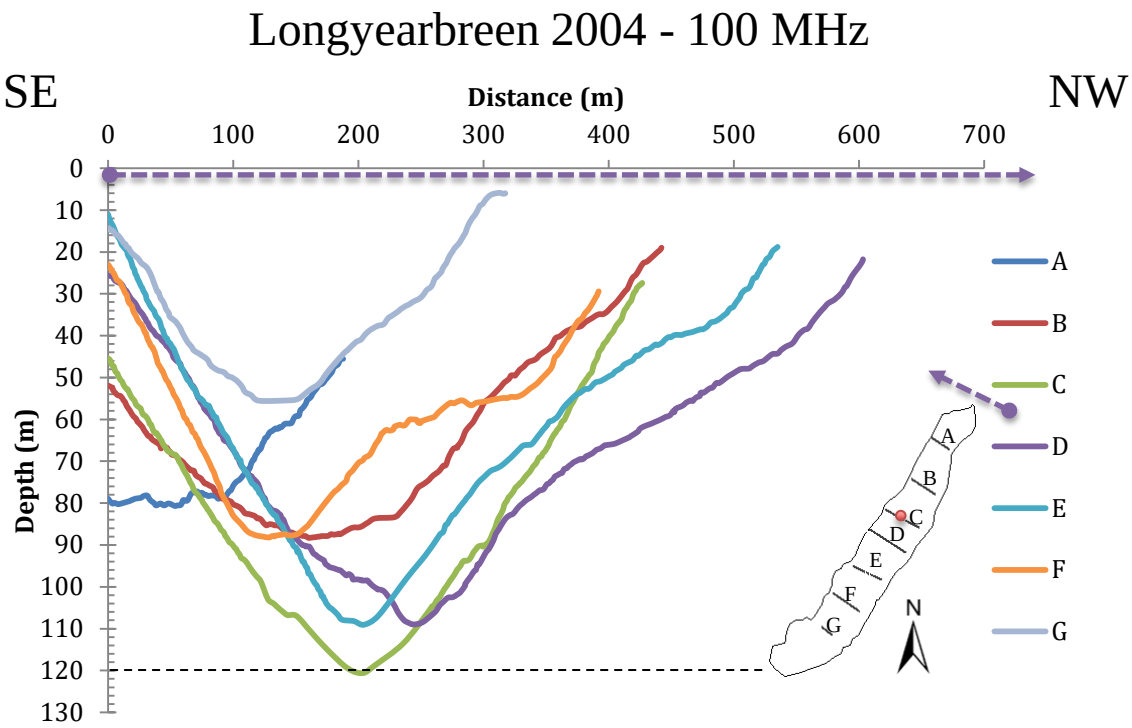


**Figure 32 – Profiles from Longyearbreen in 2004 with 100 MHz Antenna. The profiles are collected from southeast (0m) to northwest (indicated by the purple arrow). The maximum depth of ~120 m is registered in profile C (red dot).**

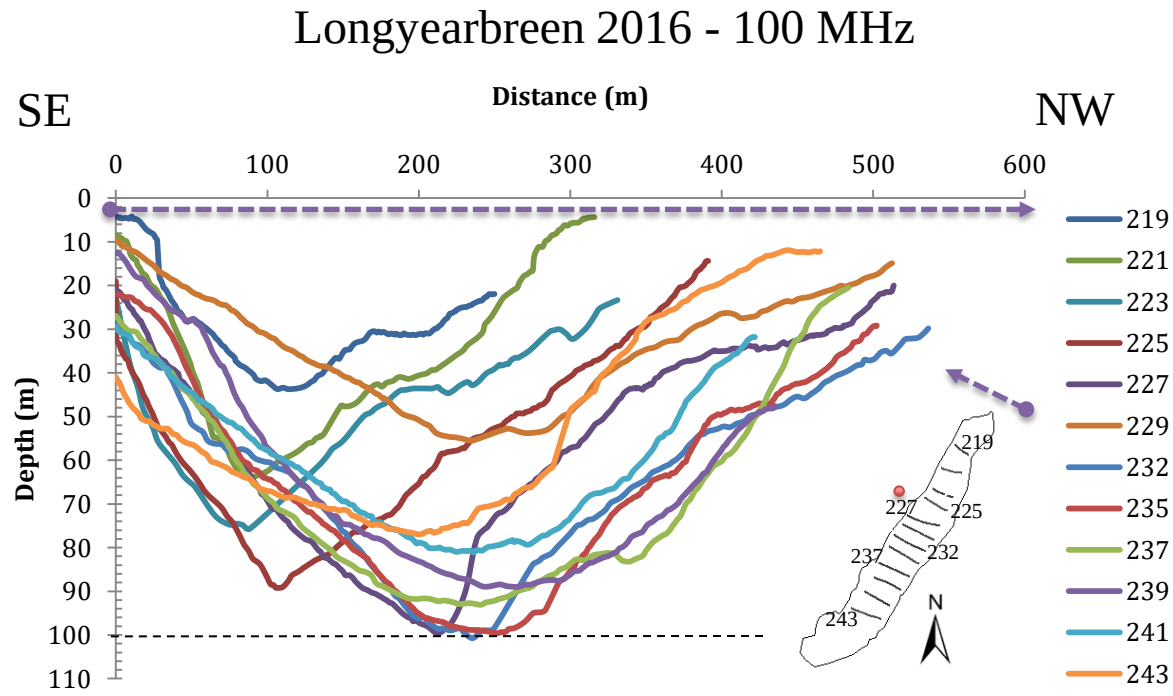


**Figure 33 - Profiles from Longyearbreen in 2016 with 100 MHz Antenna. The profiles are collected from southeast (0m) to northwest (indicated by the purple arrow). The maximum depth of ~100 m is registered near profiles 227 and 232, in the same area as the deepest profile in 2004 (C) (red dot).**

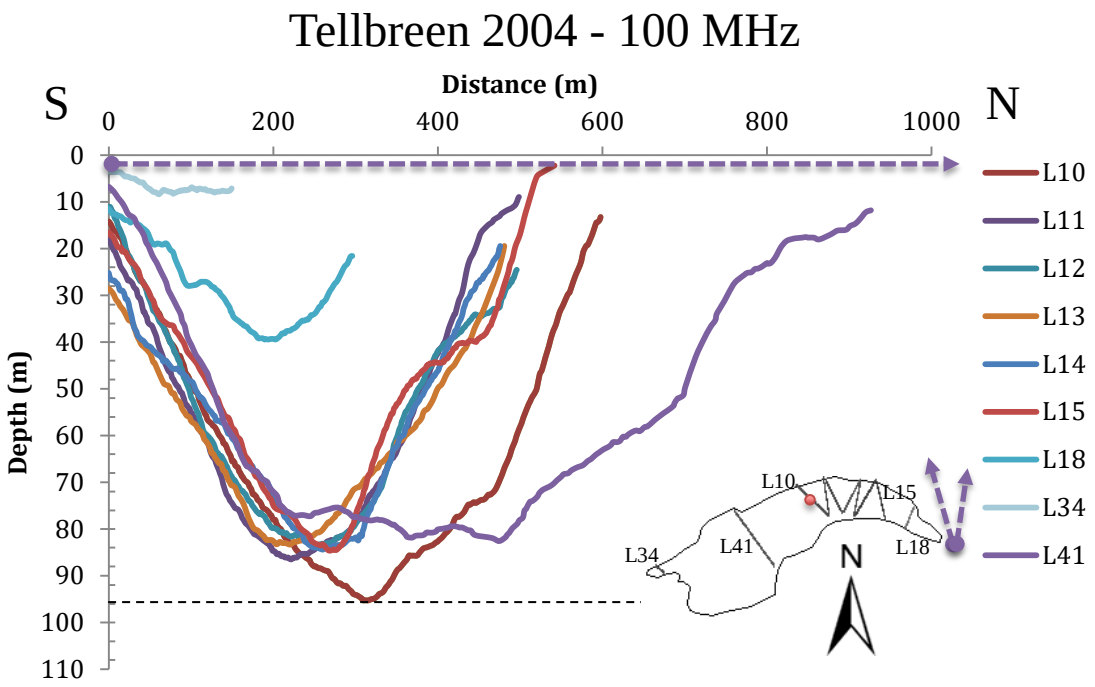


**Figure 34 - Profiles from Tellbreen in 2004 with 100 MHz Antenna. The profiles are collected from southeast (0m) to northwest (indicated by the purple arrow). The maximum depth of ~95 m is registered in profile L10 (red dot).**

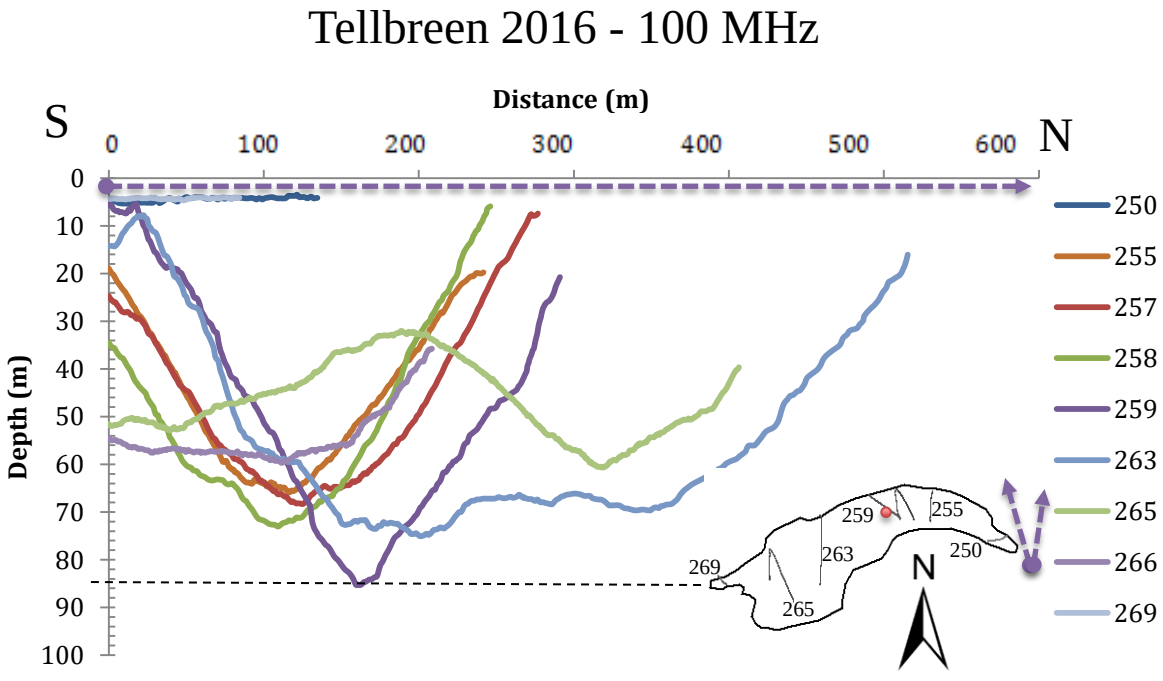


**Figure 35 - Profiles from Tellbreen in 2016 with 100 MHz Antenna. The profiles are collected from southeast (0m) to northwest (indicated by the purple arrow). The maximum depth of ~85 m was registered in profile 259, in the same area as the deepest profile in 2004 (L10) (red dot).**

### *5.1.1 Interpretation of structures*

The results from both the 100 MHz and the 50 MHz antenna generally showed strong basal reflections which were mostly easy to follow after some signal enhancing processing Typical GPR features such as multiples (Figure 36a) (repetitive reflections between strong reflectors) or scattering (noisy GPR signals) from warm ice was almost non-existent in the collected profiles. This is probably due to the cold season during field work with low water content and the lack of strong reflecting layers within the ice.

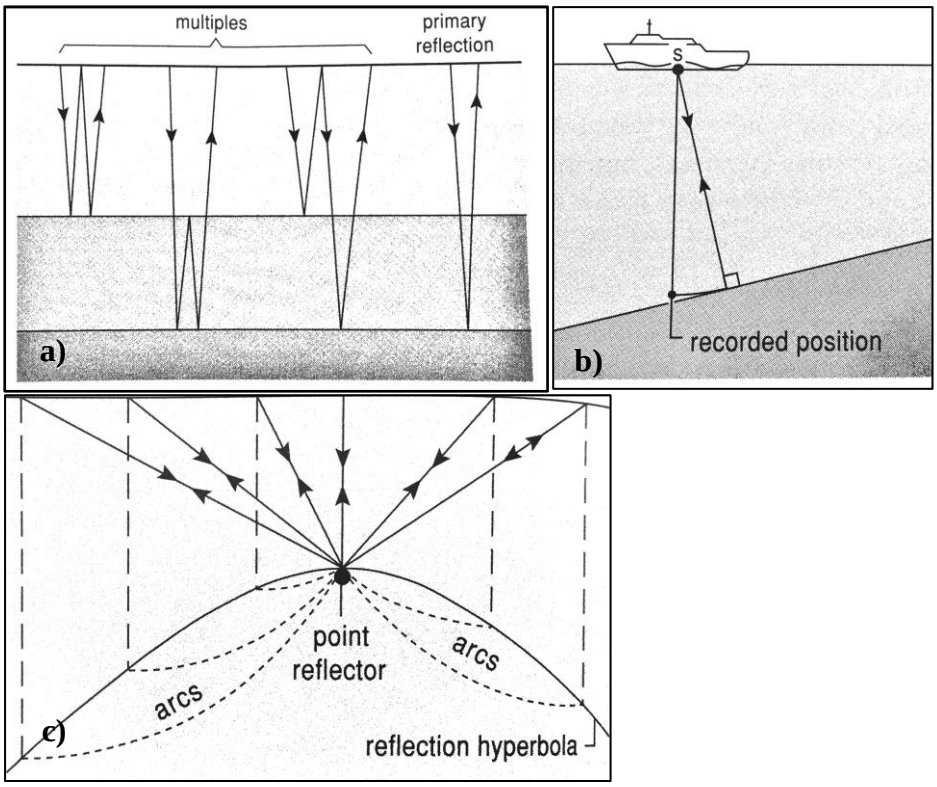


**Figure 36 – Schematic view of a) multiples, b) false dip and c) point reflectors resulting in a reflection hyperbola (Mussett and Khan, 2000)**

There were hyperbola structures in some profiles (Figure 36c) typically point reflections from the top of glacial tunnels, which were collapsed during migration of the profiles (see section 4.2.6). The reflection hyperbola is created when EM waves bounces of a point reflector. The only real measurement is the vertical one to the top of the hyperbola. The dip of the lateral parts of the basal reflections was also corrected to their real inclination by migration (Figure 36b).This is a flattening effect manufactured by the GPR since it always assumes that the reflected EM wave comes from a point straight beneath it (Mussett and Khan, 2000). In the few places where the

basal reflection was too weak to pick out, the neighboring profiles was first used as comparison. If they could not be used as guidance, a gap was left in the data set between the decipherable parts of the basal reflector (see section 4.3).

### *5.1.2 Longyearbreen*

All profiles of the 2016 survey show ice thickness, meaning that the glacier area reaches the same extent as in 2004 and has therefore not decreased noticeably since then. Figure 37 shows ice thicknesses along cross profiles perpendicular to ice flow on Longyearbreen in 2004 and 2016. The parallel profiles are aligned side by side for comparison, though the 2016 figure does not account for the distance to the glacier margin from first point of measurement. The bed reflector profiles are similar for the two surveys in all profiles, although weak basal reflections were obvious in the 2004 survey. The weak reflections has previously been thought to be caused by zones of temperate ice (Tonning, 1996), but was later interpreted as basal-rich ice (Riger-Kusk, 2006)

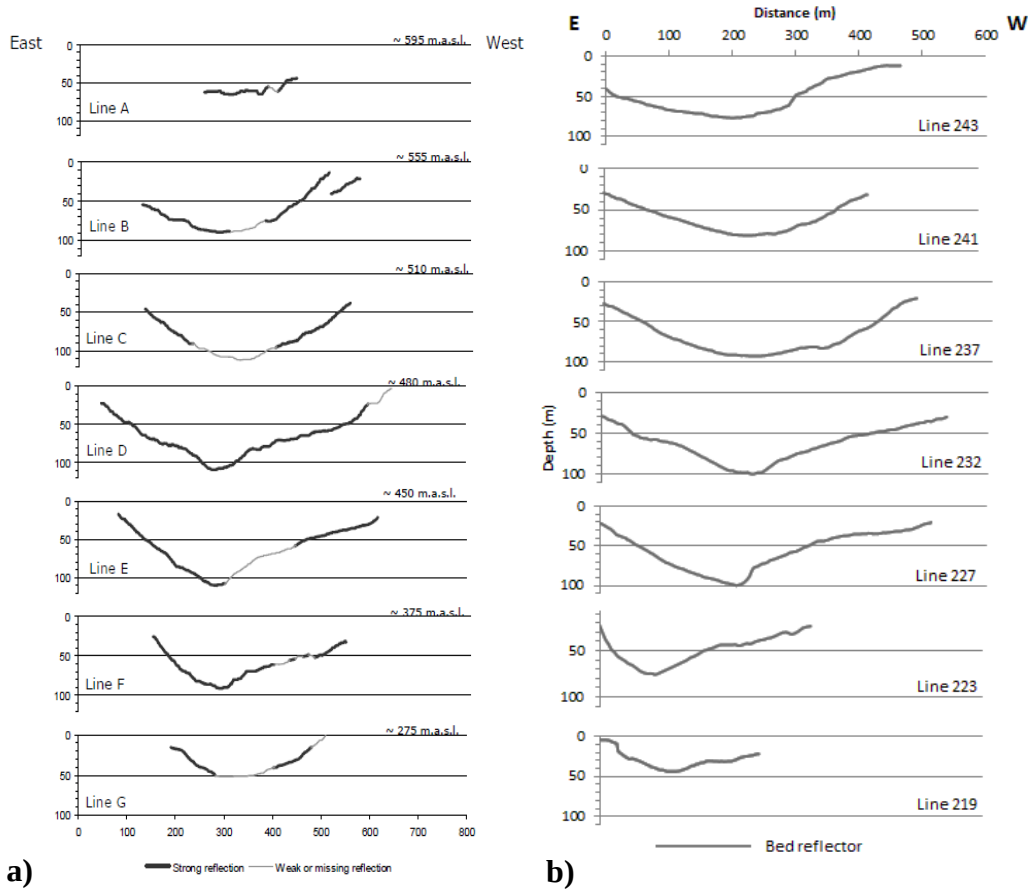


**Figure 37 – a) Ice thickness from the 2004 survey on Longyearbreen (Riger-Kusk, 2006) adjusted for lateral position compared with b) ice thickness from 2016. All profiles in the 2016 figure starts at distance 0 m. The contours of the bed reflectors are similar in all profiles. The depth of the reflector is however shallower in all 2016 profiles except for line A and 243 where the profiles are quite different from each other.**

The ice thicknesses have decreased between 2004 and 2016 for all profiles except line A and 243 where the depth seems to have increased. This is however likely to be an effect of different profile extents and slightly different profile locations in 2016. The decrease read from the figure is between 20-5 m. It is worth noting that Figure 37a was made by Riger-Kusk (2006) based on the processed profiles of the 2004 study. The reinterpretation of profile B from 2016, where the gap in picks can be seen in 2004, is shown in Figure 38. The area marked in red is interpreted as englacial structures as the same features can be seen in neighboring profiles and there still is a distinct reflector underneath it in all of them.

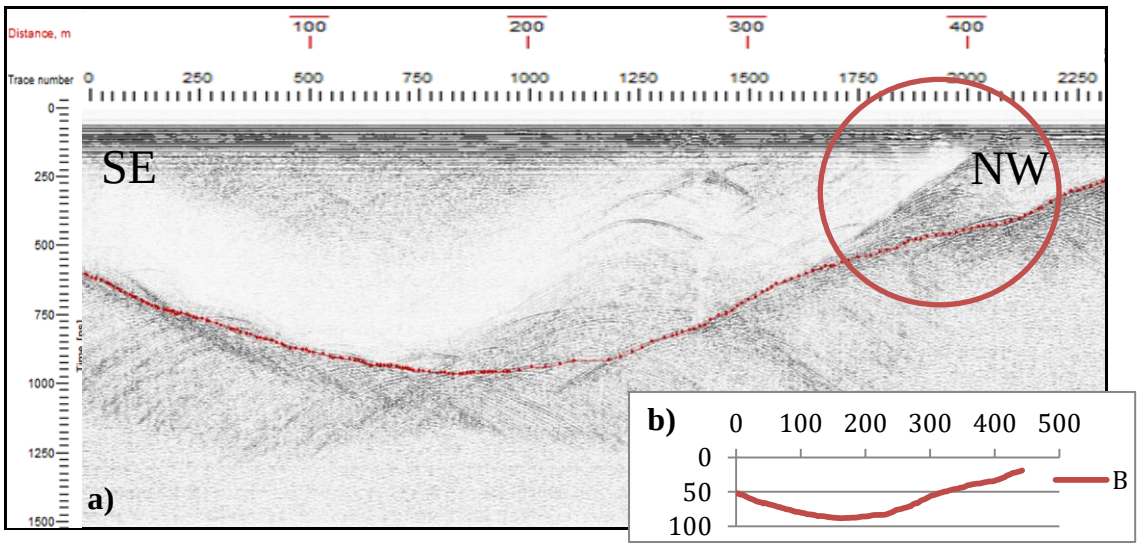


**Figure 38 – a) The 2016 reinterpretation of profile B from the 2004 survey on Longyearbreen shows that the basal reflector has been b) interpreted differently from the earlier interpretation (Figure 37a).**

Most profiles on Longyearbreen from 2016 have an easy distinguishable basal reflector. Profile 234 (Figure 39a) is a good example of a coherent basal reflector easy to pick out after processing. Figure 39b shows a good example of an air- and water filled englacial melt water tunnel lying on the western lateral side of the glacier, indicated with a blur arrow and dot. Before processing this feature looked like a large hyperbola in the profile. The top hyperbola shape stayed as the profile was migrated, though reduced in size, but the migration collapsed some of it and flat horizontal structures from the tunnel basal appeared (shown with an orange dotted line). This tunnel feature has a diameter of 22 m and can be followed through several of the neighbouring profiles towards the north and south. Profile 238 (Figure 40) shows an example of a large vertical feature on the northwestern side of Longyearbreen. The

feature looks like a crevasse which can be seen in neighboring profiles with varying distinctness as it seems be either being less developed or starting to close. The crevasse lies in the upper part of the glacier, marked with a red arrow and dot, on the same lateral side above the glacial tunnel seen in Figure 39b (profile 234). The profiles next to number 238 and 234 suggest that the feature is a continuation of the

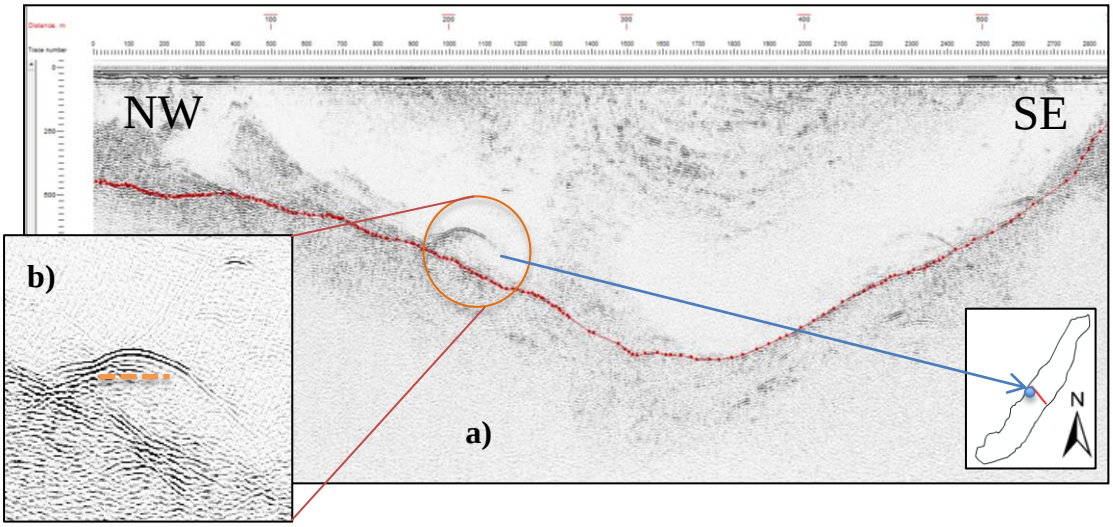


**Figure 39 – a) Profile 234 on Longyearbreen. The red dotted line shows the picked basal reflection. b) The enlargement shows an interpreted glacial tunnel (bottom of tunnel marked with orange dotted line). The blue arrow and dot indicates the location of the feature on Longyearbreen.**

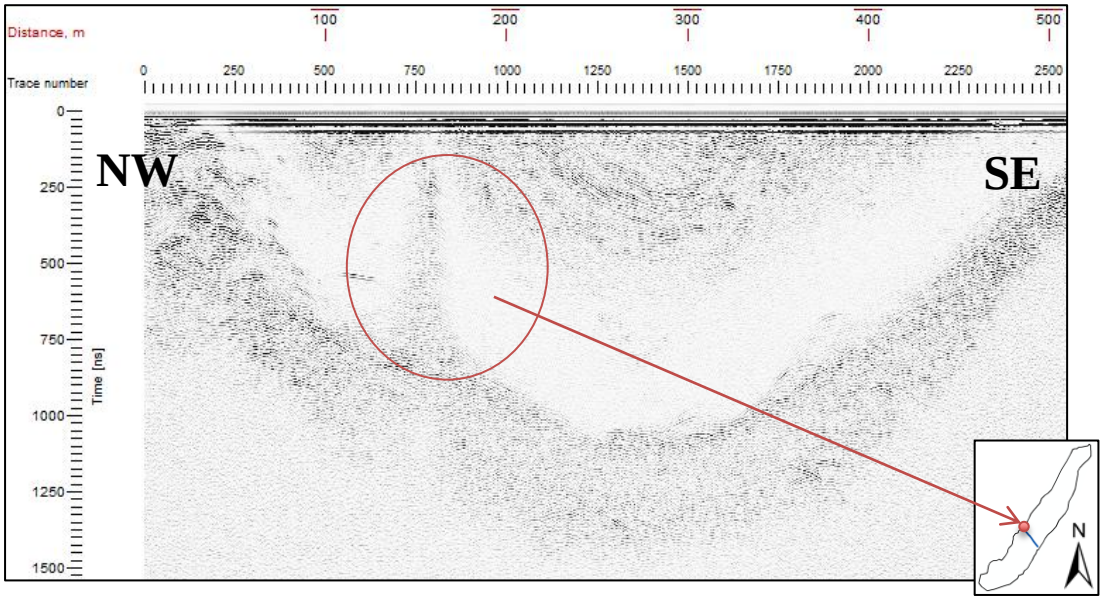


**Figure 40 – Large feature on the western lateral side of Longyearbreen. The red arrow and dot indicates the location of the feature on Longyearbreen.**

melt water tunnel as it can be seen in every profile in between. The crevasse feature could therefore be the remains after the supraglacial melt water stream that has eroded down into the ice to form the englacial melt water tunnel (Bælum, 2006). In the work by Bælum (2006), a large meandering (>10 m) melt water channel was mapped for 980 m in the same area though only a small upper portion of the channel was englacial in 2004 (Bælum, 2006). Figure 41 and Figure 42 are radargrams of parallelprofiles from the two surveys, 12 years apart. The red dotted line showing maximum ice thickness indicates that the ice thickness has decreased from ~120 m (TWT of 1400 ns) to ~100 m (TWT of 1200 ns). The profiles show the same synclinal bottom shape in both radargrams. The synclinal form produces "bow-tie" structures (Figure 41b) in both profiles which was satisfactorily removed during migration (see section 4.2.6), though can still be distinguished just below the red line in Figure 41. In the area directly below trace number 1000 in Figure 41a, there is a weak indication of a feature developing. Comparing it to Figure 42, the large anticlinal feature can appear to be the same object in a later stage. The differences in x-axis distances illustrate the problems with

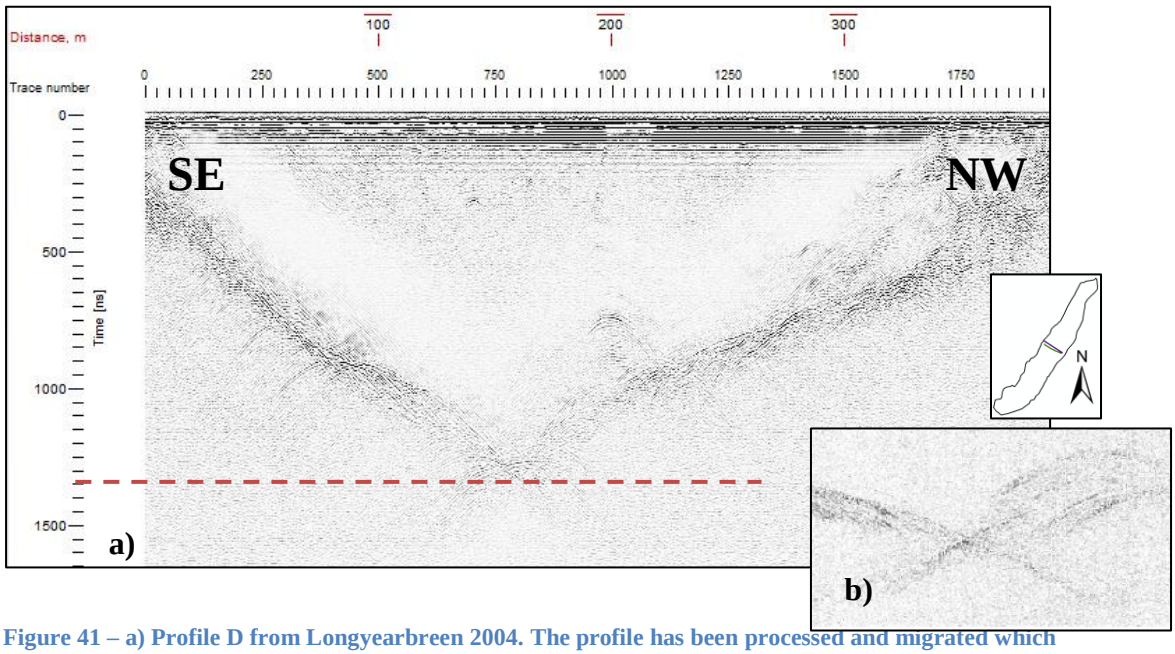


**Figure 41 – a) Profile D from Longyearbreen 2004. The profile has been processed and migrated which removed b) the artificial "bow-tie" effects (not migrated in Figure 41b).**

positioning from the 2004 survey. Measuring the distances between the start and end position of profile D in ArcMap gives a real distance of 550 m, which matches the distance of profile 232 (Figure 42).

A few of the profiles from the 2004 survey have a weak basal reflection in the lowermost parts of the radiogram (Figure 43). The weak reflections were often easy enough to pick out when turning on an extra processing routine called “reflection strength” or just zoomed in. The weak basal reflection was interpreted as a basal layer of debris-rich ice by Riger-Kusk (2006) and is thought to prove the existence of a former zone of temperate ice.

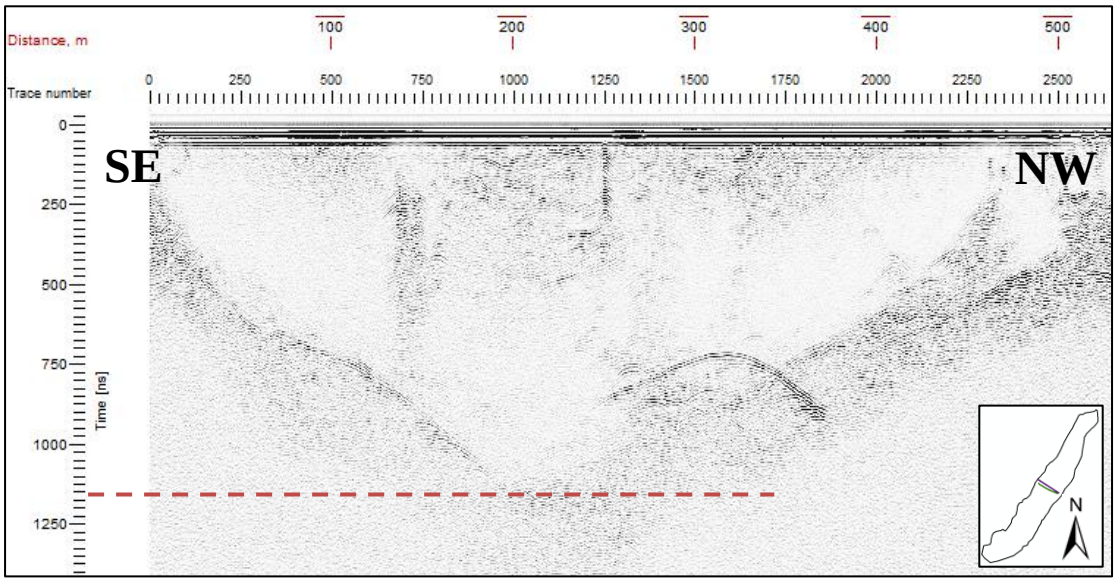


**Figure 42 – Profile 232 from Longyearbreen 2016.**

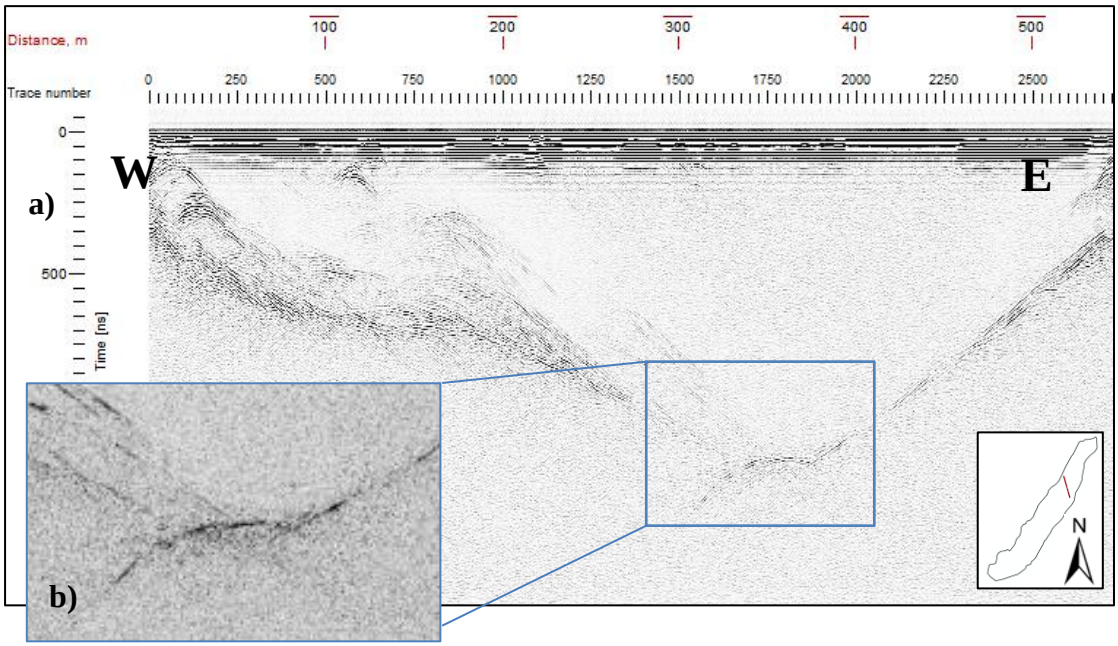


**Figure 43 – a) Profile EF from the 2004 survey on Longyearbreen. b) The deepest part of the profile, at ~100m, has a weaker basal reflector and is more difficult to interpret. The processing routine “reflection strength” can be used to boost the reflector.**

### *5.1.3 Tellbreen*

As the field work was conducted in April, the ice extent at the glacier margin was not visible under the snow. Already the lowermost profile collected on Tellbreen from 2004 (Profile L22) shows ice depths of about 30 m (Figure 44c), whereas comparable profiles from 2016 shows little to no ice at all (profile 249-251) (Figure 44b). The ice has thus retreated over 550 m from where the 2004 data sets first profile showed 0 m ice thickness (Orange line in Figure 44a) depth to where you have 0 m today (Red line). The basal reflector was strong on every profile on Tellbreen (Figure 45) and easy to pick out. Figure 45shows an example of a lateral area found in a few profiles that included strong englacial reflections thought to be caused by a high amount of

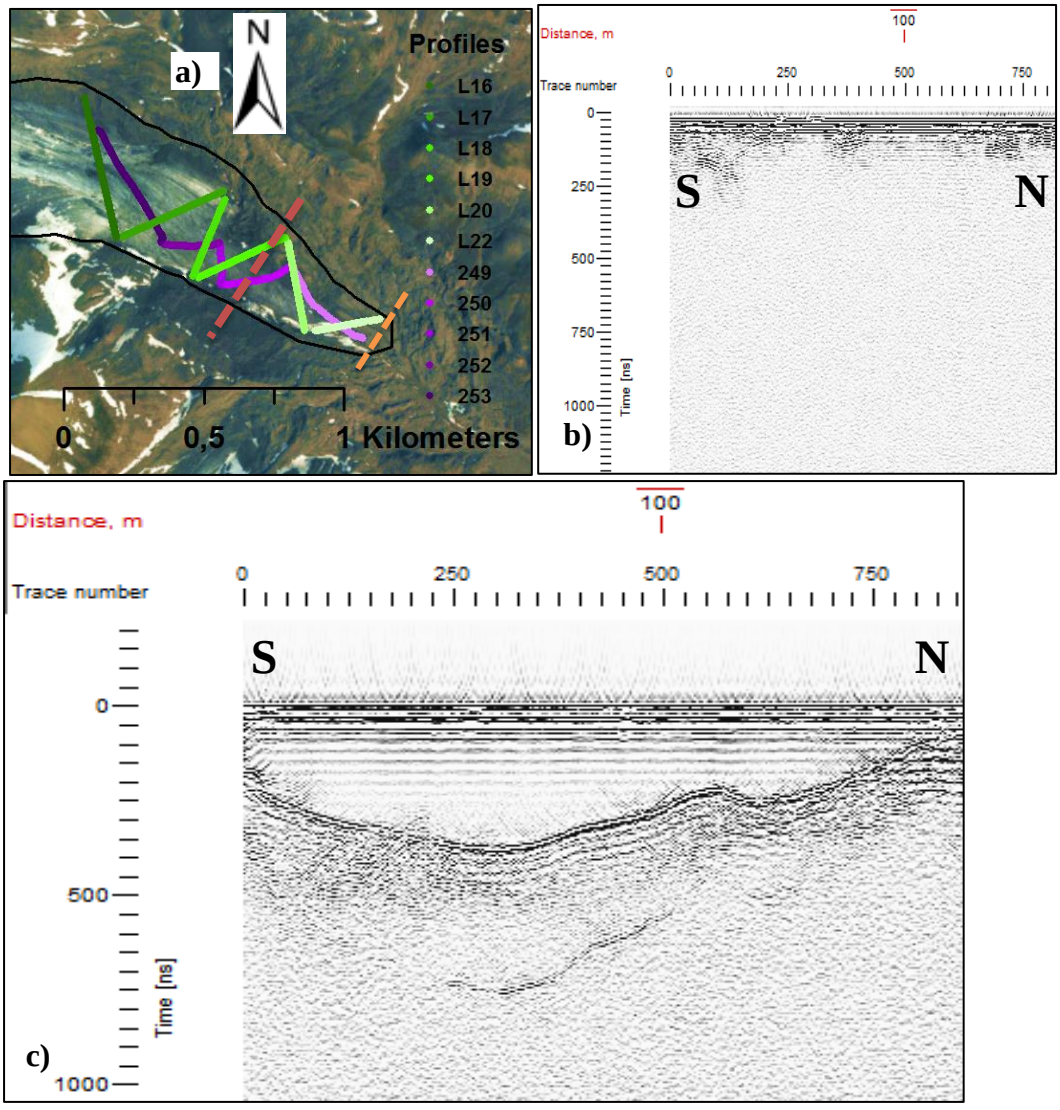


**Figure 44 – a) The lower most profiles on Tellbreen from 2004 (green) and 2016 (purple). There is ice on all profiles from 2004 while the profiles 252 and 253 from the 2016 data set show no ice thickness at all. b) Profile 250 from 2016 lies below the glacier margin and shows no ice while c) Profile L19, on the same height as profile 250, from the 2004 data set shows an ice depth of 30 m.**

sediments in the ice (indicated by red circle). Profile 294 (Figure 46) was the second longest profile collected during the 2016 survey, except for the longitudinal profiles. It crosses 1,5 km over the widest part of Tellbreen up towards the northern tributary arm, passing a threshold "dividing" the two areas into a central area and a tributary area. The ice thickness over the threshold was only 26 m at the minimum and same area shows a tail of englacial sediments coming out into the central basin, indicating the glacier movement direction downwards from the tributary area (higher elevation).

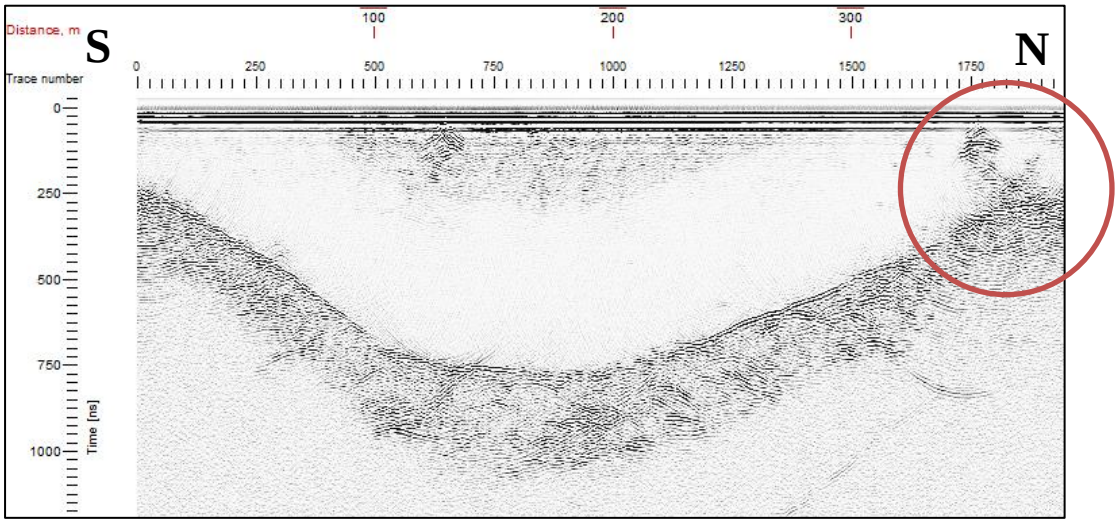


**Figure 45 – Profile 255 from Tellbreen shows a typical strong and easy interpretable basal reflector. The northern lateral side shows an area with a lot of englacial sediments.**

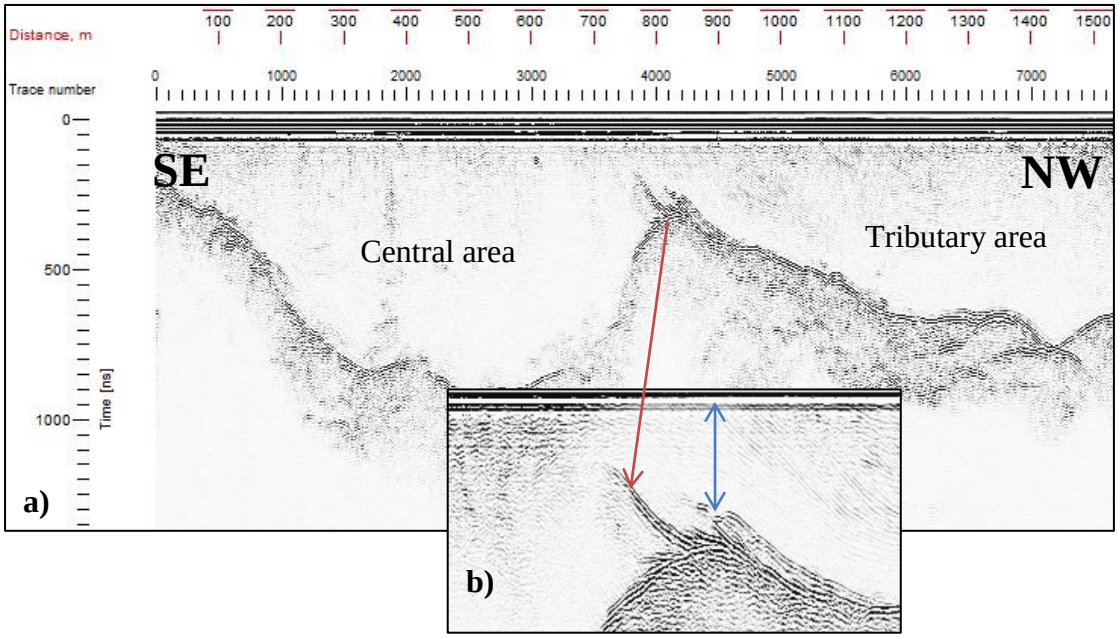


**Figure 46 — a) The second longest cross profile (294) of the 2016 data set was collected on Tellbreen across the widest area up towards the northern tributary area. b) Profile 294 crosses over the minimum ice thickness (26 m at trace number 4200) at the entry of the tributary arm (blue arrow). The enlargement of the threshold shows a tail of englacial sediments.**

## *5.2 Ice thickness interpolation*

### *5.2.1 Interpolation of Longyearbreen*

The two interpolation models of ice thickness over Longyearbreen (Figure 47) show steep inclination on the lateral sides (east and west) and low inclination along the longitudinal axis of the glacier in both models. The 2016 model shows two distinct narrowing parts into the middle of the glacier. These artifacts are discussed more in section 5.2.2. The maximum depth in the middle parts has decreased from 120 m to 100 m, whereas the lateral parts cover about the same extent only with somewhat less thickness (see section 5.1.2). The maximum depth from the 2D profiles (Figure 32 and Figure 33) confirms the detectible maximum model depths of ~120 m in 2004 and ~100 m in 2016.

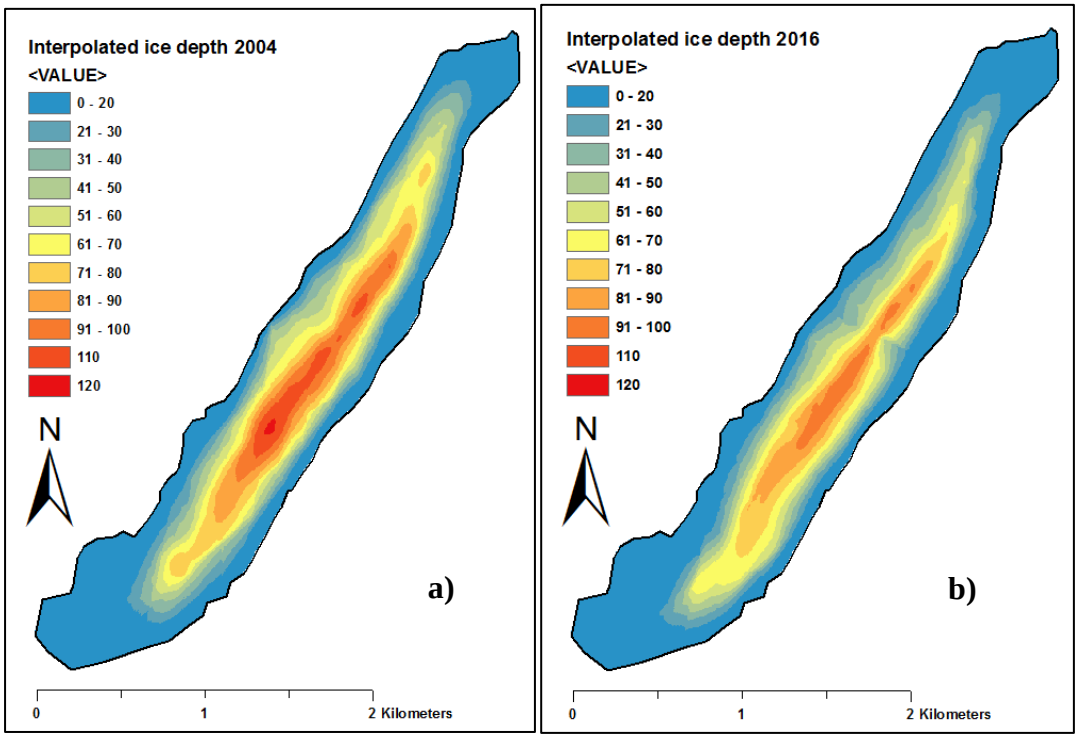


**Figure 47 – a) Interpolated depth (m) model for Longyearbreen 2004 and b) 2016.**

A more detailed map showing the differences between the two interpolation models from Longyearbreen are shown in Figure 48. The point of largest difference in ice thickness in the middle of the model is created by the narrowing parts in the interpolation model. The otherwise light red distributed colors suggest an overall thinning of the glacier (see section 2.5, Figure 11), between 5-25 m of ice thickness.

The blue area indicates an increase of between 5-30 m in ice thickness and is a result from wider cross-profiles in the southeastern area during the 2016 survey compared to the ones in 2004 (Figure 47a). The southern part (upper area of the glacier) shows less decrease in ice thickness whereas the northern two thirds show a widely distributed decrease. There is also less decrease and even some apparent increase in ice thickness along the lateral sides compared to the central line where the thinning is most widespread. The increase in ice thickness can mostly be explained by wider and denser GPR profiles during the 2016 survey as the increase areas mainly lies in areas covered closer by the 2016 profiles. The mainly shallow change in ice thickness, seen by bright colors in the figure suggests that the calculated change in ice volume between 204 and 2016 will be small.

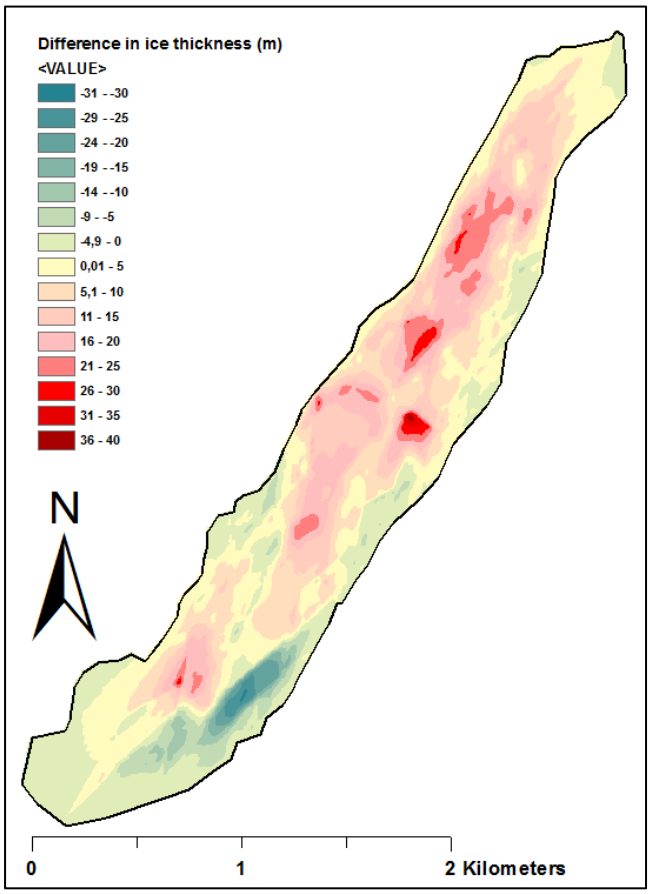


**Figure 48 – Change in ice thickness on Longyearbreen between 2004 and 2016. Red indicates where the decrease in ice thickness has been.**

### *5.2.2 Interpolation artifacts*

The interpolated model of Longyearbreen from 2016 shows a large similarity in depth distribution to the model from 2004 except for in one location in the central area (red

circle in Figure 49). Comparing the interpolated model and the closest cross profile to the narrowing area (profile 229) shows a larger difference in ice thickness between the two (15- 30 m) compared to the otherwise low differences (0-10 m). This suggests that something has gone wrong with the modeling as the interpolation has not followed the depth of the profile properly, which has similar depth distribution as neighboring profiles.

The subglacial topography under Longyearbreen has similar topographic characteristics as the features in the interpolation since the interpolated ice thicknesses were subtracted from the DEM model to construct the topography map. A solely subglacial topographic cause for the characteristics can therefore be ruled out. Though looking at the 2004 interpolation (Figure 47) there is a vague similarity which can suggest a partly subglacial cause for the narrowing parts. The color scale chosen for the interpolations separates the difference in thickness by every 10$^{th}$ meter which could contribute to a figurative exaggeration. The same types of topographic characteristics are also found on Tellbreen (Figure 51 and Figure 55).

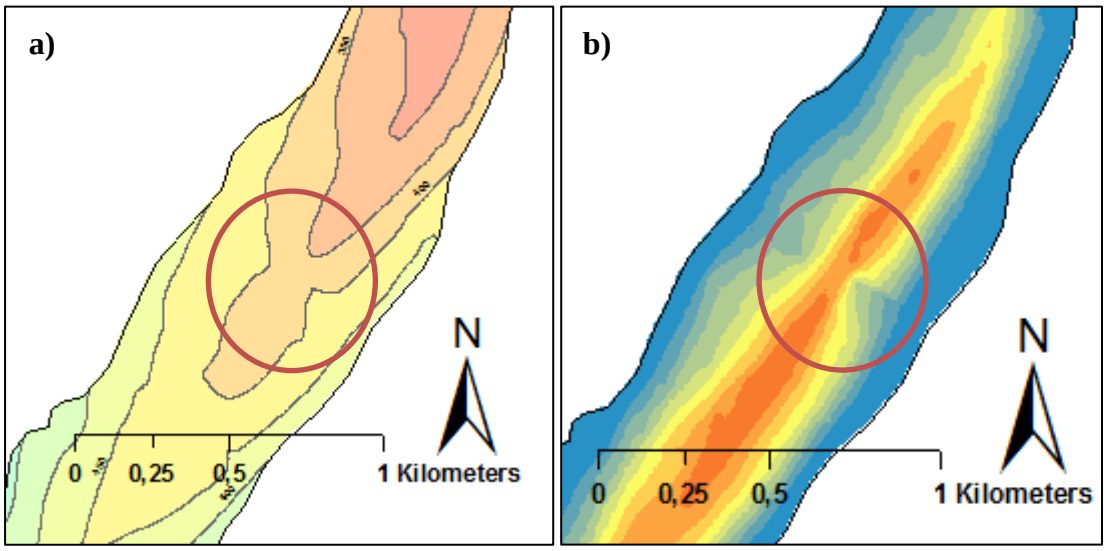


**Figure 49 – a) Zoom in on Longyearbreen subglacial topography under the b) interpolation feature seen on the 2016 model.**

### *5.2.3 Interpolation of Tellbreen*

The data collected at Tellbreen in 2004 did not cover the north-western and southernmost sections due to steep and inaccessible terrain whereas the areas was

managed to be accessed a bit more with snowmobile in 2016, creating a larger data set area. These areas must be kept in mind during the interpretation since it will increase the apparent ice volume of the 2016 data set compared to the 2004 data set (see section 5.2.4). The largest ice thickness of both models is found in the central parts along the central line of the glacier (Figure 50 and Figure 51). The interpolations

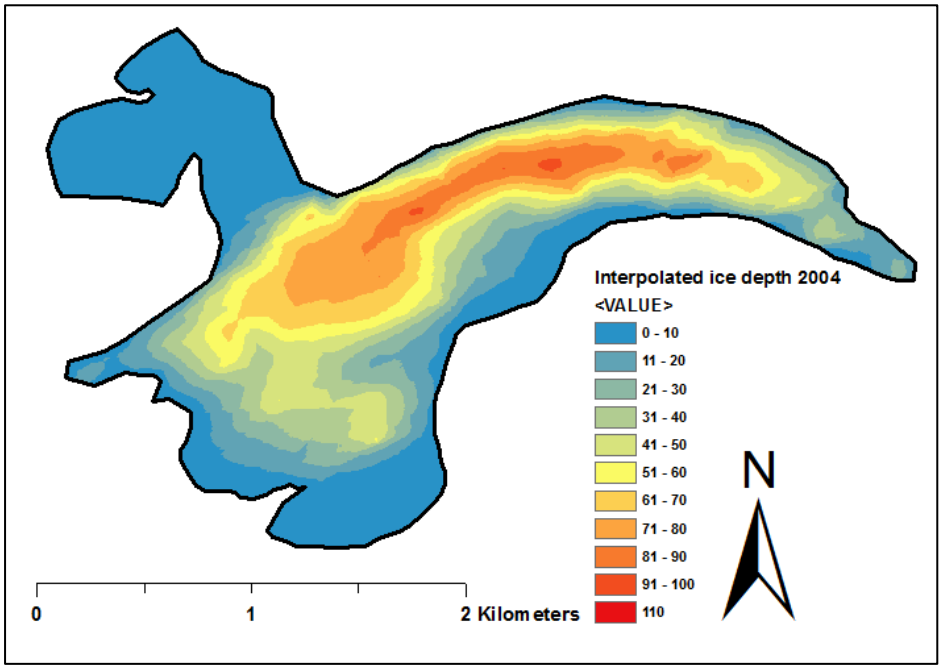


Figure 50 – Interpolated depth (m) model for Tellbreen 2004.

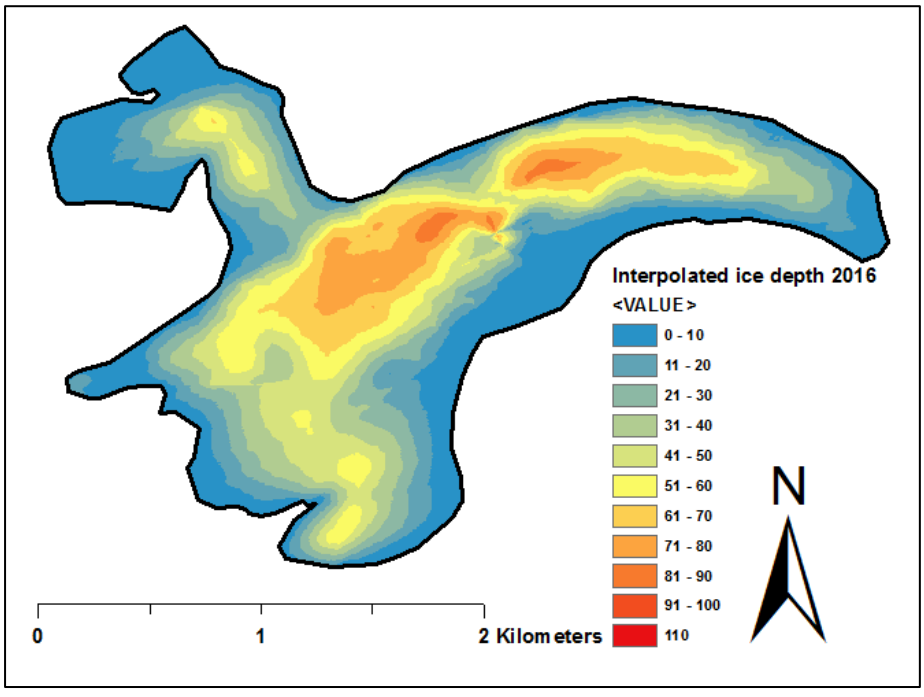


Figure 51 - Interpolated depth (m) model for Tellbreen 2016.

appear to capture the ice thickness variations observed in the 2D radargrams well, and show a similar maximum depth of ~95 m and ~85 m respectively (Figure 34 and Figure 35). The area in the middle of the 2016 model with the diagonal shallow ice thicknesses (Figure 51) between the two deeper areas) is discussed in section 5.2.2. The rest of the glacier shows an ice distribution that follows the same pattern both years (Figure 50and
Figure 51 51). The deepest areas of the 2016 data set are positioned in the same areas as in the 2004 data set and shallower parts can be recognized on both models.

Figure 52 52 shows the change in ice thickness between the 2004 and 2016 surveys. The largest decrease of 36-40 m indicated lies in the north central parts. This is also where the 2016 interpolation shows an unusual narrowing area with shallow ice thicknesses. The area should therefore be considered doubtful. The large decrease area in the

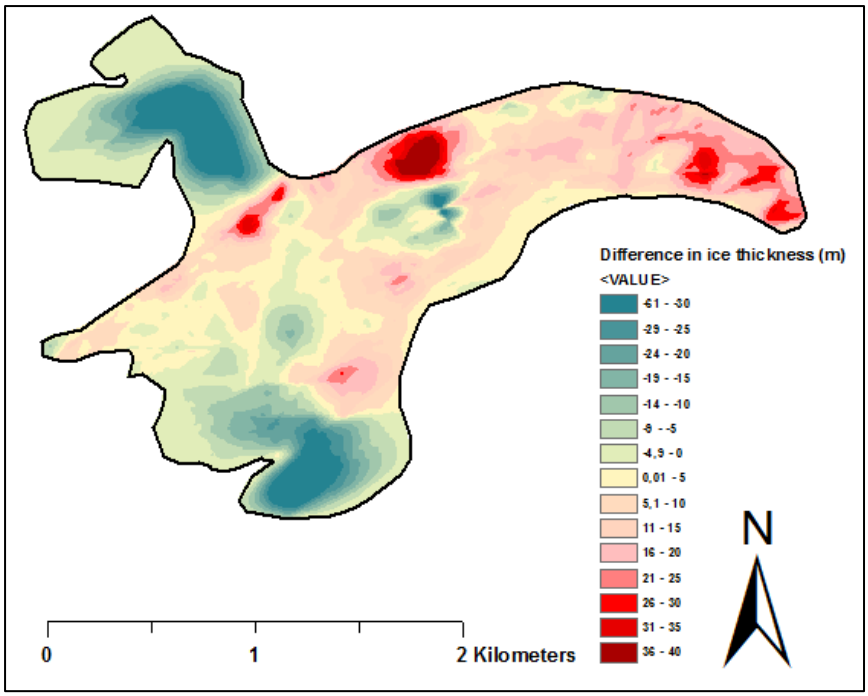


**Figure 52 – Change in ice thickness between 2004 and 2016. Red indicates where the largest decrease in ice thickness has been.**

easternmost part matches the interpretations of the 2D profiles discussed in section 5.1.2 (Figure 44), where the ice has retreated over 550m. Here the ice thickness has decreased with 15-35 m. There is a general decrease of ice thickness in the central

areas of Tellbreen of about 10-20 m. The area around the threshold for the tributary arm (Figure 46) show that the southern side of the threshold has decreased in ice thickness with 10-30 m, while the blue area north of the threshold indicates an increase in ice thickness. The two large blue areas in the north and south, with a 20-60 m increase of ice thickness, are results from the larger coverage of the 2016 survey.

### *5.2.4 Volume estimate and calculated ice volume change*

As to the actual volume change of Longyearbreen and Tellbreen the values used are specified for each interpolated model per cell in Table 4. The sum value is the sum of depth in all cells and since the cell size used during interpolation was $5 \times 5$ m, the total volume would be depth sum times 25 $m^2$ (Eq. 12).

$$(cell\ size \times mean\ depth) \times number\ of\ cells \qquad \text{Eq. 12}$$

The calculated volume values and percentage change are listed below in Table 4. The most recent volumes measured (in 2016) of the two glaciers are $8.54 \times 10^7 m^3$ (0.085 $km^3$) for Longyearbreen and $1.16 \times 10^8 m^3$ (0.12 $km^3$) for Tellbreen. As can be seen by the calculated difference in volume, both glaciers has reduced its volume during the 12 year period between the old and new data sets. The minimum estimate for the change in size on Longyearbreen is 15.8% since 2004, which can be seen as a widely distributed decrease in ice thickness in Figure 48. The numbers for Tellbreen, 4.7 %, are somewhat misleading and would be higher if the new data set would only cover the same area as the old one. As seen in Figure 52, the large blue areas are the main reason for the underestimated change on Tellbreen. To make the 2016 interpolation values more comparable with the 2004 interpolation and get a confirmation on the calculated change in volume, the interpolated areas outside the 2004 survey extent from was removed from the 2016 data (Figure 53).

The new values are listed in Table 4 as “TB 2016 (2)”. The “TB 2016 (1)” model has a much lower change in percentage between the years compared to the change on Longyearbreen. This seems illogic as the two glaciers inhibit the same small valley characteristics and lies in close proximity to each other. The adjusted interpolation on the other hand gives higher values which are more comparable and is therefore considered a much more realistic model to use for percentage comparison between 2004 and 2016, though “TB 2016 (1)” still gives more exact values of volume.

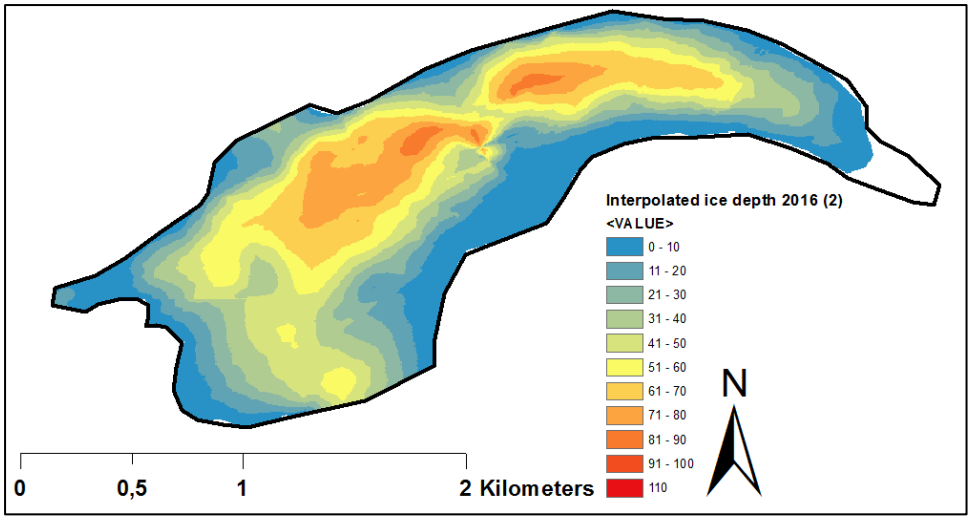


**Figure 53 – The areas outside the 2004 survey extent was removed from the interpolated model of Tellbreen 2016, creating a new model ("TB 2016 (2)") more alike to the 2004 model.**

Using the percentage change in volume from "TB 2016 (2)" to back calculate the theoretical ice volume of 2004 if the two arbitrary arms were included, as they were in the 2016 survey, gives a volume of 0.1328 $km^3$. Since the 2004 survey did not reach these areas this would be a more trustworthy volume estimate from 2004 as it covers a larger extent.

**Table 4 – Depth model values with cell count, average minimum and maximum depth per cell, sum of depth in all cells, mean depth and standard deviation from the interpolation model. Calculated volume, difference in volume and difference in percentage is derived from Equation 12. Presentation of depth values in meter. * The adjusted interpolation model for Tellbreen 2004 (see section 5.2.4)**

| **Glacier data set** | LYB 2004 | LYB 2016 | TB 2004 | TB 2016 (1) | TB 2016 **(2)*** |
|---|---|---|---|---|---|
| **Cell count** | 106748 | 106748 | 149537 | 147265 | 111370 |
| **Minimum depth (m)** | 0 | 0 | 0 | 0 | 0 |
| **Maximum depth (m)** | 110 | 98 | 95 | 86 | 86 |
| **Sum of depths in all cells (m)** | 4000000 | 3500000 | 4600000 | 4500000 | 3850117 |
| **Mean depth (m)** | 38 | 32 | 31 | 30 | 34.6 |
| **Standard deviation (m)** | 32 | 28 | 27 | 23 | 23 |
| **Calculated volume ($m^3$)** | **0.1014 $km^3$** ($1.01 \times 10^8 m^3$) | **0.0853 $km^3$** ($8.54 \times 10^7 m^3$) | **0.1158 $km^3$** ($1.16 \times 10^8 m^3$) | **0.1104 $km^3$** ($1.10 \times 10^8 m^3$) | **0.0962 $km^3$** ($0.96 \times 10^8 m^3$) |
| **Calculated difference in volume ($m^3$)** | - | **0.016$km^3$** ($16.0 \times 10^6 m^3$) | - | **0.0054$km^3$** ($85.4 \times 10^6 m^3$) | **0.020$km^3$** ($20.0 \times 10^6 m^3$) |
| **Difference in percentage (%)** | | **-15.8%** | - | **-4.7%** | **-16.9%** |

## *5.3 Subglacial topography*

The models for subglacial topography were developed in ArcMap as described in section 4.5.

### *5.3.1 Longyearbreen*

The generally concave shaped subglacial topography under Longyearbreen extends between 200–800 m a.s.l, with a height difference of 600 m (Figure 54). As the contour lines show, the steepest parts of the subglacial topography are towards the southwest and some towards the lateral margins. The upper region has a gentle U-shaped relief typical for valley glacier eroded areas (Benn and Evans, 2010). The U-shape is replaced with a steeper V-shaped relief at ~500 m a.s.l which stretches towards the northeastern front. This indicates low basal erosion of the lower parts. The deepest ice thickness of the interpolated models is found at bed elevations of between 450-350 m a.s.l (Figure 47) where the subglacial relief is deepened. The ice gets thinner towards the lateral sides of the glacier where the inclination of the bed topography is steeper. The relief shifts once again towards the glacier margin, suggesting a flattening subglacial topography towards the glacier front.

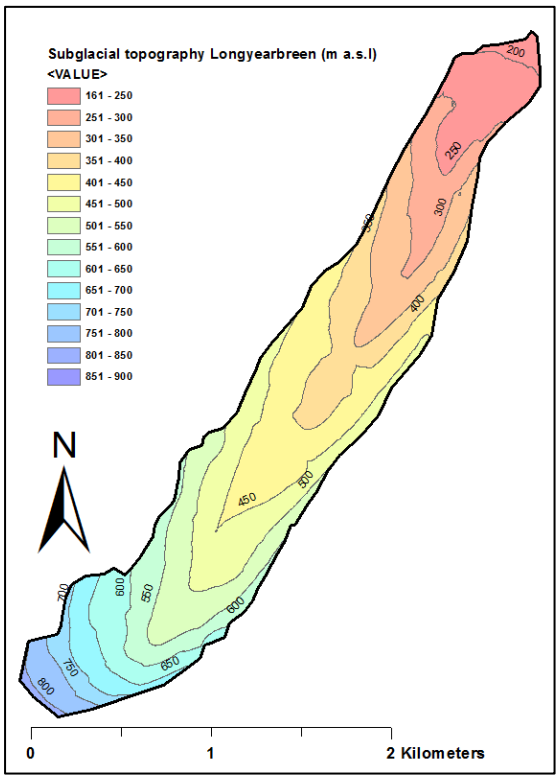


**Figure 54 – Subglacial topography of Longyearbreen.**

### *5.3.2 Tellbreen*

The subglacial topography of the northern and southern tributary ice masses of Tellbreen reaches up to 800-900 m a.s.l while the easternmost point lies on 265 m a.s.l (Figure 55). The height difference between the highest and lowest point is ~635 m. There are steep valley sides towards the northern and southern margins while the central area has a gentle U-shaped relief which turns to a steeper V-shaped relief towards the east. The southern tributary arm is the only area with a moderately convex shape which matches the thin ice thickness in the area (Figure 50 and Figure 51). The subglacial topography has an otherwise concave shape. The largest ice thickness is found at the subglacial depression between 350-450 m a.s.l. As can be seen by the central topography contours, there is a narrowing area of the 450 m a.s.l contour line no subglacial formation causing the strangely thin ice thicknesses mentioned in section 5.3.2, supporting that they are an artifact from processing.

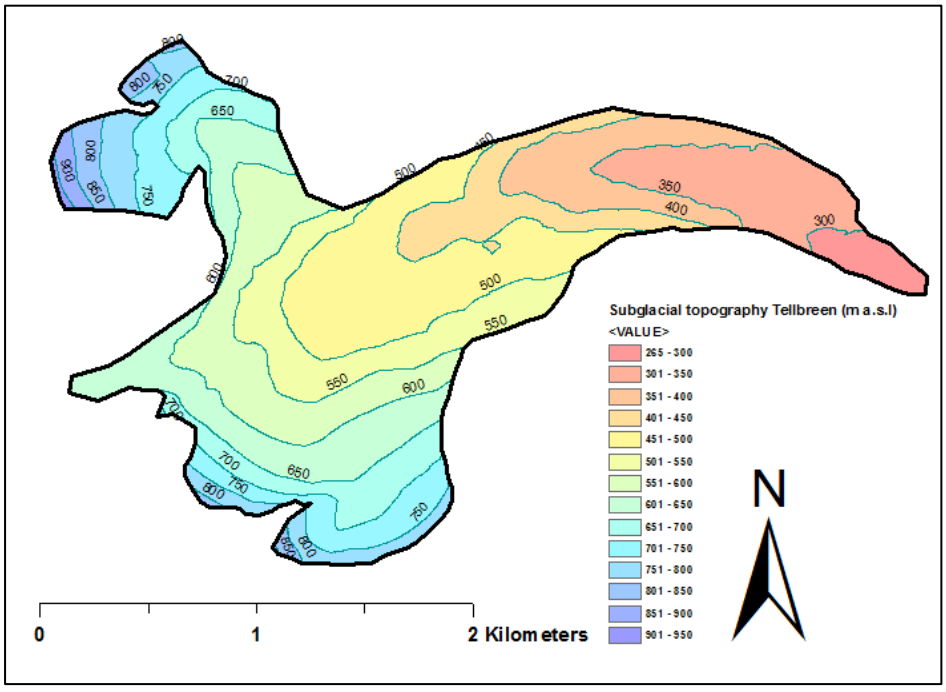


**Figure 55 – Subglacial topography of Tellbreen**

Figure 56 is a good comparison of the subglacial topography model over Tellbreen. The northern side of Tellbreen can be seen to have an evenly steep inclination downwards while the two thresholds marked with arrows steps up to the flat southern plateau (Figure 56). The profile is a typical example from Tellbreen with an easily interpretable reflector and clean ice.

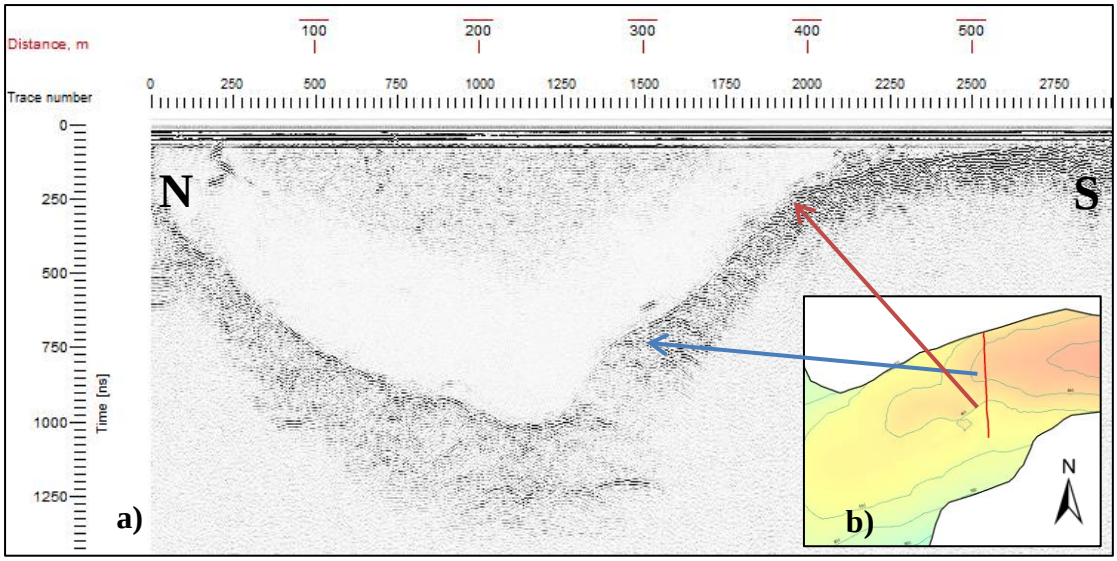


**Figure 56 – a) Profile 260 over Tellbreen shows a good example of compliance between the 2D profiles and the b) subglacial bed topography.**

# 6 Discussion

## *6.1 Uncertainties*

### *6.1.1 Data sets*

One of the main goals of this thesis is to establish the change in volume of Longyearbreen and Tellbreen. The survey in 2016 was conducted as detailed as possible in order to enable an accurate calculation of the present date ice volume. However, differences in the distribution of survey profiles between the two surveys may account for some of the observed volume change (Figure 48 and Figure 52). In order to test the effect of increased measurements on the calculated volume change, a simplified interpolation of the 2016 ice thickness was carried out (Figure 57a). Comparing the simplified interpolation with the interpolation of all the profiles from Longyearbreen (Figure 57b) gives a difference in percentage of 19.6 % and 12.5 % respectively. The addition of data in the 2016 data set does therefore lower the uncertainty with 7.1 %.

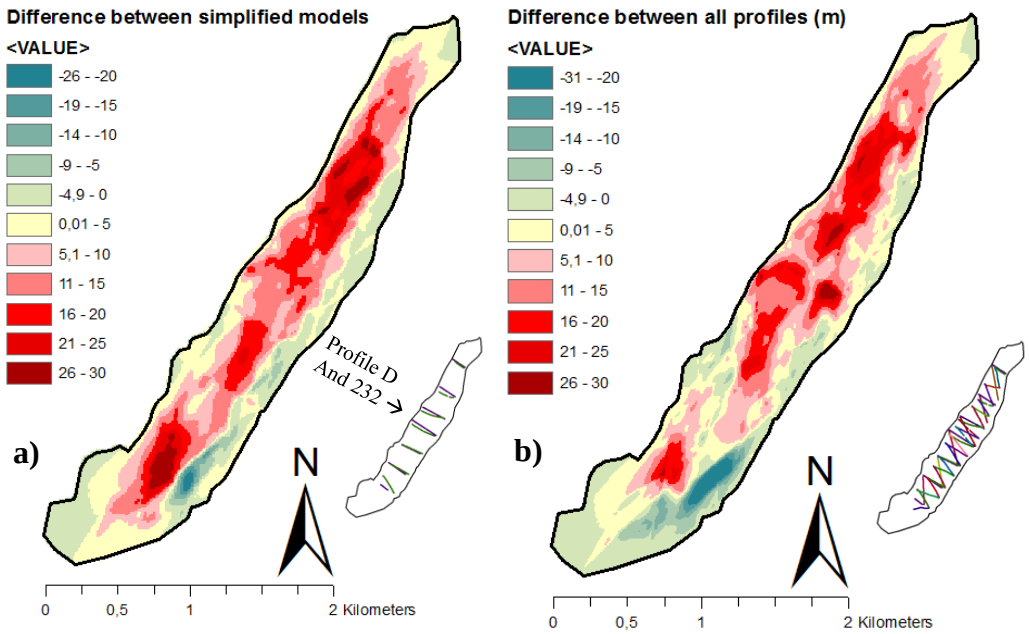


**Figure 57 – a) Simplified interpolation using only similar perpendicular profiles from the 2004 and 2016 data set. b) Interpolation of all 2004 and 2016 profiles.**

The weak reflections previously seen on profiles from the 2004 surveys were thought to be caused from temperate ice as they were first noticed in 1993 (Tonning, 1996), although not comparably weak in the profiles from the 2016 survey. The relatively

small volume of the valley glaciers implies that temperate zones like these are unlikely. A study on Tellbreen found that it would only be possible to find small pockets of temperate ice in the deepest parts (Bælum, 2006), making it unrealistic that such large extents of weak reflections (Figure 37) are caused by temperate ice. Another explanation for the weak reflections could just be that the ice/bed interface in these areas are weaker than the surrounding areas, caused by frozen debris-rich basal ice or englacial sediments causing scattering of the radar signal (Riger-Kusk, 2006). Though, englacial sediment-rich ice does suggest an earlier thermal regime with temperate ice in the glacier. This could in such case be remains from the LIA when Longyearbreen was thought to have been 20-30 m thicker than today (Bælum, 2006; Riger-Kusk, 2006). The regime of both Longyearbreen and Tellbreen are interpreted as presently cold based glaciers as they both show mainly strong basal reflectors and no other evidence of temperate ice was found.

### *6.1.2 Validation of radargram interpretations*

Ice thickness measurements for all data sets were compared where cross profiles intersect longitudinal profiles in order to evaluate the uncertainty of the 2D profile interpretations. Table 5 shows an example from cross-sections on Longyearbreen (100 MHz) from Figure 24b.

Using the absolute difference, the total average difference in depth at the intersections is 4.17 m for this data set. There are higher deviations at four different intersections (marked in yellow), the rest of the values vary between 0-10 m which is a fairly small difference considering the uncertainty of the GPS itself (see section 4.1). The average depth difference for Tellbreen in 2016 with 100 MHz antenna is 4.57 m, with only three higher deviations of 11 m (x2) and 17 m (see Appendix 1).

It is important to note that the depths of the cross profile and longitudinal profile are not precisely in the intersection point. Since the picks are not continuous lines but points, the closest point to the intersection trace number of the longitudinal profile was used (no more than 10 m). The low average difference tells that the processing and interpretation of the basal reflection has a good accuracy and that the GPS positions are precise.

**Table 5 – Deviation in depth measured and interpreted between length- and cross profile intersections at Longyearbreen (100 MHz).**

| Intersection | Longitudinal profile trace number | Longitudinal profile (m) | Cross profile (m) | Depth difference (m) |
|---|---|---|---|---|
| **246-219** | 16207 | 30 | 31 | 1 |
| **246-220** | 16036 | 30.5 | 30.9 | 0.4 |
| **246-221** | 14351 | 35.7 | 39.2 | 3.5 |
| **246-222** | 13857 | 40.1 | 40.6 | 0.5 |
| **246-223** | 12569 | 41.5 | 42.8 | 1.3 |
| **246-224** | 12408 | 42.5 | 45.6 | 3.1 |
| **246-225** | 11681 | 47 | 52.3 | 5.3 |
| **246-226** | 11348 | 48.5 | 46.4 | -2.1 |
| **246-227** | 10035 | 50.9 | 61.9 | 11 |
| **246-228** | 9607 | 55.7 | 61.5 | 5.8 |
| **246-229** | 9203 | 60.4 | 49.3 | -11.1 |
| **246-230** | 8863 | 68.3 | 69.8 | 1.5 |
| **246-232** | 8117 | 77.8 | 79.8 | 2 |
| **246-234** | 7826 | 75.7 | 76.1 | 0.4 |
| **246-235** | 7217 | 79.2 | 84.4 | 5.2 |
| **246-236** | 6832 | 87.3 | 85.9 | -1.4 |
| **246-237** | 5885 | 82.6 | 85 | 2.4 |
| **246-238** | 5528 | 76.9 | 79.2 | 2.3 |
| **246-239** | 4749 | 86.2 | 85.8 | -0.4 |
| **246-240** | 4321 | 86.2 | 82.9 | -3.3 |
| **246-241** | 3411 | 90.4 | 77.3 | -13.1 |
| **246-242** | 3054 | 88 | 74 | -14 |
| **246-243** | 1953 | 56.3 | 64.7 | 8.4 |
| **246-244** | 1535 | 55.5 | 54.8 | -0.7 |
| **Average** | | | | **4.17m** |

Both data sets from 2004 have high average depth difference of ~13 m (between 5 and 40 m) at intersections between their cross and longitudinal profiles. This is an effect of the poor quality of the longitudinal profiles and is why the longitudinal profiles were excluded from the data modeling. The poor quality of the 2004 longitudinal profiles is a result from the GPS uncertainties and difficulties of positioning the traces correctly along the profile (see section 4.5).

### *6.1.3 Snow depth*

The velocity of snow is commonly assumed to be 0.21 m $ns^{-1}$ (see section 4.1.1) (Plewels and Hubbard, 2001; Navarro et al., 2005). The velocity does however vary a lot depending on the snow density and water content even on small distances. Nevertheless, the hyperbola tool used during processing supports that this velocity is

suitable for Longyearbreen and Tellbreen. Processing of the 500 MHz profile that crosses the snow pit dug on Longyearbreen with this velocity shows that the depth at the cross-point was 1 m during the field work in 2016 (Figure 58). The snow pit showed an actual snow depth of 0.9 m which corresponds relatively well with the 1 m depth measured with the snow radar, though a bit overestimated snow velocity. Snow radar profiles from widely distributed parts of Longyearbreen and Tellbreen shows a general snow depth of 0.7-1.1 m in low, middle and high parts of the glaciers. The maximum error of the ice thickness would therefore be 0.22 m with a snow depth of 1m and a snow velocity of 0.21 m $ns^{-1}$.

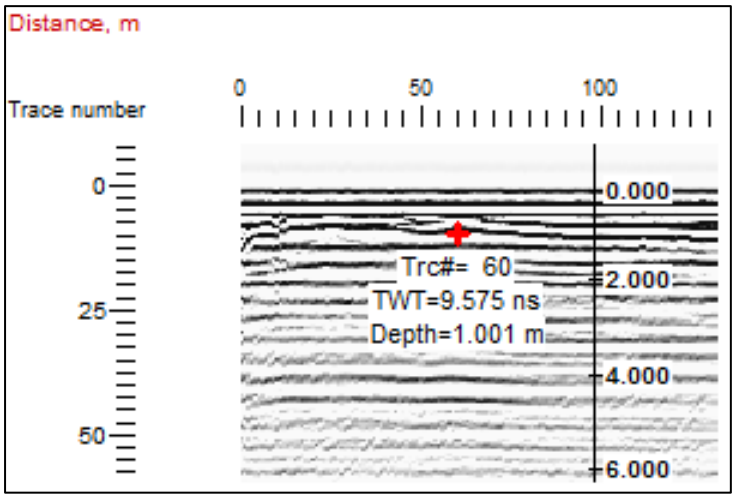


**Figure 58 – Profile 86 crosses the snow pit on trace number 60.**

## *6.2 Comparison of results*

### *6.2.1 Volume – area scaling estimate*

The resulting volume values from the interpolated models can be compared to the volume-area scaling relationship, $V = cA^{\gamma}$ (Eq. 8).

This relationship is commonly used as a reasonable method to estimate glacier volumes on a large quantity scale since the estimation can be made remotely. The areas of the glaciers used in the equation are found in ArcMap by the glacier outlines. The glacial area of Longyearbreen has not decreased noticeably since the 2004 survey (see section 6.2.1). The area is therefore assumed the same during both surveys (2.65 $km^2$). However, using GPR profile comparisons between 2004 and 2016 to outline ice covered areas; the glacial area of Tellbreen can be measured to have decreased from

4.0 $km^2$ to 3.6 $km^2$ the last decade. If $\gamma$ and $c$ have assumed values of 1.36 and 0.033 $km^{3-2\gamma}$ respectively, suited for non-steady state valley glaciers (see section 3.6) (Bahr, 2011), the values listed in Table 6 are derived.

According to the volume-area scaling relationship, the volume of Longyearbreen has not decreased at all since 2004. This is a direct result of the little to no glacier area reduction seen on Longyearbreen the last decade. It is possible that the glacier area actually has decreased some but since it was not distinguishable on the maps or aerial photographs (Figure 11) used and the 2D profiles collected both years all lies within the glacial area, a more exact glacier outline could not be mapped. Because of this, the differences in results from the measured interpolated volume and the volume-area scaling volume on Longyearbreen differ considerably (see section 5.2.4). Tellbreen on the other hand showed an over 550 m long retreat of the glacier margin (see section 5.1.3) which gives a 10 % area decrease and 13.4 % difference in volume. The measured interpolated volume change gives a 3.5 % higher result than the volume-area scaling relationship suggests.

**Table 6 – Change in area measured from glacier/data outline and change in based on the volume-area scaling relationship.**

| **Glacier data set** | LYB 2004 | LYB 2016 | TB 2004 | TB 2016 |
|---|---|---|---|---|
| **Area ($km^2$)** | 2.65 | 2.65 | 4.0 | 3.6 |
| **Difference in area ($km^2$)** | - | 0 | - | 0.4 |
| **Volume ($km^3$)** | 0.124 | 0.124 | 0.217 | 0.188 |
| **Difference in volume ($km^3$)** | - | 0 | - | 0.029 |
| **% volume difference** | - | **0 %** | - | **-13.4 %** |

$\gamma$ and $c$ are empirical numbers derived from comparing area and volume on glaciers where both can be found. They are designed to capture how a glacier shrinks or grow but the values are only approximations made from idealized assumptions from different studies, meaning that the theoretically most accurate approximations will differ between each glacier (Bahr et al., 1997). $\gamma$ and $c$ can be found from Tellbreen based on the data collected and Eq. 8. Since the values of V and A are known, the equation can be turned to (Eq. 13 and Eq. 14):

$$\gamma = \ln\frac{v_2}{v_1} \div \ln\frac{A_2}{A_1} \quad \text{Eq.13} \quad \text{and} \quad c = \frac{V}{A^{\gamma}} \quad \text{Eq.14}$$

The calculation shows that $\gamma = 1.753$ and $c = 0.011$ for Tellbreen when using the back calculated volume for 2004. These values could not be derived for Longyearbreen due to the lack of change in glacier area.

Table 7 lists volumes derived from different values of $c$ and $\gamma$ found by other studies together with the deviation from the measured volumes. In this case all the overestimated volume values results in an underestimated change in volume. The highest deviation from the change in interpolated volumes is an underestimation of 75 %. There are only three studies (marked in yellow) that underestimate the volume and thereby overestimates the change in percent. This shows that a volume overestimation is common amongst the different studies at least for cold based glaciers like Longyearbreen and Tellbreen.

**Table 7 – The interpolation volume from Longyearbreen 2004 was used as an example to calculate the estimate the volume with different values of *c* and $\gamma$. The deviation from the measured volume is also included (modified from Grinsted, 2013)**

| Study | *c* values | $\gamma$ values | Calculated volume ($km^3$) | Deviation from measured volume ($km^3$) | Percent of calculated volume |
|---|---|---|---|---|---|
| ***Erasov (1968)*** | 0.027 | 1.50 | 0.1165 | -0.02 | -14.87 % |
| ***Yafeng et al. (1981)*** | 0.036 | 1.41 | 0.1421 | -0.04 | -40.12 % |
| ***Macheret & Zhuravlev (1982)*** | 0.060 | 1.12 | 0.1778 | -0.08 | -75.33 % |
| ***Macheret et al. (1984)*** | 0.037 | 1.36 | 0.1392 | -0.04 | -37.26 % |
| ***Zhuravlev (1985)*** | 0.030 | 1.36 | 0.1129 | -0.01 | -11.33 % |
| ***Driedger og Kennard (1986)*** | 0.022 | 1.12 | 0.0652 | 0.04 | +35.71 % |
| ***Zhuravlev (1988)*** | 0.048 | 1.19 | 0.1525 | -0.05 | -50.38 % |
| ***Macheret et al. (1988)*** | 0.030 | 1.38 | 0.1143 | -0.01 | -12.71 % |
| ***Chen & Ohmura (1990)*** | 0.029 | 1.36 | 0.1070 | -0.01 | -5.51 % |
| ***Bahr et al. (1997)*** | 0.028 | 1.36 | 0.1039 | 0.00 | +2.45 % |
| ***Van de Wal & Wild (2001)*** | 0.021 | 1.38 | 0.0813 | 0.02 | +19.83 % |
| ***Radić & Hock (2010)*** | 0.037 | 1.38 | 0.1394 | -0.04 | -37.46 % |
| ***Huss & Farinotti (2012)*** | [0.024-0.042] | [1.26-1.36] | [0.0819-0.1573] | [0.02--0.06] | [+19.24 % --55.11 %] |

The $\gamma$value derived from Tellbreen is higher than all example values from Table 7 while $c$ is lower. The values closest to the measured values on Longyearbreen are the ones from Bahr et al. (1997) with only 2.45 % overestimation using $\gamma$=1.36 and $c$=0.028 and Chen and Ohmura (1990) with -5.5 % underestimation using $\gamma$=1.36 and $c$=0.029. All other values have over 10% deviation from the measured values which indicates that the method gives poor volume estimations for small cold based valley glaciers where it is expected for a slower area decrease tan "normal" given a change in volume.

Although the volume-area method is still widely used to estimate glacier volumes, advances are being made in numerical modeling of glacier volume from DEMs, glacier outlines and flow lines (Andreassen et al., 2015). However, whether or not these methods yield more exact volume estimations of small valley glaciers like Longyearbreen and Tellbreen is beyond the scope of this thesis.

### *6.2.2 Comparisons between studies*

The differences in depth between the two data sets from Longyearbreen and Tellbreen could be measured directly during the processing of the 2D profiles from both surveys, as seen in example between Figure 41 and Figure 42. Profile D and 232 on Longyearbreen are overlapping profiles from 2004 and 2016 respectively. The bed reflector has a similar relief in the two radargrams but the maximum ice depth in this location is lower for the 2016 profile by ∼20 m. The maximum measured change in ice thickness on Tellbreen was by comparison only decreased by 10 m between 2004 and 2016. The light red color distributed over Longyearbreen in Figure 48 (change between the 2004 and 2016 interpolation model) implies a comprehensive thinning of the glacier rather than a decrease in areal distribution. This can also be assumed from the 2D radar profiles from 2016 which still shows ice thicknesses in the entire area covered by the 2004 survey, meaning that the glacier extent is about the same 12 years later. The glacier front of Longyearbreen in the northernmost part is thought to retreat at such low pace due to the debris covered terminus (Etzelmüller et al., 2000; Sevestre, 2015). The debris covers the ice and will by insulating the ice-core slow down the proglacial retreat (see section 2.5, Figure 11). Tellbreen on the other hand does, in addition to extensive thinning of the central areas, have a more comprehensive reduction in ice thickness in the easternmost glacier terminus. The ice

was found to have retreated about 550 m in this area during the 12 years between the two surveys. The original interpolation results from both glaciers showed an 11.1 % difference in percentage decrease between 2004 and 2016. As the extra extent of the 2016 survey on Tellbreen was excluded (see section 5.2.4), this difference decreased to 1.1 %. This is a more reliable result and shows that the two glaciers which lie in near proximity to each other have had a similarly decrease in volume the last decade. Tellbreen has melted some more according to the adjusted interpolation which can be an appropriate result caused from the large retreat at the glacier terminus.

Figure 59 shows a comparison of net mass balance of Svalbard ice masses (Hagen et al., 2003). It shows that the 2004 measurement of Longyearbreen lies below the average mass balance altitude of Svalbard. All profiles lies within the lower average margins, except for profile G which was assumed to have an underestimated ice thickness (Riger-Kusk, 2006).

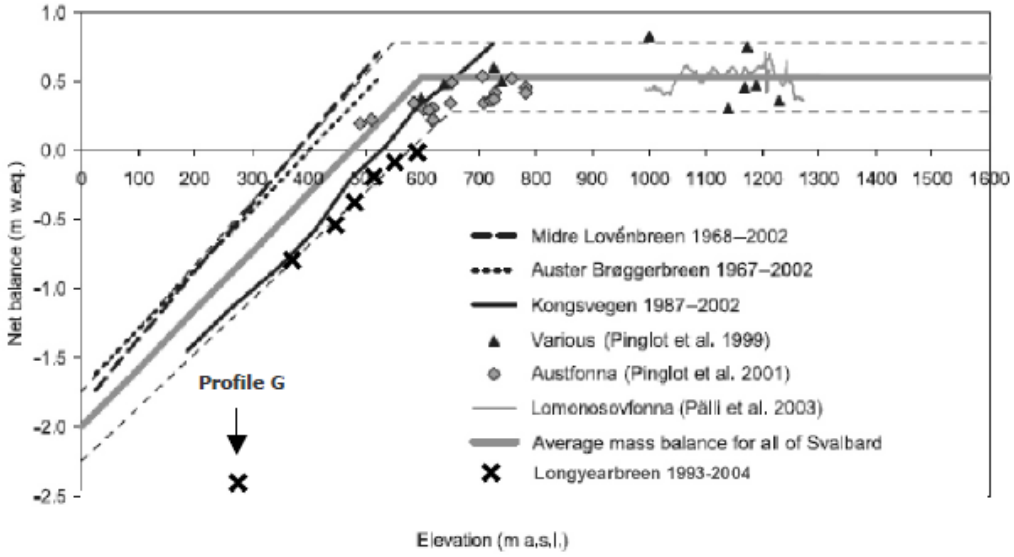


**Figure 59 – Comparisons of net mass balances of Svalbard glaciers (Hagen et al., 2003b; modified in Riger-Kusk, 2006).**

The most comparable study to the 2016 and 2004 surveys is the 1993 ice depth study of Longyearbreen (Tonning, 1996). The GPR profiles of this survey lay parallel to the perpendicular cross profiles from 2004 (see Appendix 3). This study used a radar wave velocity for ice of 0.167 m $ns^{-1}$, compared to 0.168 m $ns^{-1}$ used in this thesis, which means that the results of ice thickness will be 0.6 m thinner at a 100 m depth in the 1993 study compared to the ones in this thesis. The 1993 study did otherwise have

a similar spatial distribution of ice depth along the cross profiles as in both 2004 and 2016 (see section 5.1.2 and Appendix 3). The maximum depth was found close to profile D (Figure 62), as were the maximum depths in 2004 and 2016 (profile 232) (Figure 37). The maximum depth in this survey was 115 m in 1993 according to Tonning (1996). The total volume in 1993 was found to be ~0.122 $km^3$ (Tonning, 1993), compared to 0.101 $km^3$ in 2004 and 0.08 $km^3$ in 2016. The negative volume change of 17.2 % between 1993 and 2004 gives a close to linear decrease in ice volume between 1993 and 2016 (Figure 60).

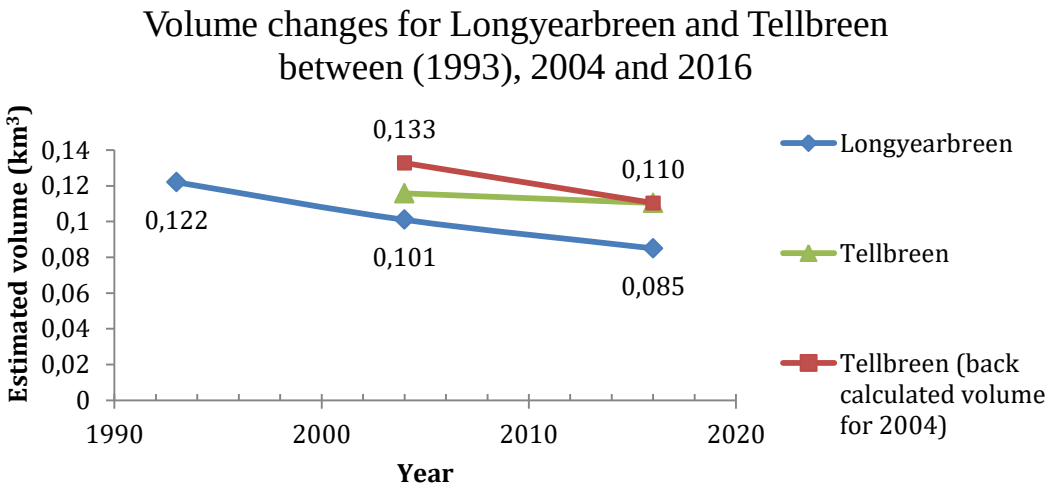


**Figure 60 – The change in volume compared between Longyearbreen and Tellbreen. The volume decrease for Longyearbreen is close to linear.**

The intervals between data sets on Longyearbreen are similar in time, which means that the glacier has had a slightly slower melt rate the last decade. Tellbreen does only show two data sets so the trend cannot be described as linear, but as the back calculated volume was used, the trend shows as parallel to the development of Longyearbreen. The green line shows the original measurements from 2004 and 2016 with an improbable low melt rate.

# 7 Conclusion

The small high arctic valley glaciers, Longyearbreen and Tellbreen, have both had a negative mass balance since the LIA maximum. Tellbreen has for example lost up to 70% since that time (Bælum, 2010). Small glaciers have short response time to climate which will affect the near future global sea level rise. As the small glaciers around the world continue to melt it is important to establish more knowledge about the volume they possess as well as the methods used for volume estimations of small glaciers (Meier et al., 2007; Bahr et al., 2009; Bahr and Radic, 2012).

The purpose with this thesis was to interpolate the thoroughly measured ice thicknesses of Longyearbreen and Tellbreen from 2D radargrams and then calculate the detailed volumes. The results have been compared to volume data measurements from 2004 as well as between the two glaciers themselves to see how the glacial progression has been during the last decade for the two glaciers. The results were then compared with the theoretical volume from the empirical volume-area scaling relationship.

The maximum ice thickness of both Longyearbreen and Tellbreen has decreased during the last 12 years between 2004 and 2016. Based on reinterpreted profiles from 2004 as well as collected and processed radargrams from 2016, interpolations were made for both glaciers. The volumes measured in 2004 were 0.1014 $km^3$ for Longyearbreen and 0.1158$km^3$ for Tellbreen. The total ice volume was found to have had a minimum decrease of 15.8 % (0.016$km^3$) on Longyearbreen and 16.9 % (0.020 $km^3$) on Tellbreen. The most recent total volume is thereby 0.0853 $km^3$ and 0.096 $km^3$ respectively for the two glaciers. The change in volume for Tellbreen was derived from an area restricted to the 2004 extent since the area covered by this survey was considerably smaller than the area covered in 2016. Therefore, back calculating the 2004 area of Tellbreen using the 16.9 % change in volume gives an estimate of the 2004 volume of 0.1328 $km^3$. The negative mass balance is observable on Tellbreen as the glacier surface area has decreased by ~0.4 $km^2$ to 3.6 $km^2$. Longyearbreen does not have visible reduction in ice volume and does still have a surface area of close to 2.65 $km^2$.

The derived volume measurements were also compared to calculated volumes from the empirical volume-area method. This scaling relationship clearly overestimates the volume of both Longyearbreen by 18.2 % (0.124 $km^3$) in 2004 and 31.13 % (0.124 $km^3$) in 2016, and Tellbreen by 46.59 % (0.217 $km^3$) in 2004 and 48.8 % (0.188 $km^3$) in 2016. Comparisons with other studies shows that all but two scaling relationships values have over 10% deviation from the measured values, which proves that the method to the greatest extent gives poor volume estimations for small valley glaciers.

This thesis concludes that the volume has decreased for the both Longyearbreen and Tellbreen as shown by direct measurements. The volume-area scaling relationship has been proven to overestimate the volume of these glaciers and most likely cold based small valley glaciers in general. The volume change of Tellbreen is noticeably overestimated, while the volume change values for Longyearbreen could not even be assessed by the method since the area of the glacier has not decreased. The volume-area method does consequently easily misjudge glaciers with volume changes due to thinning ice thicknesses rather than a decreasing glacier area/retreat of glaciers.

The results of this thesis can and will hopefully be used for further studies of the two glaciers and other similar valley glaciers. If combined with data from similar glaciers, the results can help to improve the quality of volume-area scaling relationships so that it will suit better for small but still important cold based valley glaciers and not contribute to a global ice volume overestimation.

# References

AGF212 (2014), Field report 2014—Snow and ice processes, Rep., *The Univ. Centre in Svalbard, Longyearbyen, Norway.*

Andreassen, L., Huss, M., Melvold, K., Elvehøy, H. and Winsvold, S. (2015). Ice thickness measurements and volume estimates for glaciers in Norway. *Journal of Glaciology*, 61(228), pp.763-775.

Annan, A. P. (1992). Ground Penetrating Radar - Workshop notes. *Sensors and Software Inc*: 126 pp.

Bahr, D.B., Meier, M.F. and Peckham, S.D. (1997). *The physical basis of glacier volume-area scaling. Journal of Geophysical Research volume 102,* p. 20,356.

Bahr, D., Dyurgerov, M. and Meier, M. (2009). Sea-level rise from glaciers and ice caps: A lower bound. *Geophysical Research Letters*, 36(3).

Bahr, D.B. (2011). Estimation of glacier volume and volume change by scaling methods. In Singh, V.P., Singh, P., Haritashya, U.K. (editors): *Encyclopedia of snow, ice and glaciers*, Springer, Dortrecht, The Nederlands, p. 278-280.

Bahr, D. B., and Radić, V. (2012). Significant contribution to total mass from very small glaciers. *The Cryosphere*, *6*(4), 763-770.

Benn, D. and Evans, D. (2010). *Glaciers & glaciation*. London: Hodder Education.

Björnsson, H., Gjessing, Y., Hamran, S., Hagen, J., Liestø L, O., Pálsson, F. and Erlingsson, B. (1996). The thermal regime of sub-polar glaciers mapped by multi-frequency radio-echo sounding. *Journal of Glaciology*, 42(140), pp.23-32.

Bradford, J., Nichols, J., Mikesell, T. and Harper, J. (2009). Continuous profiles of electromagnetic wave velocity and water content in glaciers: an example from Bench Glacier, Alaska, USA. *Annals of Glaciology*, 50(51), pp.1-9.

Bryhni, I., Nøttvedt, A. and Ramberg, I. (2007). Landet blir til. *Trondheim: Norsk geologisk forening.*

Bælum, K. (2006). Mapping of the general shape, depth and various internal structures of Tellbreen, a glacier on Svalbard, by means of GPR (Ground Penetrating Radar). *Unpublished master thesis. University Centre of Svalbard.*

Bælum, K. and Benn, D. (2010). Thermal structure and drainage system of a small valley glacier (Tellbreen, Svalbard), investigated by Ground Penetrating Radar. *The Cryosphere Discussions*, 4(4), pp.2169-2199.

Chen, J., and Ohmura, A. (1990). Estimation of Alpine glacier water resources and their change since the 1870s. *IAHS Publ*, *193*, 127-135.

Climate.nasa.gov, (2017). [Online] Available at: http://climate.nasa.gov/vital-signs/sea-level/ [Accessed 8 Feb. 2017].

Data.npolar.no. (2017). *Dataset*. [Online] Available at: https://data.npolar.no/dataset/eafafbb7-b3df-4c71-a2df-316e80a7992e [Accessed 24 Feb. 2017].

Davis, J. L. and Annan, A. P. (1989) Ground-penetrating Radar forhigh-resolution mapping of soil and rock stratigraphy, *Geophys. Prospect 37, No 5, 531–551.*

Eklima.met.no, (2017). Meterologisk institutt. [Online] Available at: http://eklima.met.no [Accessed 15 Feb. 2017].

ESRI (2016). ArcGIS Desktop Version 10.4. Redlands, CA: Environmental Systems Research Institute.

Etzelmüller, B., Ødegård, R., Vatne, G., Mysterud, R., Tonning, T. and Sollid, J. (2000). Glacier characteristics and sediment transfer system of Longyearbreen and

Larsbreen, western Spitsbergen. *Norsk Geografisk Tidsskrift - Norwegian Journal of Geography*, 54(4), pp.157-168.

Førland, E. and Hanssen-Bauer, I. (2003). Past and future climate variations in the Norwegian Arctic: overview and novel analyses. *Polar Research*, 22(2), pp.113-124.

Grinsted, A. (2013). An estimate of global glacier volume. *The Cryosphere*, *7*(1), 141-151.

Hagen, J. O., Liestøl, O. (1990) Long-term glacier mass-balance investigations in Svalbard 1950-88. *Annals of Glaciology 14, 1990.*

Hagen, J. O., Liestøl, O., Roland, E. and Jørgensen, T. (1993) Glacier atlas of Svalbard and Jan Mayen. *Norwegian polar institute, Oslo, (*129).

Hagen, J., Kohler, J., Melvold, K., and Winther, J. (2003a). Glaciers in svalbard: Mass balance, runoff and freshwater flux. *Polar Research 22(2), 145-159.*

Hagen, J., Melvold, K., Pinglot, F. and Dowdeswell, J. (2003b). On the Net Mass Balance of the Glaciers and Ice Caps in Svalbard, Norwegian Arctic. *Arctic, Antarctic, and Alpine Research*, 35(2), pp.264-270.

Hubbard, B. and Glasser, N. (2005). Field techniques in glaciology and glacial geomorphology. *New York: Wiley.*

IPCC, (2007). Climate Change 2007: Synthesis Report. Contribution of Working Groups I, II and III to the Fourth Assessment Report of the Intergovernmental Panel on Climate Change [Core Writing Team, Pachauri, R.K and Reisinger, A. (eds.)]. IPCC, Geneva, Switzerland, 104 pp

Isaksson, E., Kohler, J., Pohjola, V., Moore, J., Igarashi, M., Karlöf, L., Martma, T., Meijer, H., Motoyama, H., Vaikmäe, R. and van de Wal, R. (2005). Two ice-core δ18O records from Svalbard illustrating climate and sea-ice variability over the last 400 years. *The Holocene*, 15(4), pp.501-509.

Lefauconnier, B., Hagen, J. and Rudant, J. (1994). Flow speed and calving rate of Kongsbreen glacier, Svalbard, using SPOT images. *Polar Research*, 13(1), pp.59-65.

MALÅ. (2017a). *Guideline Geo | MALÅ*. [online] Available at: http://www.guidelinegeo.com [Accessed 15 Dec. 2016].

MALÅ (2017b). MALÅ XV Monitor for ProEx and X3M with Ethernet communication – Operating manual Version 1.5. *MALÅ Geoscience AB*.

MALÅ (2005). Rad Explorer 1.4 – The software for GPR data processing and Interpretation – User manual. *MALÅ Geoscience AB*.

Mauring, E., Koziel J., Lauritsen T., Rønning J S., Tønnesen J F. (1995). Målinger med Georadar. Teori, anvendelse, teknikker og eksempler på opptak. *Norges geologiske undresøkelse (NGU). Rapport nr. 94.024.*

Meier, M., Dyurgerov, M., Rick, U., O'Neel, S., Pfeffer, W., Anderson, R., Anderson, S. and Glazovsky, A. (2007). Glaciers Dominate Eustatic Sea-Level Rise in the 21st Century. *Science*, 317(5841), pp.1064-1067.

Meteorologisk institutt. (2017). *Meteorologisk institutt*. [Online] Available at: https://www.met.no/ [Accessed 10 Mar. 2017].

Mussett, A. E., and Khan, M. A. (2000). Looking into the earth: an introduction to geological geophysics. *England, Cambridge: Cambridge University Press*.

Navarro, F.J., Glazovskiy, A.F., Macheret, Y., Vasilenko, E.V., Corcuera, M.I., Cuadrado, M.L. (2005). Ice volume changes 1936-1990 and structure of Aldegondabreen, Spitsbergen. *Annals of Glaciology* 42, 158-162.

Navarro, F., Lapazaran, J., Martín-Español, A. and Otero, J. (2016). Ground-penetrating radar studies in Svalbard aimed to the calculation of the ice volume of its glaciers. *Cuadernos de Investigación Geográfica*, 42(2), p.399.

Norwegian Polar Institute. (2017a). *Kart*. [online] Available at: http://www.npolar.no/no/tjenester/kart/ [Accessed 12 Jan. 2017].

Norwegian Polar Institute. (2017b). *Svalbard*. [Online] Available at: http://www.npolar.no/en/the-arctic/svalbard/ [Accessed 10 Jan. 2017].

Nuth, C., G. Moholdt, J. Kohler, J. O. Hagen, and A. Kääb (2010), Svalbard glacier elevation changes and contribution to sea level rise, J. *Geophys. Res.*, 115, F01008, doi:10.1029/2008JF001223.

Plewes, L. and Hubbard, B. (2001). A review of the use of radio-echo sounding in glaciology. *Progress in Physical Geography*, 25(2), pp.203-236.

Riger-Kusk, M. (2006). Hydrology and hydrochemistry of a high Arctic glacier: Longyearbreen, Svalbard. Unpublished master thesis. University Centre in Svalbard.

Sevestre, H., Benn, D., Hulton, N. and Baelum, K. (2015). Thermal structure of Svalbard glaciers and implications for thermal switch models of glacier surging. *Journal of Geophysical Research: Earth Surface*, 120(10), pp.2220-2236.

UNIS. (2017). *About Svalbard - UNIS*. [Online] Available at: http://www.unis.no/studies/student-life/about-svalbard/ [Accessed 6 Jan. 2017].

Usgs.gov. (2017). *Retreat of Glaciers in Glacier National Park*. [online] Available at: https://www.usgs.gov/centers/norock/science/retreat-glaciers-glacier-national-park?qt-science_center_objects=0#qt-science_center_objects [Accessed 7 march. 2017].

Yde, J., Riger-Kusk, M., Christiansen, H., Knudsen, N. and Humlum, O. (2008). Hydrochemical characteristics of bulk meltwater from an entire ablation season, Longyearbreen, Svalbard. *Journal of Glaciology*, 54(185), pp.259-272.

Yde, J., Gillespie, M., Løland, R., Ruud, H., Mernild, S., De Villiers, S., Knudsen, N. and Malmros, J. (2014). Volume measurements of Mittivakkat Gletscher, southeast Greenland. *Journal of Glaciology*, 60(224), pp.1199-1207.

Ødegård, R.S., Hagen, J.O. and Hamran, S.-E. (1997). Comparison of radio-echo sounding (30-1000 MHz) and high resolution borehole-temperature measurements at Finsterwalderbreen. *Annals of Glaciology*, 24: 262-276.

# APPENDIX

## *Appendix 1*

Table 8 shows the cross-sections on Tellbreen (100 MHz) from Figure 25c.

**Table 8 - Deviation in depth measured and interpreted between length- and cross profile intersections at Longyearbreen (100 MHz).**

| *Cross-points* | *Longitudinal profile TRNR* | *Longitudinal profile (m)* | *Cross profile TRNR* | *Cross profile (m)* | *Difference (m)* |
|---|---|---|---|---|---|
| ***299-272*** | 18365 | 2,6 | 546 | 2,4 | -0,2 |
| ***299-273*** | 17958 | 2,8 | 429 | 2,6 | -0,2 |
| ***299-274*** | 17552 | 8,2 | 430 | 7,8 | -0,4 |
| ***299-275*** | 16078 | 28,2 | 741 | 26,8 | -1,4 |
| ***299-276*** | 15346 | 30,4 | 1037 | 30,6 | 0,2 |
| ***299-277*** | 14706 | 38,5 | 759 | 36,6 | -1,9 |
| ***299-278*** | 13913 | 57,5 | 991 | 60,3 | 2,8 |
| ***299-279*** | 13375 | 64,5 | 983 | 63,6 | -0,9 |
| ***299-281*** | 12811 | 64,1 | 1098 | 65,9 | 1,8 |
| ***299-282*** | 12369 | 65,8 | 1013 | 64,5 | -1,3 |
| ***299-283*** | 11367 | 73 | 1333 | 70,9 | -2,1 |
| ***299-284*** | 10666 | 80,1 | 1031 | 79,8 | -0,3 |
| ***299-285*** | 10057 | 82,5 | 1238 | 79 | -3,5 |
| ***299-286*** | 9474 | 62,2 | 1319 | 76,1 | 13,9 |
| ***299-288*** | 8757 | 45,7 | 1661 | 72,9 | 27,2 |
| ***299-289*** | 8199 | 58,3 | 1726 | 62,2 | 3,9 |
| ***299-290*** | 7520 | 83,4 | 1280 | 40,6 | -42,8 |
| ***299-291*** | 6880 | 83 | 1087 | 82,9 | -0,1 |
| ***299-292*** | 5935 | 69,1 | 2490 | 68,3 | -0,8 |
| ***299-293*** | 5589 | 68,8 | 970 | 69 | 0,2 |
| ***299-294*** | 4583 | 71,3 | 3137 | 71,6 | 0,3 |
| ***299-295*** | 3724 | 59,77 | 4362 | 58,2 | -1,57 |
| ***299-296*** | 1523 | 30,3 | 6361 | 33,6 | 3,3 |
| ***299-297*** | 1231 | 29,2 | 568 | 28,2 | -1 |
| ***299-298*** | 297 | 21,8 | 1344 | 24,2 | 2,4 |
| | | | | | **Absolute average 4,57** |

# *Appendix 2*

Table 9 lists volumes of Tellbreen derived from different values of $c$ and $\gamma$ together with the deviation from the measured volumes.

**Table 9 - The interpolation volume from Tellbreen 2004 was used as an example to calculate the estimate the volume with different values of $c$ and $\gamma$. The deviation from the measured volume is also included (modified from Grinsted, 2013)**

| Study | $c$ values | $\gamma$ values | Calculated volume 2004 ($km^3$) | Deviation from calculated volume 2004 ($km^3$) | Percent of calculated volume 2004 | Calculated volume 2016 (km3) | Deviation from calculated volume 2016 (1) ($km^3$) | Percent of calculated volume 2016 (1) |
|---|---|---|---|---|---|---|---|---|
| *Erasov (1968)* | 0,027 | 1,50 | 0,2160 | -0,10 | -46,34 | 0,1844 | -0,07 | -40,1 |
| *Yafeng et al. (1981)* | 0,036 | 1,41 | 0,2535 | -0,14 | -54,28 | 0,2186 | -0,11 | -49,47 |
| *Macheret & Zhuravlev (1982)* | 0,060 | 1,12 | 0,2820 | -0,17 | -58,9 | 0,2506 | -0,14 | -55,92 |
| *Macheret et al. (1984)* | 0,037 | 1,36 | 0,2434 | -0,13 | -52,38 | 0,2110 | -0,10 | -47,65 |
| *Zhuravlev (1985)* | 0,030 | 1,36 | 0,1977 | -0,08 | -41,38 | 0,1713 | -0,06 | -35,52 |
| *Driedger og Kennard (1986)* | 0,022 | 1,12 | 0,1036 | 0,01 | 10,6 | 0,0920 | 0,02 | 16,69 |
| *Zhuravlev (1988)* | 0,048 | 1,19 | 0,2485 | -0,13 | -53,36 | 0,2193 | -0,11 | -49,63 |
| *Macheret et al. (1988)* | 0,030 | 1,38 | 0,2016 | -0,09 | -42,51 | 0,1743 | -0,06 | -36,63 |
| *Chen & Ohmura (1990)* | 0,029 | 1,36 | 0,1870 | -0,07 | -38,02 | 0,1621 | -0,05 | -31,86 |
| *Bahr et al. (1997)* | 0,028 | 1,36 | 0,1818 | -0,07 | -36,25 | 0,1576 | -0,05 | -29,92 |
| *Van de Wal & Wild (2001)* | 0,021 | 1,38 | 0,1433 | -0,03 | -19,12 | 0,1240 | -0,01 | -10,93 |
| *Radić & Hock (2010)* | 0,037 | 1,38 | 0,2455 | -0,13 | -52,79 | 0,2124 | -0,10 | -48 |
| *Huss & Farinotti (2012)* | 0,024<br>0,042 | 1,26<br>1,36 | 0,1377<br>0,2748 | -0,02<br>-0,16 | -15,83<br>-57,8 | 0,1205<br>0,2383 | -0,01<br>-0,13 | -8,34<br>-53,65 |

# Appendix 3

Figure 61 shows the positions of the 1993 GPR survey profiles together with the Riger-Kusk survey profiles from 2004.

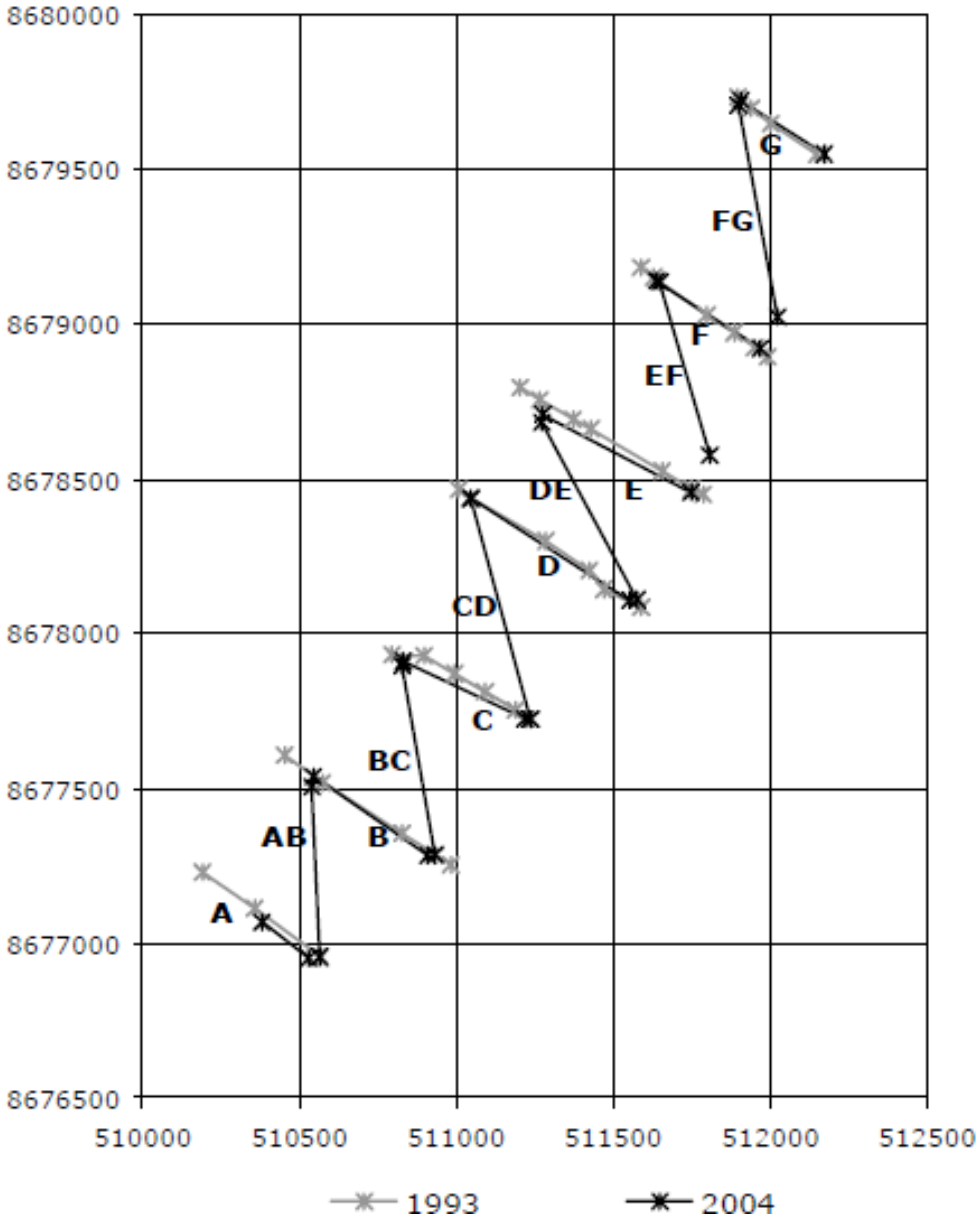


**Figure 61 – THe GPR profiles from 1993 (grey) and 2004 (black) with UTM coordinate system ED50 (Riger-Kusk, 2006)**

Figure 62 shows the spatial distribution of ice thicknesses from the survey in 1993 (Tonning, 1996).

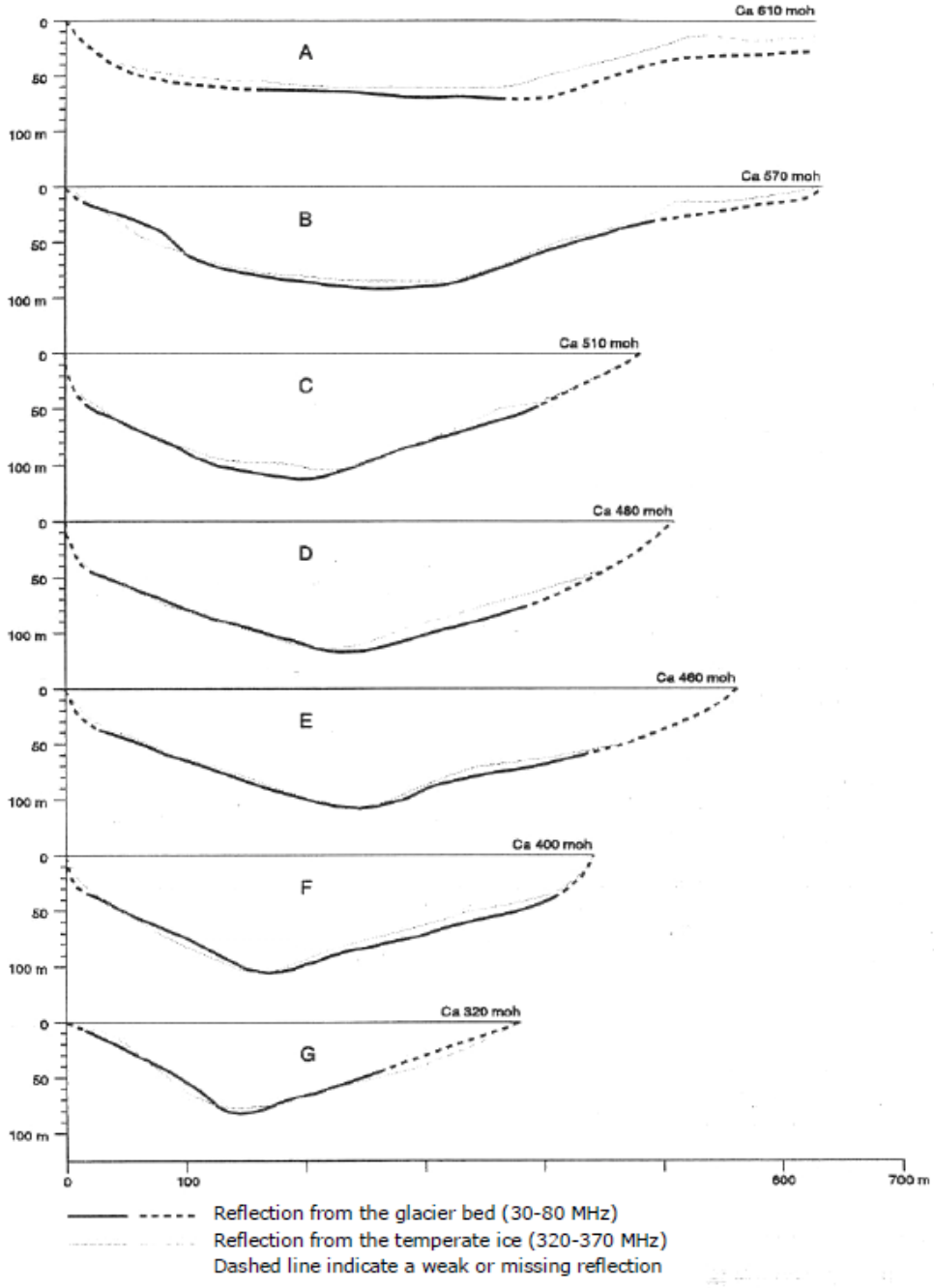


**Figure 62 – Ice thickness from the 1993 survey on Longyearbreen (Tonning, 1996). All profiles starts at distance 0 m.**